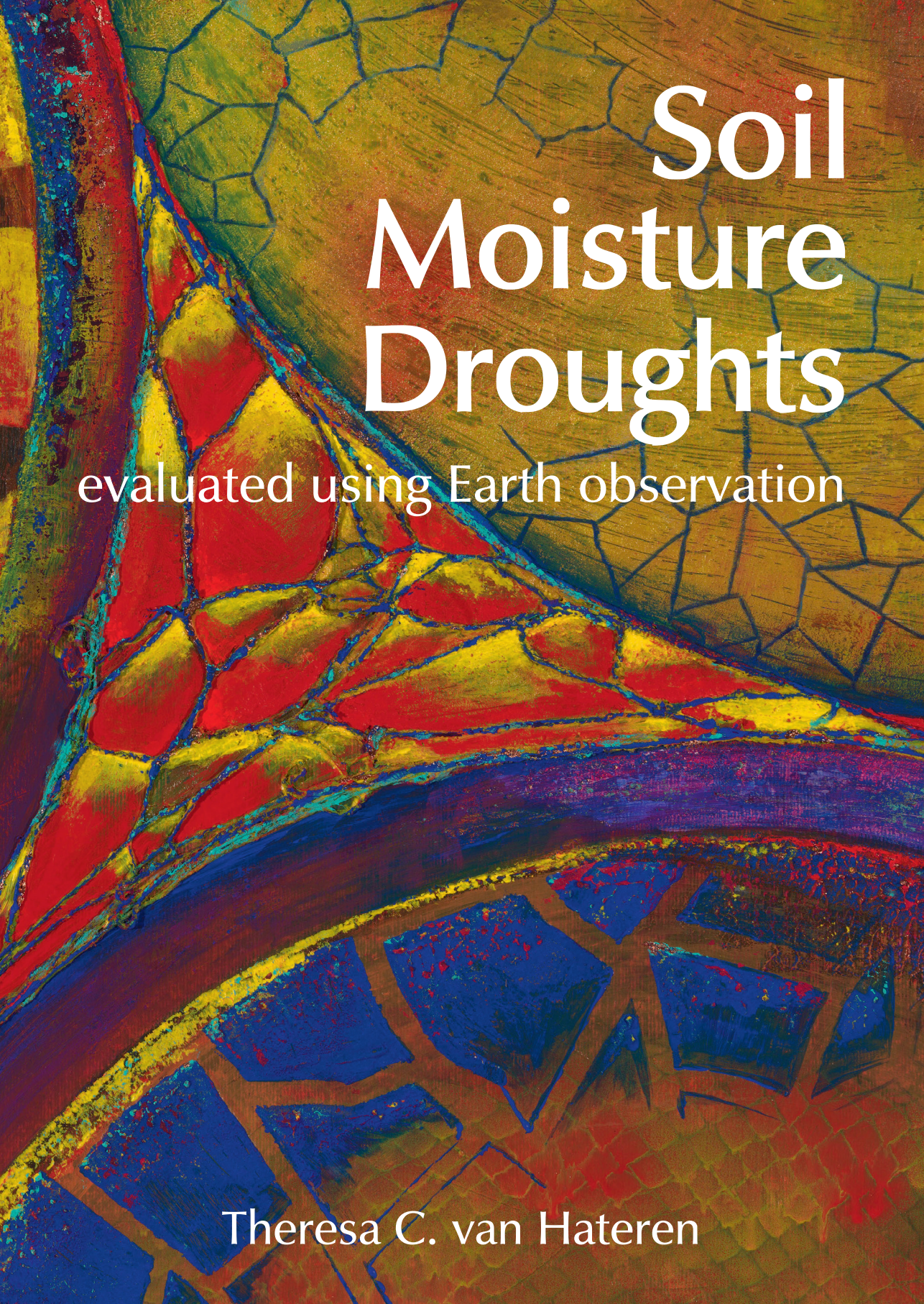
Soil Moisture Droughts
evaluated using Earth observation
Theresa C. van Hateren

Propositions

1. The pursuit of enhanced scientific accuracy of operational systems conflicts with reducing their carbon footprints.
   (this thesis)
2. In selecting a field site, spatial variation warrants precedence over practical considerations.
   (this thesis)
3. The Wageningen University doctoral degree regulations unfairly favour native English or Dutch speakers.
4. Fixed working hours are incompatible with research.
5. Physical activity during working hours improves productivity.
6. Science is valuable only when it addresses societal needs.

Propositions belonging to the thesis, entitled

Soil moisture droughts evaluated with Earth observation

Theresa C. van Hateren

Wageningen, 22 November 2023

Soil moisture droughts evaluated using Earth observation

T. C. van Hateren

Thesis committee

Promotor
Dr A. J. Teuling
Associate Professor, Hydrology and Environmental Hydraulics Group
Wageningen University & Research

Co-promotors
Dr M. Chini
Research & Technology Associate, Remote Sensing and Natural Resources Modelling Group
Luxembourg Institute of Science of Technology

Dr P. Matgen
Group leader, Remote Sensing and Natural Resources Modelling Group
Luxembourg Institute of Science of Technology

Other members
Prof. Dr K. M. de Beurs, Wageningen University & Research
Dr N. Wanders, Utrecht University
Dr A. Gruber, Vienna University of Technology, Austria
Prof. Dr A. Hildebrandt, Friedrich Schiller University Jena &
Helmholtz Centre for Environmental Research – UFZ, Germany

This research was conducted under the auspices of the Graduate School for
Socio-Economic and Natural Sciences of the Environment (SENSE)

Soil moisture droughts evaluated using Earth observation

T. C. van Hateren

Thesis
submitted in fulfilment of the requirements for the degree of doctor
at Wageningen University
by the authority of the Rector Magnificus
Prof. Dr A.P.J. Mol,
in the presence of the
Thesis Committee appointed by the Academic Board
to be defended in public
on Wednesday 22 November 2023
at 11 a.m. in the Omnia Auditorium.

T. C. van Hateren
Soil moisture droughts evaluated using Earth observation
160 pages.

PhD thesis, Wageningen University, Wageningen, The Netherlands (2023)
With references, with summaries in English and Dutch

ISBN 978-94-6447-855-6
DOI 10.18174/637197

Summary

Droughts can have wide-spread environmental, societal and financial impacts. Climate change and related amplified land-atmosphere feedbacks intensify the hydrological cycle on a global scale. This makes securing freshwater and food production for society increasingly difficult. Accurate drought monitoring and prediction strategies are therefore more and more important. Monitoring drought events is complicated as they present themselves in different parts of the water cycle (i.e. soil moisture, groundwater, surface water) in different phases of the event. When a drought affects soil moisture levels, it is called a *soil moisture drought*. Soil moisture is the direct link between precipitation and vegetation functioning and takes a central role in the water cycle and climate system, with important positive feedback cycles that can influence drought occurrence and severity.

Because of the central role of soil moisture in the water cycle, accurate soil moisture estimates at a high spatial resolution can improve numerical weather prediction, serve applications such as precision agriculture, and enhance monitoring and prediction of hydro-meteorological disasters, such as droughts. For optimal performance of these systems, accurate gridded soil moisture observations are needed, ideally at the same spatiotemporal resolution as that of the model in question. Several global or continental gridded soil moisture datasets are currently available. However, their spatial resolution does not yet allow for soil moisture drought monitoring at the scale of individual fields or even at the sub-field scale (Chapter 2). The work done for this thesis therefore had two main aims. First, to obtain accurate satellite soil moisture observations at a high resolution (Chapters 3 and 4), and second, to determine the relevance and potential of state-of-the-art soil moisture data for drought monitoring (Chapters 2 and 5).

Soil moisture droughts often affect vegetation, so they are commonly referred to as *agricultural droughts*. However, the link between soil moisture drought and its impact on vegetation is nonlinear. During short soil moisture drought events, vegetation is not always negatively affected and sometimes even thrives because the weather conditions that are associated with droughts favour vegetation growth. In **Chapter 2** ESA CCI surface soil moisture data and MODIS NDVI vegetation greenness data were used to test whether asynchronies and discrepancies occurred between major European soil moisture and vegetation droughts. A clear delay was observed between the onset of soil moisture and vegetation

drought, with correlations generally peaking at the end of the growing season. At lower latitudes, correlations peaked earlier in the season, likely due to an earlier onset of water limited conditions. In some cases, vegetation showed a positive anomaly, even during soil moisture drought events. That suggests that soil moisture and vegetation droughts should be considered separately.

In **Chapter 3** a first step towards high resolution soil moisture data was taken. Active microwave sensors can provide backscatter data on a 20 m spatial resolution. It is common practice to multilook this backscatter data prior to retrieving soil moisture to mitigate speckle noise. While such preprocessing indeed reduces speckle, it also decreases the spatial resolution and removes possibly useful high resolution information from the data. It was hypothesised that using higher resolution backscatter data for soil moisture retrieval would result in a higher retrieval accuracy. A high-resolution field study was combined with a synthetic experiment to show that calculating soil moisture prior to multilooking to the final target resolution (calculate-then-average) has substantial advantages over the average-then-calculate approach. Currently, the latter strategy is most often applied in soil moisture studies, mainly due to its computational advantage compared to the former approach. By making use of a higher source resolution backscatter data than the target resolution, soil moisture retrieval accuracy over an agricultural field was improved.

The calculate-then-average retrieval strategy was used in **Chapter 4** to explore the potential of active microwave data to monitor soil moisture at high spatial resolutions. Sentinel-1 C-band SAR data at a 20 m resolution was inverted to soil moisture at six spatial resolutions ranging from 20 to 120 m. This was compared to a closely spaced (20 m) in situ dataset collected on a non-irrigated agricultural field in the Southeast of Luxembourg. The comparison showed that soil moisture was accurately estimated at spatial resolutions of 60 m and coarser. At 60 m, sub-field variations in soil moisture were still detected. Spatial correlation was limited by the absence of soil moisture variability within the field. These results indicate that high spatial resolution soil moisture estimates from Sentinel-1 data can be valuable for monitoring temporal soil moisture variations within agricultural fields.

While it was now clear that soil moisture data could be retrieved on sub-field scales, their relevance for drought monitoring remained to be studied. To that end, the 60 m dataset that was used in Chapter 4, was extended to cover Luxembourg. In **Chapter 5**, two additional soil moisture datasets over Luxembourg were used: the vanderSat dataset with a 100 m spatial resolution and the Copernicus dataset with a 1 km resolution. Monthly anomalies of the three satellite retrieved soil moisture datasets were evaluated with those of reference in situ soil moisture and precipitation. An analysis on the national scale showed that the Copernicus data most often correctly identified a drought observed in the in situ data. Compared to precipitation anomalies, the 60 m dataset also performed well, while the 100 m data showed lower correlations. On smaller scales, both the Copernicus and vanderSat datasets showed spatially constant anomalies. Only the 60 m dataset could

distinguish local soil moisture variations. Hence, while Copernicus data allowed for soil moisture drought monitoring on the national scale, higher resolution data is needed to adequately monitor droughts on local scales.

Although this research showed that high resolution soil moisture retrieval for drought monitoring currently still has its limitations, its potential was also shown. The data can already be useful on bare soil fields for sub-field scale drought monitoring and mitigation. That means that the data can be used for precision agriculture purposes. This is especially useful when soil moisture data is combined with other types of (remote sensing) data that can provide information on vegetation functioning. For an efficient drought mitigation strategy, all these data do have to be available to farmers in near-real time.

Future work can focus on further improving the signal filtering and data processing to increase the accuracy of high resolution soil moisture products and to make the data useful for a larger range of field and climatic conditions. Improved soil moisture data can then help local drought mitigation and alleviation strategies as well as regional to national water management strategies. The continuation of the Sentinel-1 constellation and planned missions such as ROSE-L can further improve temporal resolution, retrieval accuracy and penetration depth. The resulting longer data availability will also make the data increasingly suitable for drought monitoring efforts.

Samenvatting

Droogtes kunnen grote ecologische, maatschappelijke en financiële gevolgen hebben. Klimaatverandering, en daaraan gerelateerde terugkoppelingen tussen land en atmosfeer, intensiveren de hydrologische cyclus op globale schaal. Dit maakt het veiligstellen van zoet water voor de samenleving steeds moeilijker. Nauwkeurige droogtewaarnemingen en droogtevoorspellingen worden daarom steeds belangrijker. Het monitoren van droogtes is ingewikkeld, omdat ze zich voordoen in verschillende delen van de waterkringloop (bijvoorbeeld bodemvocht, grondwater, of oppervlaktewater) in verschillende fases van de droogte. Wanneer een droogte plaatsvindt in het bodemvocht, noemen we dit een *bodemvochtdroogte*. Bodemvocht speelt een centrale rol in de watercyclus: het is het directe verband tussen neerslag en het functioneren van de vegetatie. Bovendien is bodemvocht onderdeel van belangrijke positieve feedbackcycli die invloed hebben op zowel het optreden, als de ernst van droogtes.

Gezien de centrale rol van bodemvocht in de watercyclus, hebben nauwkeurige bodemvochtschattingen op een hoge ruimtelijke resolutie verscheidende toepassingen. Zij kunnen numerieke weersvoorspelling verbeteren, toepassingen zoals precisielandbouw dienen en waarnemingen en voorspellingen van hydrometeorologische rampen, zoals droogtes, verbeteren. Voor optimale prestaties van deze systemen zijn dus nauwkeurige gerasterde bodemvochtwaarnemingen nodig, idealiter met dezelfde ruimtelijke en temporele resolutie. Er zijn momenteel verschillende continentale en zelfs wereldwijde gerasterde datasets voor bodemvocht beschikbaar. Hun ruimtelijke resolutie maakt het echter nog niet mogelijk om bodemvocht te monitoren op de schaal van individuele percelen of zelfs op nog kleinere schaal (Hoofdstuk 2). Het werk voor dit proefschrift had daarom twee hoofddoelen. Ten eerste het verkrijgen van nauwkeurige satellietwaarnemingen van bodemvocht op een hoge resolutie (Hoofdstukken 3 en 4), en ten tweede het vaststellen van de relevantie van moderne bodemvochtmetingen voor droogtewaarnemingen (Hoofdstukken 2 en 5).

Bodemvochtdroogtes beïnvloeden vaak de vegetatie en worden om die reden ook wel *landbouwdroogtes* genoemd. Het verband tussen bodemvochtdroogtes en de werking van vegetatie is echter niet-lineair. Tijdens korte bodemvochtdroogtes wordt vegetatie niet altijd negatief beïnvloed. Sterker nog, vegetatie kan zelfs goed gedijen in zulke omstandigheden.

In **Hoofdstuk 2** gebruikten we daarom oppervlakkige ESA CCI bodemvochtdata en MODIS NDVI vegetatiedata om te testen of er grote verschillen tussen de twee optraden tijdens recente Europese droogtes. Er was een duidelijke vertraging zichtbaar tussen het begin van bodemvochtdroogtes en het begin van vegetatiedroogtes. Correlaties tussen de twee droogtes bereikten in het algemeen hun piek aan het einde van het groeiseizoen. Op lagere breedtegraden waren correlaties al eerder in het seizoen op hun hoogst, waarschijnlijk als gevolg van een eerder begin van watergelimiteerde omstandigheden. In sommige gevallen vertoonde de vegetatie een positieve anomalie, zelfs tijdens droge periodes van bodemvocht. We pleiten er daarom voor om bodemvocht- en vegetatiedroogtes afzonderlijk te beschouwen, in plaats van de gezamenlijke term *landbouwdroogtes*.

In **Hoofdstuk 3** zetten we een eerste stap richting hoge resolutie bodemvochtdata. Actieve microgolfsensoren kunnen weerkaatsingsdata leveren met een ruimtelijke resolutie van 20 m. Om ruis in de data te verminderen is het gebruikelijk om deze data ruimtelijk te middellen alvorens deze om te rekenen tot bodemvocht. Hoewel een dergelijke voorbewerking inderdaad ruis vermindert, verlaagt het ook de ruimtelijke resolutie en verwijdert het daarmee mogelijk nuttige informatie uit de data. We veronderstelden daarom dat het gebruik van weerkaatsingsdata met een hogere resolutie voor de omrekening naar bodemvocht zou resulteren in een hogere nauwkeurigheid van de bodemvochtschattingen. Om dat te testen, hebben we een veldexperiment met hoge resolutie gecombineerd met een synthetisch experiment. Dit toonde aan dat het berekenen van bodemvocht voorafgaand aan het ruimtelijk middellen substantiële voordelen heeft ten opzichte van de omgekeerde benadering. Momenteel wordt de tweede strategie het vaakst toegepast in bodemvochtstudies, voornamelijk vanwege het rekenvoordeel in vergelijking met de eerste benadering. We laten zien dat het gebruik van weerkaatsingsdata met een hogere resolutie dan de doelresolutie de nauwkeurigheid van bodemvochtwaarnemingen verbetert.

De strategie die het beste werkte (berekenen en daarna ruimtelijk middellen) werd vervolgens toegepast in **Hoofdstuk 4** om te onderzoeken wat het potentieel van actieve microgolfgegevens is voor het meten van bodemvocht op hoge ruimtelijke resoluties. Sentinel-1 C-band SAR data met een resolutie van 20 m werd omgerekend naar bodemvochtdata met zes ruimtelijke resoluties (variërend van 20 tot 120 m). Deze data werd vergeleken met een hoge resolutie (20 m) velddataset, die was verzameld op een ongeïrrigeerd landbouwperceel in het zuidoosten van Luxemburg. De vergelijking liet zien dat bodemvocht nauwkeurig kon worden gemeten bij ruimtelijke resoluties van 60 m en grover. Op 60 m was de temporele correlatie 0,67 en er konden daarnaast nog steeds lokale variaties in bodemvocht worden waargenomen. Ruimtelijke correlatie werd gelimiteerd door een matige ruimtelijke variabiliteit in bodemvocht op het perceel. Deze resultaten gaven aan dat bodemvochtwaarnemingen met een hoge ruimtelijke resolutie op basis van Sentinel-1 data waardevol kunnen zijn voor het monitoren van temporele bodemvochtvariaties in landbouwgebieden.

Na het bestuderen van de mogelijkheid om bodemvocht te meten op schalen kleiner dan de veldschaal, werd hun relevantie voor droogtemonitoring bestudeerd. Daartoe werd de dataset van 60 m die in hoofdstuk 4 werd gebruikt, uitgebreid tot aan de Luxemburgse buitengrenzen. In **Hoofdstuk 5** maakten we daarnaast gebruik van de unieke beschikbaarheid van twee extra bodemvochtdatasets over Luxemburg: de vanderSat-dataset met een ruimtelijke resolutie van 100 m en de Copernicus-dataset met een ruimtelijke resolutie van 1 km. Maandelijkse anomalieën van de drie satellietbodemvochtdatasets werden geëvalueerd met die van referentie in situ bodemvocht en in situ neerslag. Een analyse op nationale schaal toonde aan dat Copernicus data het vaakst correct een droogte identificeerde die werd waargenomen in de in situ data. Vergeleken met neerslaganomalieën, presteerde de 60 m dataset ook goed, terwijl de 100 m data lagere correlaties liet zien. Op kleinere schaal vertoonden zowel de datasets van Copernicus als vanderSat ruimtelijk constante anomalieën. Alleen de 60 m dataset kon lokale variaties in bodemvocht onderscheiden. Daaruit concludeerden we dat, hoewel de gegevens van Copernicus het mogelijk maakten om droogte in de bodem op nationale schaal te monitoren, gegevens met een hogere resolutie nodig zijn om droogte op lokale schaal adequaat waar te nemen.

Hoewel dit onderzoek aantoonde dat hoge resolutie bodemvochtdata voor droogtewaarnemingen op dit moment nog zijn beperkingen heeft, hebben we ook zijn potentieel laten zien. Op kale gronden kan de data kan al nuttig zijn voor droogtewaarnemingen en -mitigatie op schalen kleiner dan landbouwpercelen. Dat betekent dat de gegevens kunnen worden gebruikt voor precisielandbouwdoeleinden. Dit is vooral praktisch wanneer bodemvochtgegevens worden gecombineerd met andere soorten (satelliet)gegevens die informatie kunnen geven over het functioneren van de vegetatie. Bovendien moeten, voor efficiënte droogtemitigatiestrategieën, al deze gegevens kort na de meting beschikbaar zijn voor boeren.

Toekomstig werk kan zich richten op het verder verbeteren van het filteren en verwerken van weerkaatsingsdata, ten eerste om de nauwkeurigheid van hoge resolutie bodemvochtproducten te vergroten en ten tweede om de gegevens bruikbaar te maken voor een groter aantal veld- en klimatologische omstandigheden. Verbeterde bodemvochtgegevens kunnen dan verder helpen bij het lokaal beperken en verlichten van droogte, evenals bij regionaal en nationaal waterbeheer. Bovendien kunnen de voortzetting van de Sentinel-1 metingen en geplande missies zoals ROSE-L de temporele resolutie, de nauwkeurigheid van de data en de penetratiediepte verder verbeteren. Een langere databeschikbaarheid zal de gegevens daarnaast steeds geschikter maken voor droogtemonitoring.

Contents


1

Chapter 1

Introduction

This chapter is partly based on:

T. C. van Hateren, H. J. Jongen, H. Al-Zawaidah, J. G. Beemster, J. Boekee, L. Bogerd, S. Gao, C. Kannen, I. van Meerveld, S. I. de Lange, F. Linke, R. B. Pinto, J. O. Remmers, J. Ruijsch, S. R. Rusli, R. C. van de Vijsel, J. P. Aerts, S. M. Agoungbome, M. Anys, S. Blanco Ramírez, T. van Emmerik, L. Galitelli, G. Chiquito Gesualdo, W. Gonzalez Otero, S. Hanus, Z. He, S. Hoffmeister, R. O. Imhoff, T. Kerlin, S. M. Meshram, J. Meyer, A. Meyer Oliveira, A. C. Muller, R. Nijzink, M. Scheller, L. Schreyers, D. Sehgal, P. F. Tasseron, A. J. Teuling, M. Trevisson, K. Waldschlager, B. Walraven, C. Wannasin, J. Wienhofer, M. J. Zander, S. Zhang, J. Zhou, J. Y. Zomer, and B. W. Zwartendijk (2023d). 'Where should hydrology go? An early-career perspective on the next IAHS Scientific Decade 2023-2032'. Hydrological Sciences Journal 68.4, 529. doi: 10.1080/02626667.2023.2170754

1.1 Drought: concept and definition

A drought is often referred to as a "creeping disaster": it is slow in nature, but it can have wide-spread environmental, societal and financial impacts (Naumann et al., 2021; Stahl et al., 2016). Over the past two decades, droughts have often plagued Europe (Bakke et al., 2020; Hanel et al., 2018; Ionita and Nagavciuc, 2021; Laaha et al., 2017). The 2003 heat wave and drought over Europe caused increased mortality, forest dieback, and agricultural losses amounted to at least 8.7 billion Euros (Buras et al., 2020; COPA-COGECA, 2003; European Commission, 2007). The 2018–2019 drought event was record-breaking and covered more than 50% of the European continent in extreme drought conditions (Hari et al., 2020). In some places this multi-year drought even lasted until 2020 (van der Wiel et al., 2023). In August 2022, 60% of the European continent was under a drought alert yet again (Toreti et al., 2022).

Unlike a flood, that can be seen as an event with a fixed threshold (i.e. flooding or no flooding, water level exceeding the height of the river bank or dike), a drought is not directly linked to a visible threshold. Instead, a drought is always defined relative to a threshold based on "normal" conditions. These "normal" conditions are different for each climate and each season, so the threshold for a drought varies in both time and space. The reason for this approach is that the impacts of dry spells are very different in different climates and different seasons. For instance, a desert is in an almost permanent state of little precipitation, so the impact of a dry spell on the ecosystem will be limited. A similarly long dry spell in a humid climate will have very different impacts. The same concept holds for seasonality: a dry spell in the wet season can have a larger impact than a dry spell in the dry season.

Many definitions of droughts exist, and at least as many indices to quantify them (Heim Jr., 2002; Zargar et al., 2011). In this thesis, the drought definition by Tallaksen and van Lanen (2004) is used: *a sustained period of below-normal water availability*. Both parts of this definition play an important role as to how droughts are characterised and quantified. Firstly, a drought only occurs when water availability to the ecosystem is low for *a sustained period*. This indicates that a system is not immediately in drought if it does not rain for a week. Instead, most large scale drought indices use moving averages or monthly timescales, to dampen the natural temporal variability in hydrological variables (Heim Jr., 2002). Secondly, *below-normal water availability* indicates that current water availability should be compared relative to conditions in the same time of year over the past climatic reference period (normally 30 years). A dry spell in the desert is now considered "normal" and thus not necessarily a drought, whereas a below-normal water availability in any climate is in fact a drought, and adequate measures can be taken.

Droughts can be further categorised based on the part of the water cycle that suffers from a below-normal water availability (van Loon, 2015). A precipitation deficit, sometimes

combined with increased evapotranspiration, is referred to as a meteorological drought. Similarly, a soil moisture drought indicates below-normal soil moisture levels. Because this second type of drought often affects vegetation, it is also often referred to as an agricultural drought. The third type of drought is a hydrological drought, where surface and subsurface water bodies experience below-normal water levels. If meteorological droughts are severe or prolonged, they can propagate into a soil moisture drought, and further into a hydrological drought (van Loon, 2015). Although droughts manifest themselves in the environment, their impacts include immense social, environmental, and economic ramifications (e.g. Nilson, 2014). For that reason, a fourth type of drought, socio-economic, is often also considered. This encompasses the impact of natural droughts on society and economy.

1.2 Droughts in a changing climate

Global warming directly influences water fluxes (Kundzewicz, 2008; Madakumbura et al., 2019; Peleg et al., 2018; Samaniego et al., 2018), and as such, climate change and related amplified land-atmosphere feedbacks intensify the hydrological cycle on a global scale. This intensification consists of increased occurrences as well as increased severity of hydrological extremes, such as floods and droughts (Berg et al., 2016; Hari et al., 2020; Samaniego et al., 2018; Teuling, 2018). This still holds if a changing hydrological regime is considered (Wanders et al., 2015). We can also expect an increase in compound events, where two extremes co-occur (i.e., hot droughts with little precipitation as well as high temperatures, Buras et al., 2020; Seneviratne et al., 2010; Zscheischler et al., 2018), and flash droughts, which have a rapid onset due to high temperatures (Christian et al., 2023; Yuan et al., 2019).

Over Europe, the impact of anthropogenic warming on drought occurrence is spatially divergent. The increasing temperature does lead to positive evapotranspiration trends throughout Europe, but precipitation trends are negative in southern Europe and positive in northern Europe. Mediterranean Europe has therefore so far seen an increase in drought occurrence, and the opposite is visible in northern Europe (Stagge et al., 2017). Under a projected 3°C global warming, which seems likely based on an intermediate emission scenario (IPCC, 2023), additional drought exposure as well as financial impact are expected to be largest in the Mediterranean sub-region, and smallest in the Boreal sub-region (Cammalleri et al., 2020; Marx et al., 2018; Naumann et al., 2021).

European summer droughts have been shown to be induced by Mediterranean winter rainfall deficits (Vautard et al., 2007; Zampieri et al., 2009). These rainfall deficits lead to anomalously warm and dry air, that is transported northward with southerly winds and increases temperature and vegetation water demand in continental Europe. The Rhine basin, one of the main hydrological systems in Northwestern Europe, is normally supplied with

atmospheric moisture from the Atlantic Ocean. During the 2003 and 2018 droughts, however, persistent high pressure systems over the Rhine basin decreased the supply from this moisture source (Benedict et al., 2021), leading to major drought events. Large-scale land-atmosphere feedbacks thus have a big influence on hydrological extremes (Schumacher et al., 2019).

An intensifying hydrological cycle makes securing freshwater for society increasingly difficult (Carvalho-Santos et al., 2017). Even more so, because ecosystems are more vulnerable to droughts in a summer following a drought (*preconditioning*, Zscheischler et al., 2020). Added to that, impacts of a subsequent drought event can be larger because of legacy effects, especially if water levels do not fully recover during the winter season (Bastos et al., 2021). Hence, increased drought occurrence due to climate change, combined with decreasing freshwater storage due to shrinking glaciers (Beniston and Stoffel, 2014), depleting high-quality groundwater aquifers (Rotzoll and Fletcher, 2013), and increasing societal water demand (Wada et al., 2013; Wanders and Wada, 2015), poses a threat for water security. Society thus needs accurate drought monitoring systems as well as improved early warning systems to limit the negative impacts of extreme events, and long-term strategies to mitigate and cope with any remaining detrimental effects.

1.3 Soil moisture's central role in the water cycle

Soil moisture levels are dependent on precipitation and temperature, and in turn they influence air temperature, moisture recycling, and evapotranspiration (Fig. 1.1, Berg and Sheffield, 2018; Teuling et al., 2006a). Via evapotranspiration, soil moisture is the direct link between precipitation and vegetation functioning. However, the relationship between soil moisture drought and its impact on vegetation is non-linear (Heim Jr., 2002; Seneviratne et al., 2010). During a soil moisture drought, vegetation growth may be limited by depleted soil moisture reservoirs, but, in humid climates, vegetation can simultaneously benefit from increased solar radiation (Jolly et al., 2005; Kowalska et al., 2020; Mastrotheodoros et al., 2020; Teuling et al., 2006c). Hence, climate change can have divergent impacts on vegetation (Berg and Sheffield, 2018), dependent not only on temperatures and increased CO_2 concentrations (Erda et al., 2005), but also on water availability.

Soil moisture thus takes a central role in the water cycle, with important positive feedback cycles that can influence drought occurrence and severity. Soil moisture's large influence on the ecosystem can also be seen in the impact of changing initial soil moisture conditions in meteorological (Liang and Yuan, 2021), hydrological (Grillakis et al., 2016; Yin et al., 2022) and land surface models (Kim and Wang, 2007). Optimal initial soil moisture conditions can reduce model warm up times, thus allowing for an optimal use of available data (Kim et al., 2018). Hence, for optimal performance of hydrological models, we need accurate

gridded soil moisture observations, ideally at the same spatiotemporal resolution as that of the model in question.

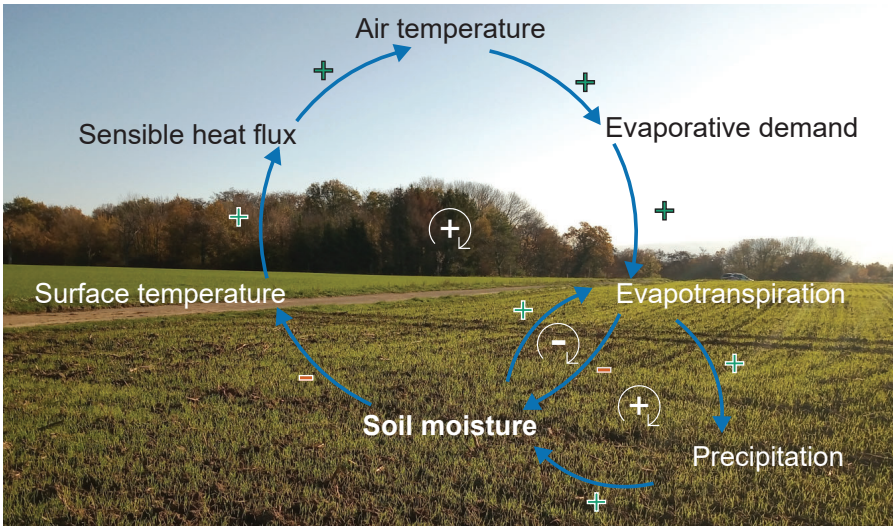

Figure 1.1: Illustration of the central role of soil moisture in the water cycle, with important feedback loops. The picture was taken in the experimental field on Nov 6th, 2020. Adapted from Teuling (2018).

1.4 Satellite soil moisture observations

Observing soil moisture is difficult because of its high small-scale spatial variability (Brocca et al., 2010). In situ observations are accurate, but made at point scale and thus lack spatial representativeness as well as spatial coverage (Babaeian et al., 2019; Crow et al., 2012b; Peng et al., 2021; Seneviratne et al., 2010; Teuling et al., 2006b). Another issue is that a large range of sensors, observation depths and sensor calibrations are used, making it difficult to compare different sites. Even though efforts are being made to collect and publish in situ soil moisture data (Dorigo et al., 2021), they remain scarce because of the costs and time involved in acquiring, installing and maintaining in situ sensors. Air- and spaceborne sensors can provide large-scale gridded estimate of soil moisture, with sizes ranging from field- to catchment scale for airborne observations and global scale for spaceborne observations. Such large-scale soil moisture data can be assimilated directly in hydro-meteorological models (Hostache et al., 2020), used for drought monitoring (Fang et al., 2021; Ford and Quiring, 2019; Liu et al., 2019), or even used to reduce farmers' drought risk exposure (Vroege et al., 2021).

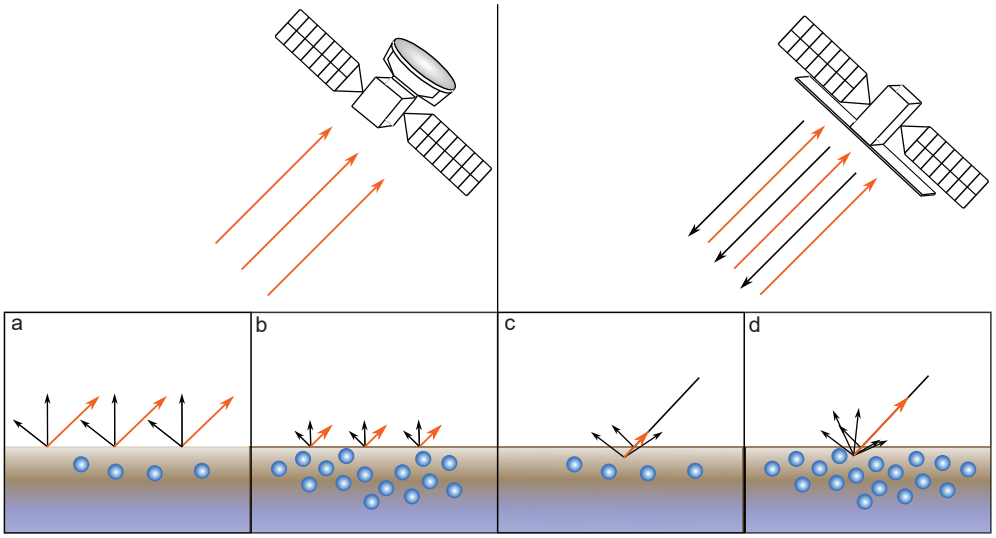

Figure 1.2: Concepts of passive and active satellite soil moisture observations. Passive sensing of dry (a) and wet (b) soils is shown on the left, and active sensing of dry (c) and wet (d) soils on the right.

Soil moisture can be estimated using a variety of satellite sensors that can be categorised by the part of the electromagnetic spectrum where measurements are taken (Babaeian et al., 2019; Li et al., 2021; Petropoulos et al., 2015; Zhang and Zhou, 2016): optical, thermal and microwave sensors. All these methods have their own advantages and disadvantages (Babaeian et al., 2019). Both optical and thermal sensors are limited to daytime retrievals and cloudless conditions. Microwave sensors do not have these disadvantages, but are influenced by surface roughness. A disadvantage that the three measurement types have in common is their sensitivity to vegetation biomass. This thesis focuses on microwave sensors because their sensitivity to longer wavelengths than optical and thermal sensors limits interference by meteorological conditions and increases penetration depth into the soil.

Both passive and active microwave sensors make use of the contrast between the dielectric permittivity of bare soil and water (Babaeian et al., 2019; Ulaby et al., 1986). Passive microwave sensors (radiometers) measure the brightness temperature of the Earth's surface. This temperature depends on the emissivity of the soil, that, in turn, inversely relates to the dielectric permittivity. Increased soil water content therefore leads to a lower brightness temperature (Fig. 1.2a, b). Active microwave sensors (scatterometers or Synthetic Aperture Radars) emit a microwave signal and measure the fraction of radiation scattered back by the Earth's surface (backscatter). Increased soil dielectric permittivity leads to increased interaction with, or scattering of, the satellite signal. This increases the backscatter that is

measured by the sensor (Fig. 1.2c, d). Passive measurements have a low spatial resolution, because of the weak signal emitted by the Earth's surface. That does allow for more frequent revisit times and results in a high temporal resolution of soil moisture products from passive sensors. For active sensors, this is the other way around: their products have a low temporal resolution but a high spatial resolution.

1.5 Spatial resolution

Accurate soil moisture estimates at a high spatial resolution can improve numerical weather prediction (Lagasio et al., 2019a; Lagasio et al., 2019b), serve applications such as precision agriculture (Vereecken et al., 2014), and enhance monitoring and prediction of hydro-meteorological disasters, such as droughts (Bierkens et al., 2015; Peng et al., 2021; Vergopolan et al., 2021; Wood et al., 2011). Several global or continental gridded soil moisture (SM) datasets are currently available (Peng et al., 2021), such as European Space Agency (ESA) Climate Change Initiative (CCI) soil moisture (Gruber et al., 2020), National Aeronautics and Space Administration (NASA) United States Department of Agriculture (USDA) Global Soil Moisture Data, and Copernicus Global Land service Surface Soil Moisture. These open data can be very useful for modelling studies thanks to their large-scale coverage. However, their spatial resolution (0.25°, 0.25°, 1 km, respectively) does not yet allow for soil moisture monitoring at the scale of individual fields or even at the sub-field scale. This can be seen clearly in Fig. 1.3, where a 1 km resolution image is compared to two images with higher resolutions (100 m and 60 m). At a 1 km resolution, we can get a global view of the region, but higher spatial resolutions are required to differentiate fields or even distinguish sub-field variation.

Active microwave backscatter data could be used to retrieve soil moisture at the sub-field scale. Two active microwave satellites are currently operating, both at C-band (wavelength of 3.75–7.5 cm): Advanced SCATterometer (ASCAT) and Sentinel-1 (S1) (Babaeian et al., 2019). ESA's S1 constellation provides high spatiotemporal resolution Synthetic Aperture Radar (SAR) data with a ground-range resolution of 20 m and a six day repeat cycle up until December 2021, when one of the two satellites failed. The function of the failed B-satellite is planned to be replaced by the C- and D-satellites in 2023 and 2024, further improving the constellation's temporal resolution. The satellites are kept under a strict acquisition scenario, and ESA is expected to continue these observations for the next few decades (Bauer-Marschallinger et al., 2019; Peng et al., 2021).

The reason that the previously discussed available datasets do not yet use active microwave data for soil moisture retrieval at its native resolution is because the SAR backscatter accuracy is limited by speckle. Speckle causes variations in the backscatter intensity that do not necessarily relate to variations in soil moisture. Speckle can be reduced by

[1] Bous, Dalheim, Mondorf-les-Bains, Remich, Schengen and Waldbredimus

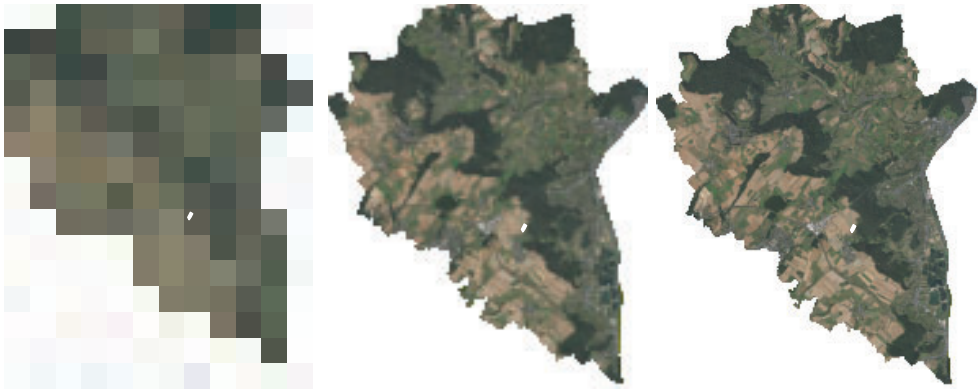

Figure 1.3: Illustration of the importance of fine resolutions for imaging purposes. Orthoimages (Portail Open Data, 2017) are shown for the six most southeastern municipalities of Luxembourg[1] with, from left to right, a 1 km, 100 m, and 60 m resolution, which are the same spatial resolutions as used in Chapter 5. The agricultural field where soil moisture was observed for Chapters 3 and 4 is indicated in white.

spatially aggregating the data, but this also reduces the spatial resolution, so the final spatial resolution of the data will be lower than that of native SAR data (Bauer-Marschallinger et al., 2019; Pulvirenti et al., 2018; Zappa et al., 2021).

1.6 This thesis

Monitoring drought events is complicated as they present themselves in different parts of the water cycle (i.e. soil moisture, groundwater, surface water) in different phases of the event (Buitink et al., 2021; van Loon, 2015). Because of the large financial implications of soil moisture droughts via its influence on crop production, this thesis focuses on the monitoring of these droughts, in the understanding that they are caused by meteorological droughts and can propagate into hydrological droughts. Remotely sensed soil moisture has shown to be useful for soil moisture drought monitoring (e.g. Bolten et al., 2010; Ford and Quiring, 2019; Martínez-Fernández et al., 2016), but this is still done on low spatial resolutions. Higher resolution data would allow for drought monitoring on the (sub-)agricultural plot scale, with applications such as crop insurance, precision irrigation and improved hydro-meteorological modelling.

In the four main research chapters, this thesis discusses the research done to answer three main research questions (Fig. 1.4):

1. What is the value of state-of-the-art satellite soil moisture products for drought monitoring?

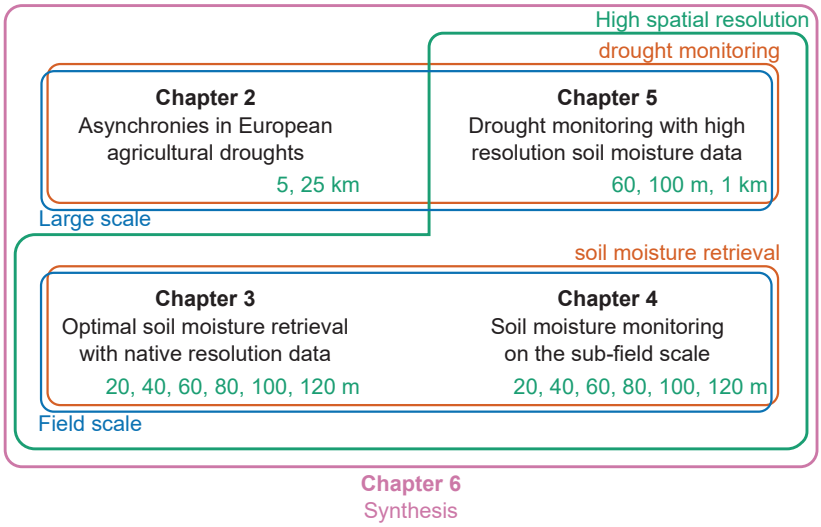

Figure 1.4: Topics and spatial resolutions discussed in each chapter.

2. What is the highest spatial resolution at which soil moisture can be accurately retrieved from satellite data?
3. Can high resolution satellite soil moisture data be used for large scale drought monitoring?

The first research question is covered by **Chapter 2**. Making use of an existing large scale satellite soil moisture dataset with a 0.25° resolution and a vegetation greenness dataset at a 5 km resolution, major European droughts are analysed for asynchronicities between soil moisture and vegetation. Long periods of decreased water availability can negatively impact vegetation. Conversely, short drought events are often linked to an increase in available energy, which can have a positive impact on energy-limited vegetation growth.

One of the main hypotheses underlying this thesis is that S1 data at its native spatial resolution (20 m) contains relevant information on sub-field moisture conditions. To that end, I set up a field experiment in the Southeast of Luxembourg (indicated in Fig. 1.3) where I collected in situ soil moisture data at the S1 native spatial resolution. This experiment together with a synthetic experiment are described in **Chapter 3** to find the best strategy to retrieve high resolution soil moisture data from Sentinel-1 backscatter intensity data. That strategy is then applied in **Chapter 4**, where soil moisture retrieval accuracy is compared to the field observations at different high spatial resolutions (20–120 m). Together, these two chapters answer the second research question.

Soil moisture retrievals at the most favourable spatial resolution are finally used in **Chapter 5** to answer the third and last research question. They are applied on a national scale, which

allows for a discussion on the use of high resolution soil moisture retrievals for drought monitoring on a large scale.

The main findings of this thesis are discussed in **Chapter 6**. The research questions are answered and reflected on in the context of recent and possible future advances in drought monitoring.


2

Chapter 2

Asynchronies in European agricultural droughts

This chapter is based on:

T. C. van Hateren, M. Chini, P. Matgen, and A. J. Teuling (2021). 'Ambiguous Agricultural Drought: Characterising Soil Moisture and Vegetation Droughts in Europe from Earth Observation'. Remote Sensing 13.10, 1990. doi: 10.3390/rs13101990

Abstract

Long-lasting precipitation deficits or heat waves can induce agricultural droughts, which are generally defined as soil moisture deficits that are severe enough to negatively impact vegetation. However, during short soil moisture drought events, the vegetation is not always negatively affected and sometimes even thrives. Due to this duality in agricultural drought impacts, the term "agricultural drought" is ambiguous. Using the remotely sensed ESA CCI surface soil moisture estimates and MODIS NDVI vegetation greenness data, we show that, in major European droughts over the past two decades, asynchronies and discrepancies occurred between the surface soil moisture and vegetation droughts. A clear delay is visible between the onset of soil moisture drought and vegetation drought, with correlations generally peaking at the end of the growing season. At lower latitudes, correlations peaked earlier in the season, likely due to an earlier onset of water limited conditions. In certain cases, the vegetation showed a positive anomaly, even during soil moisture drought events. As a result, using the term agricultural drought instead of soil moisture or vegetation drought, could lead to the misclassification of drought events and false drought alarms. We argue that soil moisture and vegetation drought should be considered separately.

2.1 Introduction

Due to climate change and enhanced land-atmosphere feedback, droughts and their impacts will likely become more severe over the coming decades (Rasmijn et al., 2018; Samaniego et al., 2018; Teuling, 2018). Droughts are generally considered to be induced by a precipitation deficit relative to normal conditions, which, when persisting over longer time periods, results in insufficient water supply to meet the demands of both human activities and the environment (Hayes et al., 2011). As a result, the impacts of droughts can range from decreased crop yield and damage to ecosystems, to land subsidence, insufficient drinking water, and the disruption of transport.

To monitor and quantify drought across the terrestrial part of the hydrological cycle, numerous drought indices have been developed over the past decades. These can be divided into indices for the three main drought types (Tallaksen and van Lanen, 2004). Meteorological droughts are defined as a prolonged period with below-normal precipitation. These droughts are typically quantified with the Standardized Precipitation Index (SPI) (McKee et al., 1993), reflecting the current dogma that droughts are measured relative to the mean climate as well as the climate variability at that location.

Meteorological droughts can propagate into hydrological droughts (Kumar et al., 2016), which entail below-normal (ground) water levels or river discharge (Seneviratne et al., 2012), and are generally evaluated using e.g., reservoir levels, the Standardized Runoff Index, or the Streamflow Drought Index (Hayes et al., 2011; Shukla and Wood, 2008). Lastly, agricultural droughts reflect droughts in the soil moisture. The few studies that provide explicit definitions of agricultural drought, agree that it concerns a soil moisture deficit severe enough to hamper vegetation growth, agricultural production, or crop yield (Panu and Sharma, 2002; Tallaksen and van Lanen, 2004; Wilhite and Glantz, 1985).

Other definitions exist (e.g. IPCC, 2012); however, these also relate soil water status to vegetation state. Due to its direct relation to food production (through crop yield) and water management (through irrigation), agricultural drought is often the key focus of drought monitoring and forecasting. In line with their definition, agricultural droughts have traditionally been quantified based on the soil moisture conditions in the root zone (e.g. Bolten et al., 2010; Carrão et al., 2016; Martínez-Fernández et al., 2016; Sridhar et al., 2008). The well-known and widely-used Palmer Drought Severity Index (PDSI) calculates a simple water budget based on the monthly values of precipitation and the potential evapotranspiration, in combination with parameters that have been optimised to ensure similar PDSI values correspond to similar impacts on vegetation and crop yield even in different climate conditions (Briffa et al., 1994; Palmer, 1965; Raible et al., 2017).

The development of high-resolution land surface models applied at continental scales also allows a more physically-based alternative to PDSI, which can account for the local soil and vegetation properties. In other cases, ranked or standardised in situ or remotely sensed

soil moisture observations have been used directly as an agricultural drought index (e.g. Crow et al., 2012a; Mozny et al., 2012; Peled et al., 2010). Helped by the readily available satellite observations of vegetation indices, such as NDVI, EVI, SIF, fPAR, NIRv, or VOD, other studies have focused on the use of these vegetation indices to quantify agricultural drought (Anyamba and Tucker, 2012; Buitink et al., 2020; Hu et al., 2019).

Similarly, Narasimhan and Srinivasan (2005) developed two separate indices for agricultural drought monitoring: one focused on soil moisture, and the other on evapotranspiration deficits. In other studies, other combinations were made to quantify agricultural drought, such as precipitation, potential evapotranspiration, and soil moisture (Cao et al., 2019). The current definition of agricultural droughts described earlier, i.e., a soil moisture deficit severe enough to hamper vegetation growth, thus, does not seem to be compatible with a single index that describes either its cause (soil moisture deficit) or its impact (hampered vegetation growth).

Whereas soil moisture and vegetation-based indices both aim to quantify agricultural drought, the relation between soil moisture and vegetation is characterised by considerable complexity and nonlinearity. This complexity was already acknowledged late in the nineteenth century, when Abbe (1894) stated that "a drought affecting agriculture is a complex result of many considerations" (Heim Jr., 2002). Although combined indices have since been proposed as a solution to circumvent the nonlinear relation between soil moisture and vegetation (Sepulcre-Canto et al., 2012; Sivakumar et al., 2010; Yurekli and Kurunc, 2006), it is questionable whether agricultural drought and its impact can be adequately quantified by a single normalised index across climate gradients.

From the small scale to the continental scale, distinct water- and energy-limited soil moisture regimes can be identified (Denissen et al., 2020), with the relation between soil moisture and the evaporative fraction often being represented by a bilinear relation (Seneviratne et al., 2010). Above the so-called critical moisture content, which is an absolute value of soil moisture, evapotranspiration and plant functioning will not be limited nor affected by a lack of precipitation.

In fact, in humid climates, increased incoming solar radiation during meteorological drought periods can even enhance evapotranspiration (Teuling et al., 2013) often leading to positive anomalies in vegetation indices, relative to the mean conditions, despite relatively dry conditions (Jolly et al., 2005; Kowalska et al., 2020; Mastrotheodoros et al., 2020; Teuling et al., 2006c), as illustrated in Fig. 2.1.

We hypothesise that because of this duality in agricultural drought impacts, the use of the term *agricultural drought* is ambiguous, because vegetation impacts might depend on the absolute rather than relative soil moisture conditions, in a way that differs from a simple delayed response. The threshold behaviour associated with the "absolute" critical moisture content is clearly at odds with the current dogma that drought and its impacts should be expressed relative to the mean conditions.

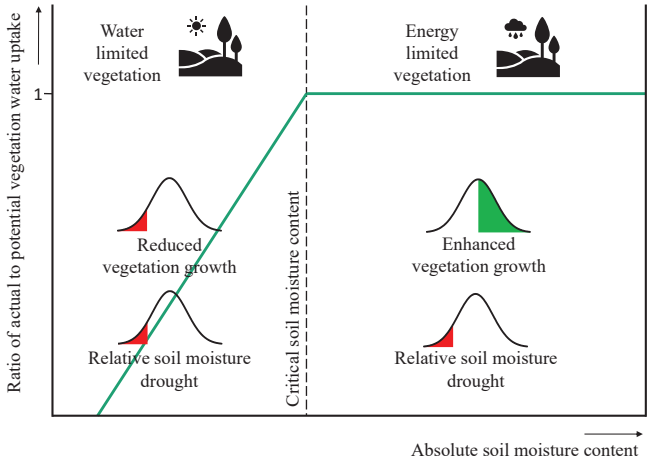

Figure 2.1: The ambiguity of agricultural drought. Normalised agricultural drought indices across a range of climates or mean soil moisture contents can show contrasting signs due to the non-linearity between the soil moisture and vegetation water uptake. In water-limited (arid) climates, a normalised soil moisture drought (i.e., negative soil moisture anomaly) will generally be accompanied by a drought in the vegetation indices (i.e., a negative growth anomaly). In humid climates, where the soil moisture generally does not limit the evapotranspiration and plant functioning, normalised soil moisture indices might indicate drought, whereas vegetation indices might show positive anomalies, as long as the soil moisture is above the absolute critical soil moisture content.

To address the issues surrounding the definition of agricultural drought, we aim to characterise the synchrony and similarity between droughts in the soil moisture and vegetation using readily available long-term (2000–2018) gridded datasets of precipitation, vegetation functioning, and remotely sensed soil moisture. We additionally aim to contribute to the debate on the use of drought indices (for agricultural drought in particular), and how routine global-scale Earth observation products can be used for this.

The relation between soil moisture and vegetation during drought periods has been studied (Chen et al., 2014; Nicolai-Shaw et al., 2017; Papagiannopoulou et al., 2017; Szczypta et al., 2014; Zscheischler et al., 2015), and significant correlations have been found, in addition to a lag between the soil moisture and vegetation response (Chen et al., 2014; Nicolai-Shaw et al., 2017), especially in water-limited ecosystems (Papagiannopoulou et al., 2017). Such lags are not expected in humid areas where the soil moisture content, though relatively low, might not decrease below the absolute critical moisture content.

Based on the aforementioned studies, and the concept of critical soil moisture (Denissen et al., 2020; Peled et al., 2010), we hypothesise that the link between soil moisture and vegetation droughts is more direct in the water-limited Mediterranean region, whereas a more

complex behaviour is expected in the more humid Northern Europe depending on the intensity and duration of the drought. Though a move toward the more unambiguous separate use of the two drought types has started over the past years (e.g. van Loon, 2015), there are ongoing challenges related to the understanding, quantification, and operational monitoring of agricultural drought at larger (sub)continental scales that encompass a range of climate conditions.

Here, we investigate the relation between the surface soil moisture and vegetation drought, as observed in negative (< -1) anomalies in soil moisture (SM) and Normalized Difference Vegetation Index (NDVI) from routine and widely-used Earth observation products. We investigate six widespread meteorological drought events that occurred over the past two decades in Europe, including the severe 2003 and, more recent, 2018 events, that occurred in water- as well as energy-limited regions. In addition, we critically evaluate the practice of using soil moisture to predict the observed agricultural drought (i.e., the vegetation impact, e.g. Chakrabarti et al., 2014; Hao and AghaKouchak, 2013; Martínez-Fernández et al., 2015; Martínez-Fernández et al., 2016; Sridhar et al., 2008).

2.2 Data and methods

2.2.1 Data

Daily remotely sensed surface SM data were obtained from the ESA CCI Combined SM v04.5 dataset (Dorigo et al., 2017; Gruber et al., 2017; Gruber et al., 2019), with a 0.25° resolution, spanning from January 1979 until December 2018. The combined CCI algorithm includes the masking of uncertain soil moisture estimates, for instance in the case of frozen soil, water bodies, or dense vegetation (Scanlon et al., 2020), though masking can be insufficient at times (van der Vliet et al., 2020). The information contained in the satellite soil moisture data mainly contains the surface soil moisture content, rather than the root-zone soil moisture content (Nicolai-Shaw et al., 2017), where the latter has a more direct impact on the vegetation performance.

Regardless, remotely sensed data were deemed the most suitable for this study due to the long time period and large spatial scale of the analysis, and the unavailability of root zone soil moisture measurements on such scales. Existing large scale root zone soil moisture datasets are either inferred from surface soil moisture using land surface models (e.g. Beaudoing et al., 2017; Crow and Tobin, 2018; Houborg et al., 2012) or using water balance models (e.g. Bauer-Marschallinger et al., 2018; Crow, 2012; Owe et al., 2008). For a comparison between the performance of modelled soil moisture and satellite soil moisture products, we refer to Beck et al. (2021).

As we used the surface soil moisture rather than the root zone soil moisture, the possibility exists that we overestimated any observed asynchrony between the water content

and vegetation. This will be accounted for in the discussion of our results. The monthly precipitation data were collected from the NASA GPM IMERG final precipitation L3 dataset with a 0.1° spatial resolution (Huffman et al., 2020; Huffman et al., 2019) from June 2000 until February 2020.

The monthly NDVI data were gathered from the Moderate-resolution Imaging Spectroradiometer (MODIS) dataset on a monthly timescale with a 0.05° resolution, spanning February 2000 to December 2018 (MODIS MOD13C2) (Didan, 2015; Tucker, 1979). Although MODIS vegetation indices are available on a 16-day resolution, we opted for a monthly mean rather than a temporal composite, to have a more consistent sensing date throughout the dataset.

In addition to the NDVI – a measure for the amount of live green vegetation and, thus, the crop health (Ji and Peters, 2003) – numerous other products exist that reflect the vegetation water status and/or productivity. These include other indices based on optical imagery (e.g., NIRv and EVI) or on microwave data (e.g., VOD). Though each of these different indices might produce slightly different results in this analysis, their application should not affect the fundamentally different response of the soil moisture and vegetation to meteorological drought.

SM and NDVI data were spatially and temporally resampled to the lowest spatiotemporal resolution and shortest time span of both datasets, resulting in data with a monthly 0.25° resolution ranging from 2000 to 2018. These were then cropped to our European study area (11°W–45°E, 35–72°N). On this monthly time scale, we assumed that large-scale patterns in both the soil moisture and vegetation would remain similar, although lags between the surface soil moisture and vegetation patterns were expected due to travel time toward the root zone (Crow et al., 2012a). The main vegetation evolution occurs on a monthly timescale, not on a day-to-day basis, as near-surface soil moisture does. For comparison purposes, the monthly timescale, which is common in drought analyses, is thus more appropriate.

Both the SM and NDVI datasets were then masked to only include grid cells where at least 80% of the area was covered by agricultural activities, to ensure any ambiguity based on land cover was removed from the equation. The 80th percentile was chosen as a trade-off between sufficient agricultural areas and a sufficient number of grid cells in the resulting mask. The 2018 ESA CCI land cover map (ESA, 2017) was used as the basis of the mask. The categories included in the present analysis are rainfed, irrigated, and mosaic cropland and grassland (IDs 10, 11, 12, 20, 30, and 130), resulting in the mask shown in Fig. A6. All of the used datasets have been extensively validated (e.g. Beck et al., 2021; Lahoz et al., 2018; Lange et al., 2017; Navarro et al., 2019; Reinhart et al., 2021); so a validation was not conducted here.

2.2.2 Drought event selection

To study the relation between negative soil moisture and vegetation anomalies, growing seasons where significant precipitation deficits occurred were selected based on the 6 month aggregated SPI (McKee et al., 1993). The SPI6 was computed from the precipitation data contained in our reference period (2000–2018) using a Gamma distribution. The SPI6 in September of each year was compared, as that reflects the integrated precipitation deficit over a typical growing season (Apr–Sep).

A fixed growing season was chosen for the drought event selection, though we are aware that differences exist in the onset of the growing season, when high and low latitudes are compared. This will be accounted for in the discussion of the results. Interconnected grid cells over relatively large areas with a moderate to extreme precipitation deficit (SPI6 < -1, Lloyd-Hughes and Saunders, 2002) were chosen, resulting in the six selected seasons/areas as indicated in Fig. 2.2: the 2002 precipitation deficit over the Baltic states and north-western Russia (Rimkus et al., 2017), the 2005 event on the Iberian Peninsula (Sepulcre-Canto et al., 2012) and the infamous 2003, 2015, and 2018 events over central Europe (Buras et al., 2020; Hanel et al., 2018; Ionita et al., 2017). Due to the large north–south extent of the 2018 event, this event was split into two parts (hereafter referred to as "2018N" and "2018S"). Grid cells in these selected areas were then used for further analysis as discussed below.

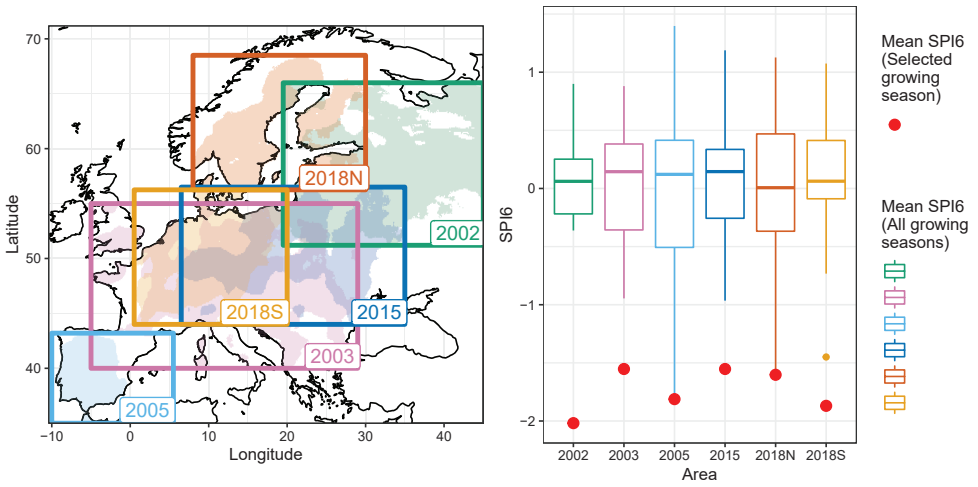

Figure 2.2: Properties of the selected summer droughts. Left: the location and spatial extent, right: SPI6 over the selected growing season (red), compared to the distribution of SPI6 in the remaining growing seasons for the same region.

2.2.3 Analysis

To allow for a fair comparison between anomalies of different variables, and to remove seasonal variations from the drought definition, the data were normalised by subtracting the long-term monthly mean from the SM/NDVI at each time step in a grid-wise manner, and subsequently dividing by the long-term (2000–2018) monthly standard deviation, following Eq. 2.1:

$$z = \frac{X_{ij} - \mu_i}{\sigma_i} \tag{2.1}$$

where X_{ij} is soil moisture in a specific month and year, μ_i and σ_i are the mean and standard deviation in the same month in the reference period. This resulted in z-scores between approximately -3 and $+3$, indicating negative and positive anomalies, respectively. These anomalies can be compared with SPI6 directly.

Other indices, such as the ESSMI for soil moisture data (Carrão et al., 2016), or the VCI for NDVI data (Kogan, 1990), are available and comparable to normalisation; however, a more general approach was adopted here to increase the comparability of two different variables. We recognised anomalies in SM (SMA) and anomalies in NDVI (NDVIA) below -1 as grid cells in soil moisture drought and vegetation drought, respectively, to include moderate, severe, and extreme droughts in the analysis (Lloyd-Hughes and Saunders, 2002). To account for seasonality in the variables, data for each month of the year were taken separately, and grid cells with less than seven data points were removed from the analysis.

After the data normalisation, for agricultural grid cells belonging to each event, the percentage of the selected grid cells in drought was determined for each variable. Then, for each selected grid cell in each event and time step, the Pearson correlation between SMA and NDVIA was quantified. While correlation is useful for an overview of the similarity between two variables, it is not sensitive to bias or scale errors (Brier and Allen, 1951; Murphy and Epstein, 1989). Skill scores, on the other hand, provide a more in-depth and well-rounded view on the use of soil moisture as a predictor for agricultural impact.

As soil moisture indices are often used as a proxy for vegetation drought (e.g. Bolten et al., 2010; Carrão et al., 2016; Martínez-Fernández et al., 2016; Sridhar et al., 2008), predictions using soil moisture drought are implicitly assumed to be skilful. Therefore, the number of Hits (H), Misses (M), Correct Rejections (CR), and False Alarms (FA) were determined for a case where the soil moisture drought (SMA < -1) was used to predict the vegetation drought (NDVIA < -1). These were used to compute five different skill scores, each highlighting a different aspect of the prediction accuracy. First, the Frequency Bias (FB) is given by:

$$\mathrm{FB} = \frac{\mathrm{H} + \mathrm{FA}}{\mathrm{H} + \mathrm{M}} \tag{2.2}$$

and expresses the difference between the mean drought frequencies. Next, the Frequency of Hits (FOH) is a measure of discrimination that shows the fraction of forecasted vegetation droughts that were correct, which is given by:

$$\mathrm{FOH} = \frac{\mathrm{H}}{\mathrm{H} + \mathrm{FA}} \tag{2.3}$$

The Frequency of Misses (FOM) is given by:

$$\mathrm{FOM} = \frac{\mathrm{M}}{\mathrm{H} + \mathrm{M}} \tag{2.4}$$

and expresses the fraction of observed vegetation droughts that are incorrectly forecasted by the soil moisture drought. The Hanssen–Kuipers score (HK) (Hanssen and Kuipers, 1965) measures the ability of the soil moisture drought to discriminate between (or correctly classify) vegetation drought events and non-events:

$$\mathrm{HK} = \frac{\mathrm{H}}{\mathrm{H} + \mathrm{M}} - \frac{\mathrm{FA}}{\mathrm{FA} + \mathrm{CR}}. \tag{2.5}$$

Lastly, the Odds Ratio (OR) (Stephenson, 2000) is used to measure the strength of the association between soil moisture and vegetation drought:

$$\mathrm{OR} = \frac{\mathrm{H} \cdot \mathrm{CR}}{\mathrm{FA} \cdot \mathrm{M}}. \tag{2.6}$$

We refer to Hogan and Mason (2011) for an overview of these skill scores as well as their advantages and disadvantages.

2.3 Results

A general check of the full data time series, including all land cover types, revealed that, during each event, asynchronies between the spatial patterns in the soil moisture and vegetation anomalies were widespread. Fig. 2.3 shows the spread of different drought types during the 2015 growing season and serves as an illustration for these asynchronies, which occur in all green and purple grid cells (See Figs. A1–A5 for other events).

Regionally more humid areas, such as mountain ranges and high latitude regions, can be easily distinguished by their relatively low Pearson correlations between the soil moisture and NDVI anomalies (Fig. A7), in line with our hypothesis where we suggest that low correlations could be found in energy-limited regions, though other factors may play a role in this correlation, such as high local heterogeneity in the topography, soil moisture, and other vegetation types, as compared to the remaining region. Furthermore, correlations

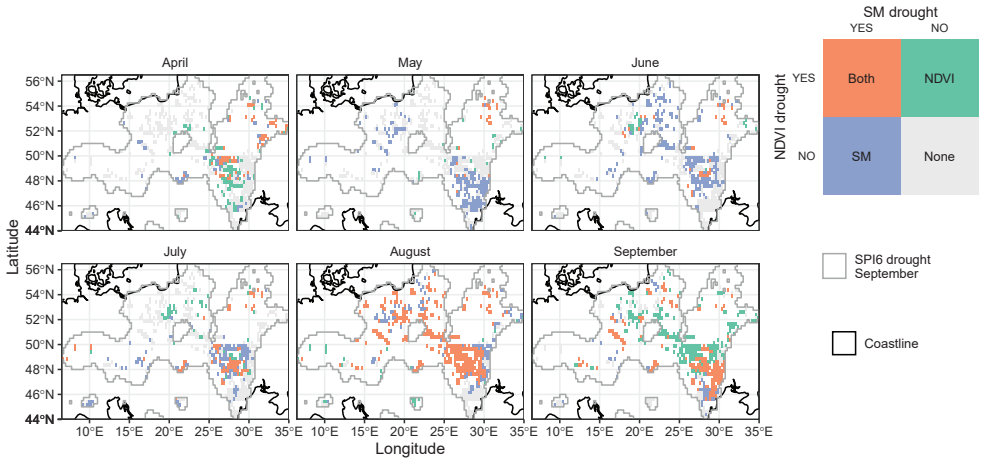

Figure 2.3: Synchrony between the soil moisture and vegetation droughts during the 2015 growing season in the agricultural grid cells. Note the asynchronous development of soil moisture and vegetation drought, with soil moisture drought dominating in May–June, and vegetation in April and September. Similar figures for the other drought events are included in the Appendix (Figs. A1–A5).

between the anomalies were low in April and generally increased toward September; however, in some areas, the correlations peaked in August.

Not all of the six studied events were equally affected by deficits in SM and/or NDVI. A comparison between drought extents using the fractions of the area affected by a soil moisture and/or vegetation drought is provided in Fig. 2.4. The 2002, 2015, and both 2018 events are characterised by a clear overlap between the "NDVI" and "Both" lines, indicating that an area affected by a vegetation drought also has a soil moisture drought. Interestingly, in 2003 and 2005, some vegetation droughts occurred in the absence of a soil moisture drought.

Fig. 2.5 shows the severity of each drought event for both the vegetation and soil moisture and the Pearson correlation between NDVIA and SMA. Asynchrony between the two variables is visible in the irregular shape of the arrows and the deviation of the linear regression from the 1:1 line. Generally, a delay can be distinguished between the negative SMA and NDVIA values. This delay was expected as discussed in Section 2.2.1.

Interestingly, positive anomalies were more common in NDVIA than in SMA, showing that soil moisture droughts do not always negatively affect vegetation, and can sometimes even coincide with the opposite, i.e., positive, impacts in vegetation. High monthly correlations between SMA and NDVIA generally occurred later in the growing season as shown by yellow colours in Fig. 2.5. For example, in the 2002 event, the NDVIA–SMA correlation

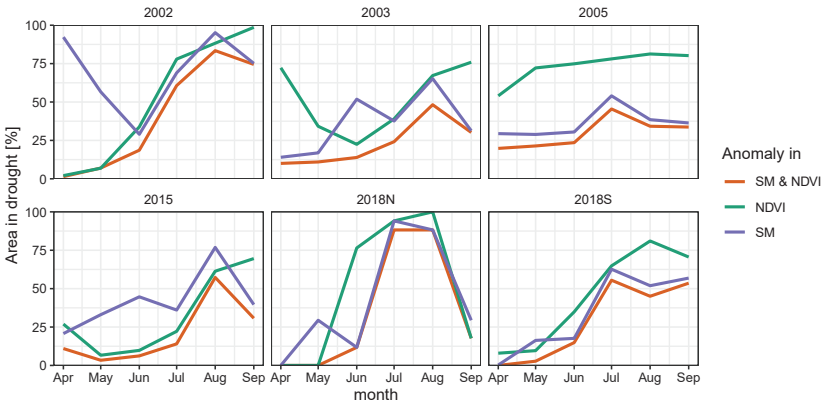

Figure 2.4: The growing season evolution of the percentage of area in soil moisture and/or vegetation drought in the selected agricultural grid cells in each studied meteorological drought event. Panels show the six events, where the vegetation (NDVI, green) and soil moisture (SM, purple) grid cells in drought (defined as an anomaly < -1) are shown separately, as well as the percentage of grid cells affected by droughts in both variables simultaneously (orange).

increased from −0.45 in May to 0.68 in July, and correlations in the 2003 (2005, 2015, 2018N, and 2018S) event peaked in September (Sep, Aug, Sep, and Jul), at 0.51 (0.49, 0.68, 0.77, and 0.71).

Given the clear asynchrony and discrepancy in the soil moisture and vegetation under water-limited conditions, it is relevant to question how well soil moisture-based indices, such as the widely-used SSMI and PDSI, perform when targeting to quantify vegetation drought. The skill scores of the agricultural drought impacts, as reflected in NDVIA < -1 and as predicted using SMA < -1, are shown in Fig. 2.6. From the low density of lines in the parts of the skill score plots shaded green, it is clear that the overall skill was rather low.

Similar to the Pearson correlation, the skill scores generally increased in August. Over-forecasting, i.e., when more droughts were forecasted using soil moisture than there were droughts observed in vegetation, as seen in a FB > 1, generally occurred in the beginning of the growing season, whereas underforecasting (FB < 1) occurred near the end of the growing season. The respective increase and decrease in FOH and FOM show the result of the changing frequency bias.

The HK, showing the accuracy of events minus the accuracy of non-events, was rather stable throughout the growing season although it peaked in the second half as did the OR, which showed the number of correct forecasts. None of the drought events stood out in all of the skill scores. A sensitivity analysis showed that different thresholds for the drought selection and skill scores did not substantially change the results.

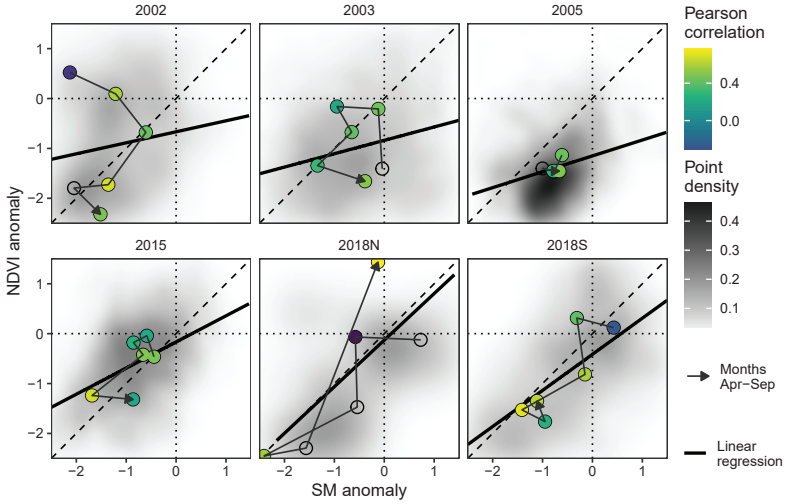

Figure 2.5: The relations between anomalies in the soil moisture (SM) and vegetation (NDVI). Panels show the six drought events, with both soil moisture and vegetation drought defined when the anomaly < -1. The point density in the background indicates the number of grid cells with a certain combination of anomalies in soil moisture and vegetation. The centroids of each month are chronologically connected with an arrow and shaded by the Pearson correlation in that month if $p \leq 0.05$.

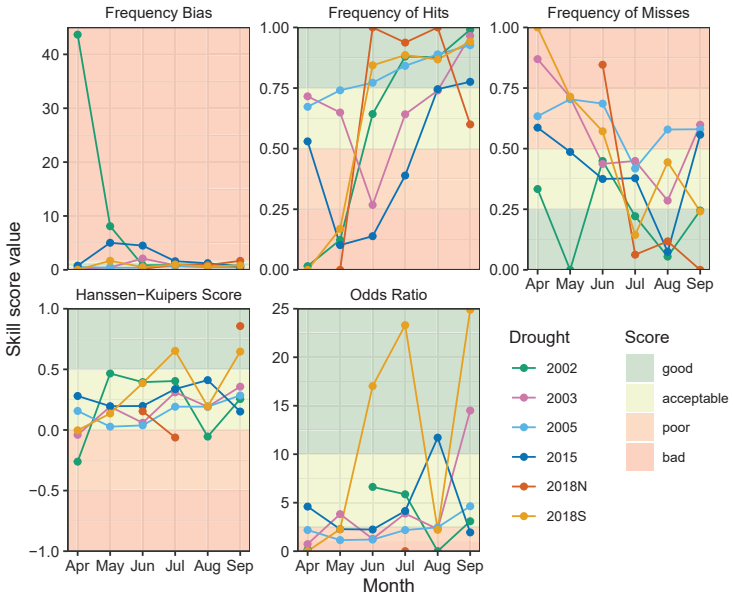

Figure 2.6: Skill scores for the soil moisture drought as a proxy for vegetation drought. The background colours indicate the quality of the skill scores (see Section 2.2.3 for their description), and the lines show different drought events.

2.4 Discussion

2.4.1 Soil moisture regimes

Our results showed that, in some cases, most notably during the 2003 and 2005 meteorological droughts, vegetation growth was not obviously limited by the current water content but possibly by other factors, such as the energy, heat stress, antecedent low soil moisture conditions, or pests and diseases. Since these events were located further south than most other selected events, energy limitations could be ruled out. Heat stress could well have been the limiting factor for vegetation, as well as antecedent soil moisture (Figs. A8–A11).

Additionally, we showed, using a correlation analysis, that a general pattern in which NDVI remains largely unaffected by small anomalies in the SM content when vegetation is energy limited as is often the case at the start of the growing season. Under water-limited conditions, which are more likely to occur near the end of the growing season, higher correlations were found, consistent with the results of Jolly et al. (2005). The southernmost 2005 event is the only event in which correlations peaked early in the season, which can be related to the water-limited conditions that are likely to occur earlier in the Mediterranean than in the geographic locations of the other events.

The extremely low correlations in the beginning of the 2002 event might also have been caused by the low temperatures that can occur early in the year in these latitudes, under which soil moisture estimates are highly uncertain (Scanlon et al., 2020; van der Vliet et al., 2020), and the growing season might not have started. Finally, the skill scores were generally found to improve in the second half of the growing season; however, we expect the usefulness of end-of-season NDVIA prediction to be limited for agricultural purposes. These results do confirm our hypothesis that there is a more direct link between the soil moisture and vegetation state under water-limited conditions, i.e., when the available water content is below the critical soil moisture, although this is only the case at the end of summer, instead of solely being related to geographical location.

2.4.2 Data

The complexity of agricultural droughts is not a local or regional issue but a global one and, thus, should be considered that way. While this study was performed over the European continent, it covers a range of climates found around the globe, from arid regions in the Mediterranean to boreal regions in northern Scandinavia. It is therefore expected that the behaviour will be similarly asynchronous in other regions. The limitations of this approach are on a local scale, rather than a global scale, due to the low spatial resolution of the analysis. Even though each dataset was carefully selected based on the length, spatial resolution, and validation results over Europe, resulting in a selection of datasets

best suited for this analysis, uncertainties are inherent to any type of data, and the results should, therefore, be interpreted with care.

In complex landscapes, high-resolution information can sometimes reveal a range of anomalies, even containing contrasting signs that are not visible at a coarser scale (Buitink et al., 2019). The normalising of the soil moisture data in this study can be criticised, because soil moisture data can show bimodality (Teuling et al., 2005; Vilasa et al., 2017). In addition, a dataset length of 18 years can be considered short when compared to the traditional 30-year reference period as recommended by the WMO (WMO, 2017).

On the other hand, uncertainties due to areal properties are decreased, because the grid cell values are compared to other values of the exact same grid cell, while the resulting anomalies can easily be compared to other grid cell values. This, next to the possibility to fairly compare different variables, led to the decision to use a standard normalisation for both the vegetation and soil moisture data, regardless of the method's limitations.

In this research, we used available long-term satellite records of soil moisture and NDVI. Whereas current satellite soil moisture products are limited to the soil surface, a soil moisture drought assessment is ideally based on observations over the entire root zone. However, such observations are currently only available in several regional-scale observation networks (Mittelbach et al., 2011). By opting for surface soil moisture estimates rather than root zone soil moisture data, we performed this study using observations only.

On the other hand, the asynchrony between the surface soil moisture and vegetation index is likely larger than the asynchrony between the root zone soil moisture and vegetation, and thus asynchronies found here might be overestimated. For that reason, a skill score analysis was performed with a one month lag in the surface soil moisture (to account for the travel time to the root zone), which did not show large differences compared to the analysis presented in this paper (Fig. A12).

2.4.3 Separating soil moisture and vegetation droughts

The inherently complex and nonlinear relation between soil moisture and vegetation status has important implications for drought monitoring where a distinction is traditionally made between meteorological, agricultural, and hydrological drought events. Though it might seem to be a logical step, based on our results, to redefine agricultural droughts from the traditional definition as a soil moisture drought, to be identical to vegetation droughts, this would disregard any information contained in the soil moisture anomalies.

For instance, it would be unclear whether any negative vegetation anomalies are caused by water stress, or by other factors, such as diseases or heat stress. We, therefore, argue that a distinction is necessary between soil moisture drought (reflecting water status) and vegetation drought (reflecting the impact of the drought on vegetation). This is particularly true when evaluating droughts across climate zones. The distinction between

soil moisture drought and vegetation drought is important because shorter soil moisture droughts can even have a positive rather than negative impact on productivity, thus, risking the misclassification of drought events and false drought alarms.

2.5 Conclusions and outlook

Agricultural droughts are generally quantified using anomalies in soil moisture; however, our results show that a clear asynchrony and discrepancies existed between the surface soil moisture drought and the impact of these droughts on vegetation. Occasionally, soil moisture droughts even coincided with positive anomalies in the vegetation. In some of the studied events, a vegetation drought could not be attributed to a soil moisture drought alone.

While the asynchrony of soil moisture and vegetation droughts is not a novel finding (e.g. Crow et al., 2012a), the term agricultural drought is still being used as a synonym for soil moisture drought (e.g. Chakrabarti et al., 2014; Hao and AghaKouchak, 2013; Martínez-Fernández et al., 2015; Martínez-Fernández et al., 2016; Sridhar et al., 2008). To overcome this duality in the definition of agricultural droughts and to prevent false drought alarms, drought monitoring and prediction may benefit from a move away from the combined term *agricultural drought* (which can lead to confusion between soil moisture and vegetation effects) toward two separate terms: soil moisture drought and vegetation drought, each with their own indices and use in drought monitoring and forecasting.


3

Chapter 3

Optimal soil moisture retrieval with native resolution data

This chapter is based on:

T. C. van Hateren, M. Chini, P. Matgen, L. Pulvirenti, N. Pierdicca, and A. J. Teuling (2023c). 'On the Use of Native Resolution Backscatter Intensity Data for Soil Moisture Retrieval'. IEEE Geoscience and Remote Sensing Letters 20, 1. doi: 10.1109/LGRS.2023.3264732

Abstract

The accuracy of soil moisture estimated from Synthetic Aperture Radar backscatter data at high resolution is limited by speckle. Common practice to mitigate speckle is to multilook the data prior to retrieving soil moisture. While multilooking indeed reduces speckle, it also decreases the spatial resolution and removes possibly useful high resolution information from the data. We therefore hypothesised that using higher resolution backscatter data for soil moisture retrieval would lead to higher retrieval accuracies. A high-resolution field study combined with a synthetic experiment showed that calculating soil moisture prior to multilooking to the final target resolution (calculate-then-average, CtA) has substantial advantages over the average-then-calculate (AtC) approach. Currently, the AtC strategy is most often applied in soil moisture studies, mainly due to its computational advantage compared to the CtA approach. We show that by making use of a higher source resolution backscatter data than the target resolution, we could improve the soil moisture retrieval over an agricultural field.

3.1 Introduction

Soil moisture strongly influences meteorology, climate and hydrology via its direct impact on evapotranspiration (Seneviratne et al., 2010). Soil moisture conditions influence drought events (van Loon, 2015) and flash flood magnitude (Grillakis et al., 2016). Observations of soil moisture are therefore imperative to monitoring and predicting extreme hydrological events. Unfortunately, large scale in situ soil moisture observations are scarce, because they are labour-intensive and made at point scale. Large scale soil moisture observations are thus best made using satellites (Brocca et al., 2017; Li et al., 2021) equipped with an instrument like an optical sensor, radiometer, scatterometer, or Synthetic Aperture Radar (SAR).

Space-borne SAR sensors emit microwaves and measure the fraction of radiation scattered back by the Earth's surface. This backscatter intensity can be used to retrieve soil moisture with a forward model. ESA's Sentinel-1 constellation currently provides high spatiotemporal resolution SAR data with a ground-range resolution of 20 m and a six day revisit time until the failure of the B satellite in December 2021. At these high spatial resolutions, SAR backscatter accuracy is limited by speckle that is inherent to the data. Speckle causes variations in the backscatter intensity that do not necessarily relate to variations in soil moisture. Multilooking the data reduces the speckle and for that reason, soil moisture products are often presented at relatively low resolutions (500–1000 m) (Bauer-Marschallinger et al., 2019; Pulvirenti et al., 2018; Zappa et al., 2021).

Multilooking is generally performed on the backscatter data (e.g. Das et al., 2019), rather than multilooking soil moisture data after its inversion (e.g. Balenzano et al., 2021). This choice has the advantage of higher computational efficiency. However, applying a multilook means assuming that the mean of the surrounding pixels is equal to the central pixel of interest (Mansourpour et al., 2006). This assumption does not hold when there is a significant spatial variability in soil moisture or other soil parameters that influence backscatter intensity (Teuling and Troch, 2005). Over such heterogeneous surfaces, multilooking of the backscatter not only averages speckle and soil moisture conditions, but also other types of information that are contained in the backscatter signal (land cover, vegetation water content, roughness), and in turn, they cannot be easily removed from the signal as the information on individual pixels is now lost.

Ma et al. (2020) have briefly compared the use of high resolution backscatter data to the use of multilooked backscatter data for soil moisture estimation. Two strategies were applied and compared (Fig. 3.1): the Average-then-Calculate (AtC) strategy and the Calculate-then-Average (CtA) strategy. The AtC strategy consists of multilooking backscatter data to the target resolution and then converting it to soil moisture, whereas the CtA strategy consists of computing soil moisture from high resolution backscatter data, and then multilooking it to the target resolution. Ma et al. (2020) found that the CtA strategy showed

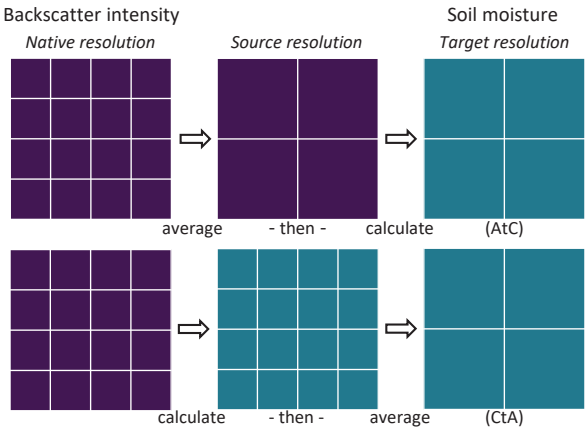

Figure 3.1: An illustration of the terms used in this manuscript: the average-then-calculate (top) and calculate-then-average (bottom) strategies, and native, source and target resolution. Purple represents backscatter intensity, and blue represents soil moisture.

significantly better results than the AtC strategy, at a spatial resolution of about 125,000 m. In a related study, Satalino et al. (2004) use a synthetic dataset to show that increased accuracy of the CtA strategy occurs especially when model errors are expected to be large. To the best of our knowledge, the difference between the two aggregation strategies has not been tested on a sub-field scale, even though the processes underlying the effects of multilooking (e.g. heterogeneity) change with changing spatial resolution. The strategies have also not yet been tested with in situ soil moisture data.

We hypothesise that a substantial loss of information occurs in the AtC strategy compared to the CtA strategy. Hence, reducing the spatial source resolution (i.e. resolution of data going into the retrieval algorithm) to mitigate the speckle, especially at high target resolutions, can negatively impact soil moisture retrieval accuracy. To test this hypothesis, we performed a synthetic experiment with increasing variation in soil moisture content and roughness and applied the two strategies on these data. The experiment was duplicated using in situ data to determine whether the results from the synthetic experiment could be confirmed in a field in southeastern Luxembourg.

3.2 Data and methods

3.2.1 In situ soil moisture data

We focused our study on a non-irrigated agricultural field (~110 by 250 m) in South-eastern Luxembourg (Fig. 3.2). Luxembourg is located in Central Western Europe and marked by its moderate climate. The field's soil can be classified as a moderately gleyic clay on

a calcareous substrate, according to the Luxembourgish Geoportal. Their high spatial resolution elevation data shows a slight slope in the field from the northern to the southern corner (~9 m elevation difference, Fig. B1).

In situ SM data were gathered in the field between March 2020 and June 2021 (with a gap in between April and September 2020, Fig. 4.1), on all days coinciding with S1 overpasses and under varying SM and weather conditions. On each campaign day, five SM measurements were taken at each location on a 12×6 grid, with a grid spacing of approximately 20 meters (Fig. 3.2). SM was measured with a FieldScout Time Domain Reflectivity (TDR) 350 with 3.8 cm metal pins. These short pins were used to have a similarly superficial measurement depth as the S1 retrieved SM estimates. Prior to the analyses, the five TDR measurements at each sampling location were averaged to obtain a single value per location. Additionally, on some of the field days, 12 volumetric soil samples were taken at random TDR sampling locations. The soil samples were then weighed, oven-dried for 24 hours, and weighed again to determine the soil bulk density and the SM. These SM values were used to calibrate the TDR measurements (Fig. 3.3). A linear relationship existed between the two measurement types, so that a linear transformation could be applied to all raw TDR data: $TDR = 0.098 + 0.97 \cdot rawTDR$. The analyses described here were performed with these calibrated TDR data.

Finally, on field days, vegetation height was determined at various locations in the field to be compared with NDVI data. No roughness measurements were performed.

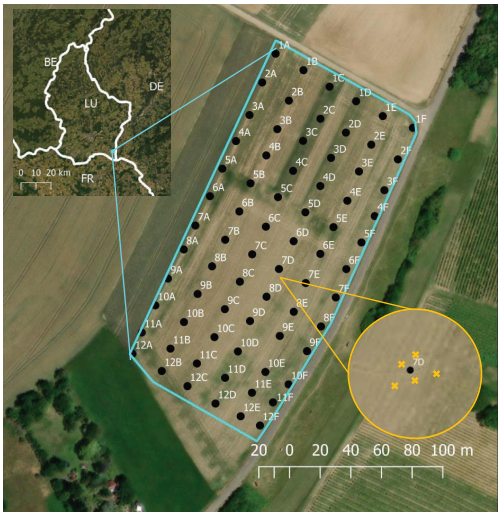

Figure 3.2: Location of the study area and the sampling points for the reference dataset (centre at 6.31774°E, 49.51109°N). At each of the 72 sampling points, five TDR measurements were taken, of which an example lay-out is given in the circular inset. In total, 360 TDR measurements were thus taken per measurement day.

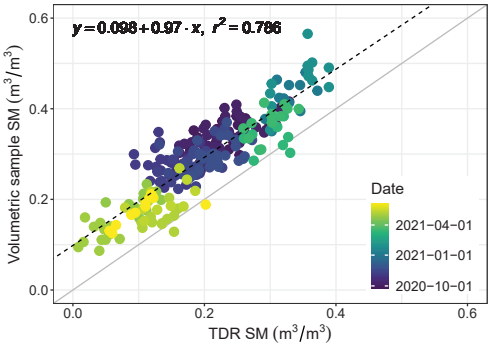

Figure 3.3: A comparison of the two in situ measurement approaches. The x-axis shows the SM content as measured by the TDR device, and the y-axis the SM content as derived from the soil samples. The dashed line shows the linear regression model and the solid line follows the 1:1 line.

3.2.2 Satellite soil moisture data

Satellite soil moisture was retrieved from descending S1 Interferometric Wide swath (IW) ground-range detected (GRD) backscatter intensity (σ^0) data. The data were preprocessed with ENVI SARscape. The precise orbit files were applied, thermal noise was removed, and data were radiometrically calibrated, multi-looked (4 pixels in the range direction) and geocoded using the Shuttle Radar Topography Mission (SRTM) Digital Elevation Model (DEM) on the WGS 84 / UTM zone 32N coordinate system to finally obtain a square pixel of 20×20 m^2. The Local Incidence Angle (LIA) and the slope over the study area were also extracted using the SARscape tool. Soil moisture data were then retrieved using the MUltitemporal LEast Square Moisture Estimator (MULESME) algorithm (Pulvirenti et al., 2018), a multitemporal physically-based algorithm.

MULESME has been evaluated previously and has been shown to accurately estimate SM on a pixel-by-pixel basis (Pulvirenti et al., 2018). The inversion of SM content and surface roughness is performed in each pixel using an least-square-errors approach. The algorithm assumes that SM content changes considerably faster than surface roughness, and in doing so reduces the ill-posedness of the soil moisture retrieval problem (Pierdicca et al., 2014). If only one image was used, there would be two unknown values (soil moisture and roughness) and one known value (backscatter) per pixel. By using five images over a period with constant roughness, the number of knowns increases to five, but the number of unknowns only increases to six. Over shorter periods, the constant roughness assumption is more likely to be valid. Over longer periods, the estimation accuracy is higher but computation time increases dramatically. The use of five images is thus a compromise between accuracy and efficiency (Pierdicca et al., 2014). For more information on the algorithm and its underlying theory, we refer to Pierdicca et al. (2014) and Pulvirenti et al. (2018).

In comparison to other retrieval algorithms, the first advantage of the MULESME algorithm is that it is versatile in its application since it can be run at a varying spatial resolution "on demand". Secondly, the algorithm does not require a calibration for every pixel since the underlying empirical equations have been calibrated. This pixel-by-pixel calibration is required for other methods relying on the availability of a long record of backscatter data (Bauer-Marschallinger et al., 2019). Thirdly, MULESME implements a multitemporal approach which enables us to mitigate the uncertainty caused by roughness.

The MULESME algorithm first resamples all input data (LIA, σ^0, NDVI, slope, land cover) to the specified spatial resolution. Then, each σ^0 pixel is corrected for the influence of vegetation. Any σ^0 values higher than −2 dB or lower than −18 dB after vegetation correction are masked out, since these values lie outside of the range of backscatter values under which soil moisture can be accurately retrieved (Pulvirenti et al., 2018). SM and surface roughness are finally inverted, making use of a Look Up Table (LUT) that contains 7956 unique combinations of backscatter, SM, roughness and LIA based on the Oh forward model using a least-squares minimisation approach. The use of a LUT is considerably faster than computing the forward model repeatedly (Pulvirenti et al., 2018).

One MULESME run finally results in five S1 SM maps, and a unique roughness map. The algorithm was run with a temporally moving window of five σ^0 images: for each new run, one new σ^0 image was added and the eldest one was removed from the computation (Fig. 3.4).

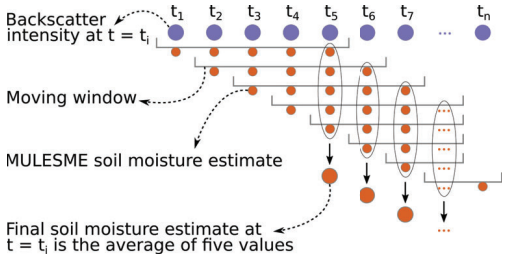

Figure 3.4: Graphical illustration of the moving window approach

3.2.3 Field experiment

For the field experiment, SM maps were retrieved with MULESME from backscatter intensity data at six different resolutions (20, 40, 60, 80, 100, and 120 m) following the two strategies depicted in Fig. 3.1. For both strategies, backscatter images were preprocessed to a square 20 m pixel. For the AtC strategy, these images were then multilooked into the five lower resolutions, and finally the SM was retrieved for all six resolutions. Alternatively, for the CtA strategy, the SM was retrieved at the 20 m resolution, and subsequently multilooked into the different target resolutions.

Table 3.1: Data variability in the three synthetic experiments

	Exp.	1	2	3
SM	Space	constant	varying	varying
	Time	varying	varying	varying
Roughness	Space	constant	constant	varying
	Time	constant	constant	constant
Speckle	Space	varying	varying	varying
	Time	varying	varying	varying

3.2.4 Synthetic experiments

Three synthetic experiments with increasing data variability were set up to study how the computation strategy impacts SM retrieval accuracy. A square region of 18×18 km (or 360,000 pixels at a 20 m resolution) was used for the synthetic experiments. Synthetic data for the experiments consisted of 15 days of soil moisture, roughness, NDVI, land cover, LIA and backscatter intensity data. In all three experiments, speckle was added to the synthetic backscatter data, since speckle is inherent to SAR data and does not contain relevant information for the soil moisture retrieval. SM and roughness were varied in time and/or space as presented in Table 3.1. In experiment 1, SM varied only in time and roughness was constant in time and space. Any multilooking therefore only removed speckle, and no information on SM or roughness was lost. In experiment 2, spatial SM variation was added, so that during multilooking some information on SM was lost since the resulting aggregated backscatter is an average of different values of SM. In experiment 3, roughness also varied in space, thereby losing even more information during the multilooking. The synthetic data were used as input data for the MULESME algorithm and processed according to the two different strategies as outlined in Section 3.2.3.

Synthetic data were sampled from either a normal or a uniform distribution, with their parameters derived from in situ (Section 3.2.1) and satellite (Section 3.2.3) field data. Both sets of experiments (i.e. "normal" and "uniform") were performed, because using a uniform distribution leads to increased spatial variability in soil moisture compared to the normal distribution. However, the uniform distribution is less comparable to a ground truth scenario, where neighbouring soil moisture pixel values are usually similar. Hence, the results from the "normal" analysis were compared to the in situ data, and the results from the "uniform" analysis were used to demonstrate a more extreme case. Since random sampling was used, the entire experiment was carried out 15 times with different random values to reduce the chance that the presented results are merely the result of a stochastic artefact. The random sampling is described for every variable in the following subsections.

Soil moisture

For the synthetic SM dataset based on normal distributions, data were sampled from two truncated normal distributions, one for the temporal and one for the spatial variation. The mean of both distributions was set to the spatiotemporal average of the S1 retrieved SM data over the studied field (i.e. 0.19 m^3m^{-3}) and the distribution was truncated at the 5^{th} and 95^{th} percentile of the S1 retrieved SM data (i.e. 0.08 and 0.29 m^3m^{-3}). The standard deviation for the spatial variation was taken to be the same as the spatial standard deviation in the in situ SM data, and for the temporal variation it was taken to be the same as the temporal standard deviation in the in situ SM data. For the uniform distributions, the lower and upper limits were set to the same as for the normal distribution: 0.08 m^3m^{-3} and 0.29 m^3m^{-3}.

Roughness

In the experiments with a constant value for roughness, the spatiotemporal field average roughness was taken from the MULESME runs that were performed for the field study (1.2 cm). In the case of spatially variable roughness, the data were sampled from a normal distribution, based on the same mean, and supplemented with the standard deviation (0.48 cm) and 5^{th} and 95^{th} percentiles (0.50, 3.8 cm) of the MULESME output. For the uniform distribution, the same percentiles were used as lower and upper limits, respectively.

NDVI, land cover and LIA

The synthetic NDVI, land cover and LIA data were set to be constant in both space and time. NDVI was set at 0.15 to mimic near-bare soil conditions, optimal for soil moisture retrieval. The land cover was set to class 211 (non-irrigated arable land in Corine Land Cover (CLC)), which is the same classification as the field in the in situ study. LIA was set to the field average from the 37 orbit (33.5°).

Backscatter intensity

The Oh forward model was then used to infer synthetic VV and VH backscatter from the sampled values of SM, roughness, and LIA. Noise was added to all three experiments, based on the noise in the real S1 backscatter data over the field. By inferring the noise from real data, we accounted not only for speckle multiplicative noise, but also for thermal noise (Palmisano et al., 2021).

Noise was added to the synthetic data by multiplying the synthetic linear backscatter at 20 m resolution by a random sample from a truncated normal distribution with a mean of one and a minimum of zero. The standard deviation of the distribution was derived from backscatter data over pixels that showed homogeneous soil moisture conditions: in that

case, any remaining variation in backscatter is most likely caused by speckle. Homogeneous pixels were identified by first selecting days where in situ SM data had a spatial standard deviation lower than 0.03 m^3m^{-3}. Second, the 30% pixels where the in situ SM was closest to the field average were selected. Satellite backscatter was then extracted over the selected pixels and their spatial standard deviation was computed. Finally, the median of these standard deviations was used as the standard deviation of the speckle distribution.

3.2.5 Analysis

For both the synthetic and the field experiment, two performance metrics were used to compare observed and retrieved soil moisture: the Pearson correlation (r), and the unbiased Root Mean Square Error (ubRMSE) (Entekhabi et al., 2010). The analysis was performed for both retrieval strategies.

In the results section, r is not shown for the "uniform" synthetic data. In those cases, when moving to lower spatial resolutions, the soil moisture values in the field converge towards the mean of the uniform distribution. Hence, variation in the data decreases with coarser resolutions and the resulting r cannot be fairly compared between different resolutions.

3.3 Results and discussion

The analysis performed on the "normal" synthetic data (Fig. 3.5a, top two rows) shows that for all source resolutions and experiments, r increases and ubRMSE decreases with a coarser target resolution. Differences in performance were found in the results of the two computation strategies CtA (circles) and AtC (triangles). For every target resolution, the CtA strategy outperforms the AtC strategy. This indicates that retrieving soil moisture at fine resolutions prior to multilooking results in higher retrieval performance at both fine and coarse target resolutions. The CtA performance is especially good when the difference between source resolution and target resolution increases, and peaks at the lowest target resolution.

When moving from experiment 1 to 3, i.e. with increasing spatial variability in the data, the performance variations between the different source resolutions grow (Fig. 3.6). A general decrease in performance is visible, especially in r. The difference between performance of the two strategies also increases. In experiment 1, no spatial variation in soil moisture and roughness was simulated. We hypothesised that under these conditions, the difference between the performance of the two strategies would be minimal as any spatial variation in backscatter is only due to speckle, and multilooking to mitigate speckle thus indeed only reduces speckle without losing any other type of information. The results confirm our hypothesis, with small but consistent differences in performance between different resolutions and between the AtC and CtA strategies. In experiment 2, where spatial variation in

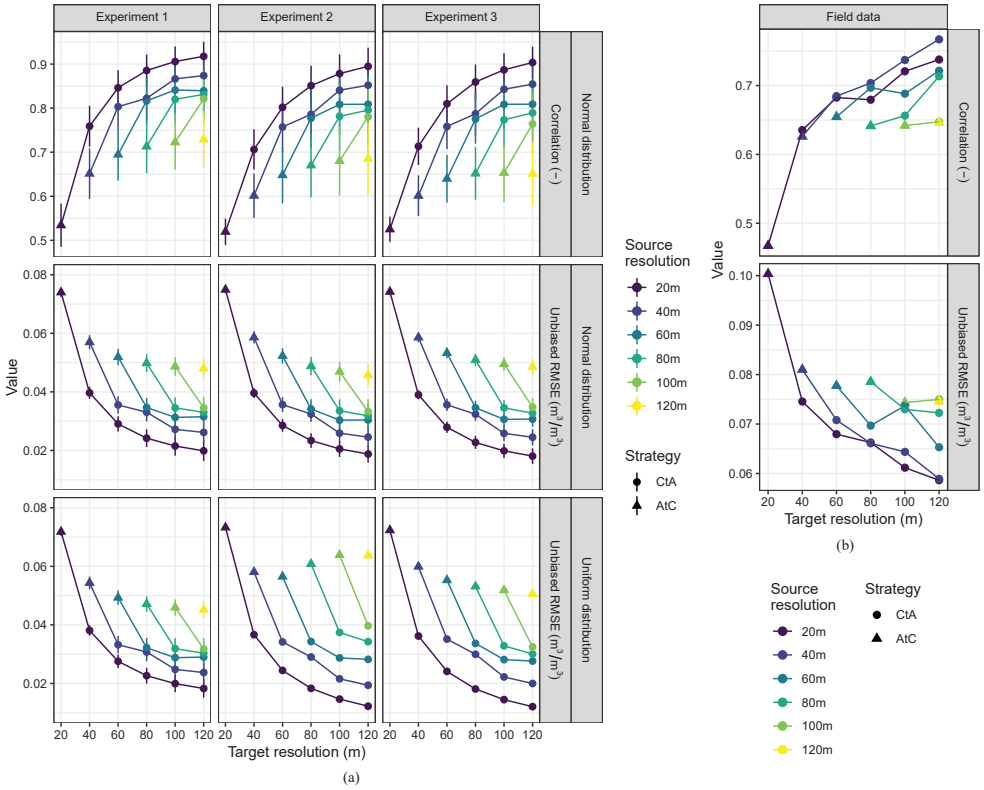

Figure 3.5: Resolution- and strategy-dependent accuracy of soil moisture retrieval performance. (a) shows the mean results and their 95% confidence interval of the 15 synthetic experiments with a normal distribution in the top two rows and of the 15 synthetic experiments with a uniform distribution in the bottom row; (b) shows the results of the two different strategies applied on the field data. In panels where confidence intervals are not visible, their lines are smaller than the diameter of the circles.

SM was added, the performance metrics deteriorated compared to experiment 1. Furthermore, the difference between the two strategies as well as the difference between the six source resolutions increased. In this second experiment, multilooking not only averages the speckle but also different values of SM. This trend continued when spatial variation in soil roughness was added to the simulation in experiment 3: the difference in performance further increased, as hypothesised.

Even stronger patterns were found in the "uniform" synthetic data (Fig. 3.5a, bottom rows). Again, for all source resolutions and experiments, ubRMSE decreases with coarser target resolution, and for each target resolution, the best performance is found for data with high source resolutions. In comparison with the normal distribution, the performance differ-

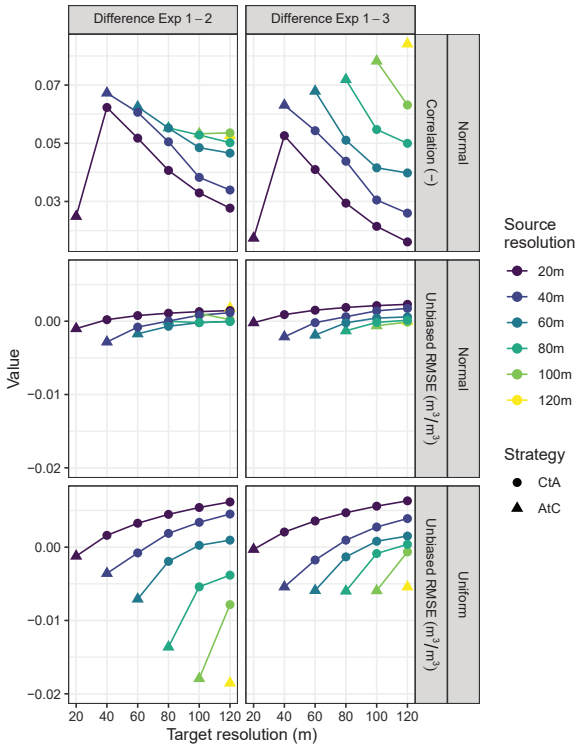

Figure 3.6: Impact of increasing spatial variation in the different synthetic experiments. Differences between results from synthetic experiments 1 and 2 are shown in the left panels and between 1 and 3 in the right panels, with a normal distribution in the top two rows and a uniform distribution in the bottom row.

ences between the two strategies are larger, as well as the performance differences between the first two experiments. Interestingly though, the difference between the first and third experiment is smaller than the difference between the first and second experiment, contrary to the experiments based on synthetic data with a normal distribution (Fig. 3.6).

In this idealised synthetic scenario, it is possible that speckle has a smaller effect on the results than in a field experiment. An analysis based on the field experiment (Fig. 3.5b) confirms this. However, the patterns found in the synthetic data are still visible in the field experiment data. The best SM accuracy on any target resolution is obtained when the calculation is performed with backscatter data with a finer source resolution. At the same time, this does not mean that at any target resolution, the highest possible source resolution should be used: at resolutions of 80 m or lower, the data with a 40 m source resolution shows better performance than data with a 20 m resolution. This could indicate that at 20 m resolutions, the soil moisture signal in the backscatter data was still too

weak compared to the speckle to produce consistent soil moisture estimates over the field, and a performance improvement at lower target resolutions was possible by aggregating the source data to 40 m before calculating soil moisture. At high target resolutions (20 or 40 m), using the highest possible source resolution remains the best choice.

In summary, the results from the synthetic and field experiments confirm our hypothesis: the CtA strategy leads to better retrieval performance than the AtC strategy. Moreover, we saw that in general, when more information is contained in the backscatter data, more information is lost in multilooking and the resulting performance difference between the two computation strategies increases. The exception to this was found in data derived from uniform distributions. In those data the CtA–AtC performance difference was more pronounced in experiment 2 than in experiment 3, indicating that the added spatial variation in roughness does not have as big of an impact on the results as the added spatial variation in soil moisture content, although it could also have been caused by the numerical set-up of the synthetic experiment.

3.4 Conclusions

We performed a synthetic experiment using Sentinel-1 C-band SAR data to test the performance of two retrieval strategies: calculate-then-average (CtA) and average-then-calculate (AtC). We hypothesised that the AtC strategy leads to the loss of important information on soil moisture conditions, which would mean that applying the CtA strategy would lead to higher accuracies over the area of interest. Our results showed that, indeed, applying the CtA strategy to native resolution (20 m) Sentinel-1 data led to a smaller ubRMSE and a higher r on all tested target resolutions (20–120 m). The results from the synthetic experiment were confirmed in a 2.5 ha field in Southeastern Luxembourg that was intensively sampled for in situ soil moisture conditions. Since in both the synthetic and the field experiment an increase in performance was found even at small resolution gaps between source and target data, we expect that the presented results are also relevant for coarser resolutions and for soil moisture applications on larger scales.


4

Chapter 4

Soil moisture monitoring on the sub-field scale

This chapter is based on:

T. C. van Hateren, M. Chini, P. Matgen, L. Pulvirenti, N. Pierdicca, and A. J. Teuling (2023a). 'On the potential of Sentinel-1 for sub-field scale soil moisture monitoring'. International Journal of Applied Earth Observation and Geoinformation 120, 103342. doi: 10.1016/j.jag.2023.103342

Abstract

Soil moisture datasets at high spatial resolutions are beneficial for a wide range of applications, such as monitoring and prediction of hydrological extremes, numerical weather prediction, and precision agriculture. For large scale applications in particular, remotely sensed soil moisture has advantages over in situ data because it provides gridded estimates and because it is less labour-intensive. However, until present, active microwave SM data have not been presented at their native spatial resolution, since the quality of these data is limited by speckle. We explored the potential and limits of high spatial resolution of active microwave soil moisture observations. We used a Sentinel-1 C-band SAR soil moisture dataset at six spatial resolutions ranging from 20 to 120 m. This was compared to a closely spaced (20 m) in situ dataset collected on a non-irrigated agricultural field (~2.5 ha) in the Southeast of Luxembourg. A comparison of the field and satellite datasets demonstrated how Sentinel-1 data with a high spatial resolution can be used to quantify temporal within-field soil moisture variability. Soil moisture was accurately estimated at spatial resolutions of 60 m and coarser, where the temporal correlation was found to be 0.67 and sub-field variations in soil moisture were still detected. Spatial correlation was limited by the absence of soil moisture variability within the field. These results indicate that high spatial resolution soil moisture estimates from Sentinel-1 data can be valuable for monitoring temporal soil moisture variations within agricultural fields.

4.1 Introduction

Soil moisture (SM) is an important variable in the water cycle as it controls the exchange of both water and energy between the land surface and the atmosphere (Seneviratne et al., 2010; Vereecken et al., 2014), in particular during droughts and heatwaves (Miralles et al., 2019; Teuling, 2018). SM observations at high spatiotemporal resolutions can improve numerical weather prediction (Lagasio et al., 2019a; Lagasio et al., 2019b), serve applications such as precision agriculture (Vereecken et al., 2014), and enhance monitoring and prediction of hydro-meteorological disasters (Bierkens et al., 2015; Peng et al., 2021; Vergopolan et al., 2021; Wood et al., 2011).

In situ SM observations, though accurate, are still scarce because of costs and time involved in acquisition, installation, and maintenance of sensors. Furthermore, observations are effectively made at point scale and thus lack spatial representativeness and spatial coverage (Babaeian et al., 2019; Crow et al., 2012b; Peng et al., 2021; Seneviratne et al., 2010; Teuling et al., 2006b). Remotely sensed SM products, on the other hand, are less labour intensive and provide a gridded estimate of SM with a large spatial coverage. Consequently, these data can be assimilated in hydro-meteorological models directly (Hostache et al., 2020).

Several global or continental gridded SM datasets are currently available (Peng et al., 2021), such as ESA CCI soil moisture (Gruber et al., 2020), NASA USDA Global Soil Moisture Data, and Copernicus Global Land service Surface Soil Moisture (CSM). These open data can be very useful for modelling studies thanks to their large-scale coverage. However, their spatial resolutions (0.25°, 0.25°, 1km, respectively) do not yet allow for SM monitoring at the scale of individual fields or even at the sub-field scale that is most relevant for (precision) agriculture.

SM can be observed at sub-field scales with the use of active microwave data, as provided for instance by the S1 satellites. Active microwave sensing has the benefits of a high native spatial resolution, and can be performed day and night and under all weather conditions (Babaeian et al., 2019). On the other hand, SM retrieval accuracy is hampered by uncertainties caused by speckle, surface roughness, the presence of vegetation, water bodies, and frozen soils. These uncertainties have to be accounted for in the SM retrieval and might limit the effective spatial resolution at which SM can be inferred.

An integral part of any SM retrieval is the forward model that predicts the backscatter for given surface conditions. Multiple forward models exist, such as the physical Advanced Integral Equation Model (Fung et al., 1992), the Water Cloud Model (Attema and Ulaby, 1978), and the semi-empirical Oh model (Oh, 2004). The Oh model has been applied successfully in many SM retrieval studies (e.g. Choker et al., 2017; Ezzahar et al., 2020; Pulvirenti et al., 2018; Wang et al., 2018). Retrieval algorithms are even more numerous, with different underlying methods to account for uncertainties, such as change detection

(e.g. Balenzano et al., 2011; Bauer-Marschallinger et al., 2019; Wagner et al., 1999), artificial neural network (Del Frate et al., 2003; El Hajj et al., 2017; Elshorbagy and Parasuraman, 2008; Hachani et al., 2019), or multiple least squares (Kim et al., 2014; Mattia et al., 2009; Pierdicca et al., 2014; Zhu et al., 2019) methods.

In addition to the retrieval process, evaluating the accuracy of SM retrievals with high spatial resolutions poses it own challenges (Gruber et al., 2020). Since in situ SM data lack spatial representativeness, the reference in situ point dataset must be of sufficient spatial density (i.e. small spacing, Western and Bloschl, 1999) and account for sampling uncertainty. Big efforts have been made to monitor SM and to make these datasets publicly available, such as in the International Soil Moisture Network (ISMN) (Dorigo et al., 2021) or during numerous ground validation experiments (SGP97, NAFE'06, SMAPVEX12, 16, SMAP Cal/Val, Colliander et al., 2017; Colliander et al., 2019; Colliander et al., 2015). Unfortunately, currently available in situ datasets like these do not have sufficiently small spacing and/or their measurement period does not overlap with S1 acquisitions. Dedicated field experiments using robust and intensive spatiotemporal sampling are required for a fair analysis of a satellite dataset on multiple high spatial resolutions: the pixel-average in situ SM must be known at all of the studied resolutions. For that reason, a field campaign with small spacing was set up in Luxembourg, where topography is limited and a strong seasonality in surface SM exists (Matgen et al., 2012).

We hypothesise that even S1 data at its native spatial resolution contains relevant information on sub-field moisture conditions and aim to find the minimal spatial resolution at which speckle still allows for accurate SM estimates. For this purpose, we use a multitemporal pixel-based algorithm introduced by Pulvirenti et al. (2018) to retrieve SM at different high spatial resolutions (20–120 m). The S1 retrieved SM dataset was then evaluated against an in situ dataset whose spacing matches the S1 native spatial resolution. This dataset resulted from a field campaign on a non-irrigated agricultural field of ~2.5 ha in the Southeast of Luxembourg during 2020 and 2021. The evaluation for the entire time period is supplemented with a case study, entailing a short period with strongly varying SM conditions. We then discuss benefits and limitations of SM monitoring at these high spatial resolutions.

4.2 Study area and data

4.2.1 Study area

A field experiment was performed on a ~2.5 ha non-irrigated agricultural field in southeastern Luxembourg (Fig. 3.2). This specific field was chosen for its close proximity to a permanent meteorological station, and because of its availability for in situ measurements over a long time period. The long time period was necessary in order to obtain measurements at a large range of moisture conditions. Vegetation state in the field varied throughout the measurement period (Fig. C1): during the 2020 growing season maize

covered the field, and winter wheat was sown in the fall of 2020. The winter wheat grew to a few cm before low temperatures stagnated their growth, hence a slight coverage of vegetation was present in the 2020–2021 winter season. Growth then continued from March onward.

4.2.2 In situ data

In situ soil moisture data were collected and calibrated as described in Section 3.2.1 on the days indicated in Fig. 4.1. Additionally, at a nearby permanent meteorological station (6.32893°E, 49.49475°N), hydrometeorological variables such as SM (at 10, 20, 40, 60 cm depth), air temperature, and precipitation are measured continuously. These data were used in the analysis, where meteorological conditions in the field were assumed to be similar to conditions at the station.

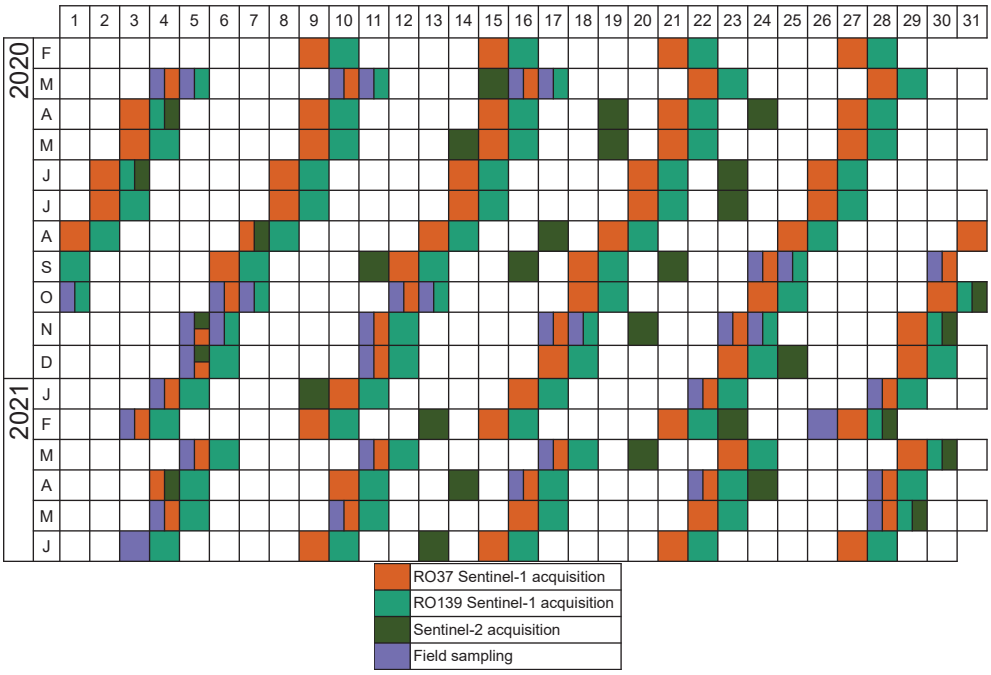

Figure 4.1: Overview of the timing of S1 (RO37, RO139), S2, and in situ data acquisitions.

4.2.3 Satellite data

Amongst the presently available active microwave sensors (see e.g. Babaeian et al., 2019), S1 data is the most promising: ESA freely provides S1 data at a 20×22 m^2 resolution (ESA Sentinel Online, 2023), keeps the satellites under a strict acquisition scenario, and is expected to continue these observations for the next few decades (Bauer-Marschallinger

et al., 2019; Peng et al., 2021). Every S1 orbit provides backscatter data with a revisit time of 6 days. Data from two different descending orbits (RO37 and RO139) were retrieved, with an average LIA of respectively 33.5° and 42.1° over the study area. S1 data were downloaded in Level-1 high resolution IW GRD format in VV polarisation for the days indicated in Fig. 4.1.

As an indication of vegetation state over the study area, NDVI data were used. These data were derived from Sentinel-2 (S2) Level-2 optical data. Although each S2 orbit has a five day revisit frequency, fewer data were available for this study because only images that are cloud-free over the study area were used. Moreover, only data from the 108 orbit were used. Data were finally retrieved on days shown in green in Fig. 4.1.

The 100 m resolution CLC map 2018 was used as land cover input data for the soil moisture retrieval algorithm. Although this is at a lower spatial resolution than the other input data, the results of the present study are not affected since the studied field is characterised under the same land cover type. Finally, the DEM over the study area was extracted from the SRTM (EROS, 2017).

4.3 Methods

4.3.1 Pre-processing

S1 GRD backscatter intensity data (σ^0) were preprocessed with ENVI SARscape. The precise orbit files were applied, thermal noise was removed, and data were radiometrically calibrated, multi-looked (4 pixels in the range direction) and geocoded using the SRTM DEM on the WGS 84 / UTM zone 32N coordinate system to finally obtain a square pixel of 20 m. The LIA and the slope over the study area were also extracted using the SARscape tool.

S2 optical data were converted to NDVI data with ESA's Sentinel Application Platform (SNAP) 7.0 tool.

4.3.2 Soil moisture retrieval

The retrieval algorithm

Soil moisture was retrieved following the methods discussed in Section 3.2 for all S1 images indicated in Fig. 4.1. The two different orbits were processed separately to ensure constant geometrical acquisition conditions (i.e. the same incidence angle) between the five consecutive backscatter images. Then, the SM maps were further processed (Section 4.3.3) and the roughness maps could be analysed immediately. Although no site-specific calibration was performed, estimated roughness conditions did approach their boundary

conditions (Fig. 4.2) and their temporal dynamics were as expected, with large changes occurring only during sowing and harvesting of the crops (Bousbih et al., 2017).

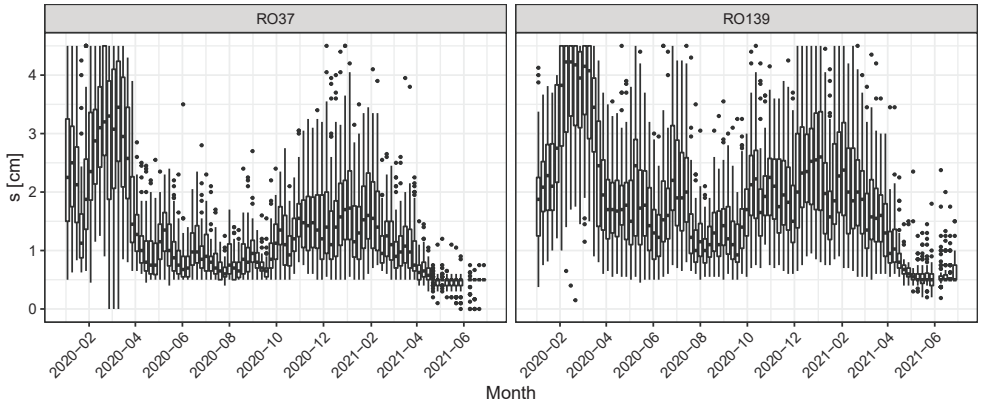

Figure 4.2: Illustration of the temporal dynamics of inferred roughness during the field campaign, provided in root mean square surface height [cm]. Boxplots with their minimum, 25th quartile, median, 75th quartile, maximum, and outliers as dots, are provided for every overpass day. The left panel shows results for RO37 and the right panel for RO139.

Minimising retrieval uncertainties

Several uncertainties in the retrieval have to be accounted for in the analysis, most notably speckle, surface roughness, frozen soils and the presence of vegetation.

Speckle in the σ^0 image is caused by inhomogeneities in the scattering natural target and results in grainy backscatter images (Lee, 1986). Speckle is generally reduced with spatial aggregation (e.g. Attarzadeh et al., 2018; Tripathi and Tiwari, 2020) or dedicated speckle filtering (e.g. Schonbrodt-Stitt et al., 2021). In this case, we only multi-looked the image four times in the range direction because we aimed to catch SM variation at a high spatial resolution. Applying a more rigorous speckle filter could hamper this since variations in backscatter could be interpreted as speckle rather than SM variation.

Surface roughness influences the scattering of microwaves and is corrected by assuming that moisture conditions change faster than roughness conditions (Pulvirenti et al., 2018).

Frozen soils decrease dielectric constant of the soil substantially (Hallikainen et al., 1985; de Rosnay et al., 2006) and are therefore flagged and removed after retrieval. Images acquired at a time when air temperatures at the meteorological station dropped below 2 °C were excluded from the computation of the temporal performance metrics. They were

included in the spatial analysis because in that case the data show how frozen soils affect the retrieval, but do not influence performance metrics for the entire time period.

Vegetation water content influences the scattering of the microwave signal and is often corrected in the retrieval as a dynamic parameter that changes in time, as does MULESME. It uses NDVI as a proxy for Plant Water Content (PWC), which is used to correct the σ^0 images for signal scattering by vegetation following Section 2.3 in Pulvirenti et al. (2018). PWC is derived from the NDVI images with an empirical equation that depends on the land cover of the pixel. The studied field is located in an area classified as agricultural, and as such, the conversion follows Eq. 4.1 (Chan et al., 2011).

$$\mathrm{PWC} = (1.9134 \cdot \mathrm{NDVI}^2 - 0.3215 \cdot \mathrm{NDVI}) + 3.5 \cdot \frac{(\mathrm{NDVI} - 0.1)}{0.9} \tag{4.1}$$

σ^0 is corrected for the vegetation signal if $0.25\ \mathrm{kg/m^2} < \mathrm{PWC} \leq 5\ \mathrm{kg/m^2}$. When $\mathrm{PWC} > 5\ \mathrm{kg/m^2}$, the pixel is masked from the backscatter image.

Backscatter pixels that are higher than −2 dB or lower than −18 dB after vegetation correction are masked out, since these values lie outside of the range of backscatter values under which soil moisture can be accurately retrieved (Pulvirenti et al., 2018).

4.3.3 Post-processing

During post-processing, any MULESME runs that included a known roughness change (e.g. due to ploughing in Oct 2020, Fig. C1) were removed from the analysis. Moreover, SM images were averaged to create a single ensemble mean per overpass day (Fig. 3.4, Lee et al., 2021; Zhu et al., 2020). A combination of a moving window and this averaging has two advantages. First, a moving window allows us to work with a shorter set of images so the hypothesis of constant roughness is more reasonable. Second, the averaging reduces the uncertainty in the SM estimate by exploiting more backscatter measurements.

Then, lower spatial resolution SM maps were created (i.e. 40, 60, 80, 100, 120 m) by multi-looking the retrieved 20 m SM map. Although multi-looking before SM retrieval is a more common approach to reduce speckle, this approach leads to the mixing of pixels that potentially have different SM, vegetation and roughness conditions. This could hamper SM retrieval, especially at high spatial resolutions. By retrieving SM first, and multi-looking second (CtA), different conditions are accounted for in the retrieval. Both this approach and the inverse (i.e. retrieving after multilooking, AtC) have been tested in a synthetic experiment and over the study area, of which the results are presented in Chapter 3. Those experiments showed that multi-looking after retrieval results in higher retrieval accuracy.

4.3.4 Data analysis

The accuracy of the SM images was evaluated by comparing the S1 retrieved SM maps to the in situ reference data at all six derived spatial resolutions. To that end, the in situ SM data were converted from point to raster data by averaging all TDR estimates located in the overlying pixel. Then, S1 retrieved and in situ SM images were compared to analyse the satellite's ability to capture the spatial SM variability.

We also computed two performance metrics to quantify the accuracy and error of the SM retrieval at the six different spatial resolutions: spatial and temporal r (Eq. 4.2) and spatial and temporal ubRMSE (Eq. 4.3). The RMSE quadratically penalises any deviation from in situ observations, but is sensitive to any bias in the data. The ubRMSE removes that from the equation and is thus useful for SM datasets, since in their application, an accurate estimate of the temporal SM variation is more relevant than its exact value (Entekhabi et al., 2010; Reichle et al., 2007). The Pearson correlation is a useful addition as it quantifies the agreement in space or time between the satellite dataset and the in situ dataset.

$$r = \frac{\sum_{i=1}^{n}(y_i - \overline{y})(x_i - \overline{x})}{\sqrt{\sum_{i=1}^{n}(y_i - \overline{y})^2}\sqrt{\sum_{i=1}^{n}(x_i - \overline{x})^2}} \tag{4.2}$$

$$\text{ubRMSE} = \sqrt{\frac{1}{n}\sum_{i=1}^{n}((y_i - \text{ME}) - x_i)^2} \tag{4.3}$$

$$\text{ME} = \frac{1}{n}\sum_{i=1}^{n} y_i - x_i \tag{4.4}$$

In Equations 4.2 – 4.4, y stands for the estimated SM, x for the in situ observed SM, n for the number of samples and i for each individual pair of observations.

4.3.5 Comparison with Copernicus surface soil moisture

To confirm the suitability of the MULESME algorithm for SM retrieval, we not only include a comparison of MULESME SM to a field study, but also to results of the more widely used TU Wien Change Detection model (Bauer-Marschallinger et al., 2019). This model has been used by the Copernicus Global Land Service to operationally retrieve global SM from S1 at a 1 km resolution (CSM dataset, https://land.copernicus.eu/global/products/ssm). Whereas MULESME retrieves absolute SM based on the forward Oh model, the TU Wien model interprets changes in backscatter as changes in SM and thus ends up with a relative estimate of SM in % saturation.

We performed a comparison with MULESME SM aggregated to the same spatial resolution and with average field in situ values. All three datasets were filtered for frozen soils and adverse vegetation conditions. We hypothesised that MULESME SM trends align with

TU Wien SM trends, and assume that will be the same on higher spatial resolutions. Conclusions drawn in applying this method will therefore likely be transferable to the use of a different algorithm.

4.4 Results

4.4.1 Soil moisture conditions during field campaign

SM conditions in the field are provided for each day in Appendix C (Figs. C2 and C3). A temporal average (Fig. 4.3) shows that SM was not homogeneous in the field, but that spatial variability within the field was considerably smaller than temporal variability. On days coinciding with the 139 overpass (RO139), the field was slightly wetter than on days coinciding with the 37 overpass (RO37). A wetness gradient in the field from northwest to southeast is visible in the high resolution satellite images (i.e. 20, 40, 60 m), but it can no longer be detected in the images with a larger pixel size. The gradient is comparable between the in situ and satellite data and between the RO37 and RO139 data. However, a clear bias exists in the results: the temporally averaged TDR values range from 0.30 to 0.40, whereas the satellite values range from 0.16 to 0.26.

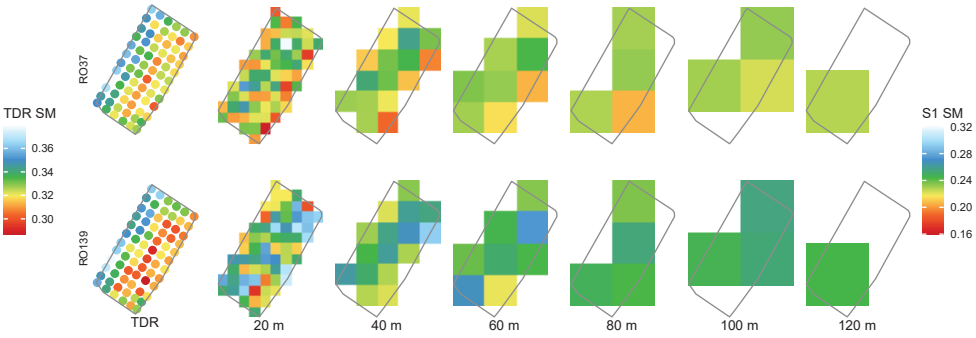

Figure 4.3: Temporal average of SM content throughout the field measurement campaign. The first column shows the in situ TDR data, and the remaining columns show the S1 SM data on six different spatial resolutions. Upper and lower panels show data for the two different orbits, and thus for different days in the measurement period (Fig. 4.1). This figure excludes days when temperatures were below 2°C, when standing water was observed and when vegetation hampered the SM retrieval (Section 4.4.2).

4.4.2 Temporal metrics

The bias in average SM conditions is also apparent in the temporal SM dynamics (for the complete dataset we refer to the appendix: Figs. C2 and C3). The centre panel

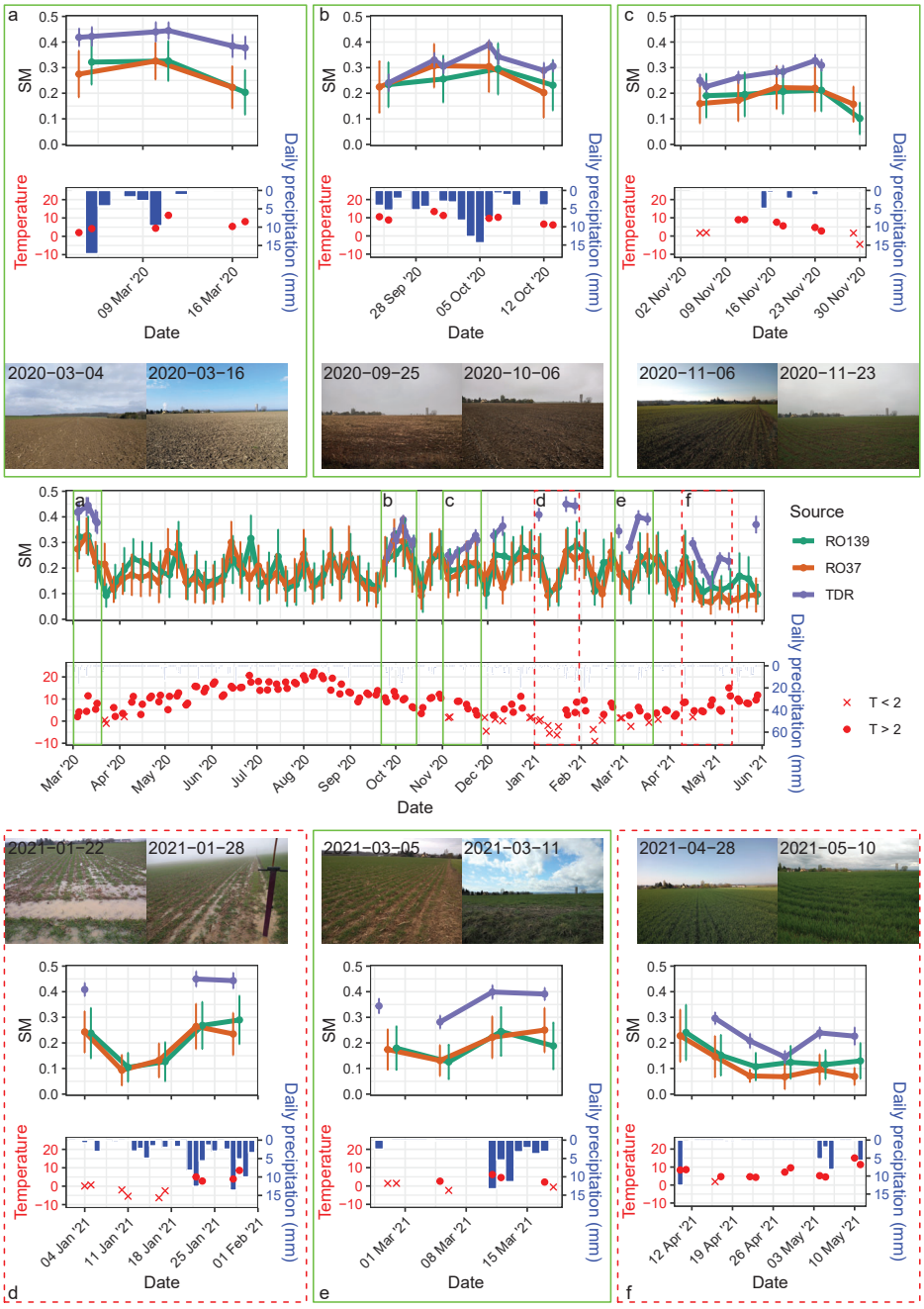

Figure 4.4: Illustration of the temporal SM dynamics during the field campaign. The centre panel shows TDR (purple) and S1 (green, orange) time series through the 2020–2021 winter and beginning of the 2021 growing season, with error bars indicating the standard deviation, and meteorological conditions: daily precipitation in blue and air temperature at the time of overpass in red. Subplots a, b, c, d, e, and f zoom in on periods that are discussed in the text.

in Fig. 4.4 shows the S1 retrieved SM time series, as well as air temperature and daily precipitation at the permanent station at the time of the satellite overpass. The time series show that the bias between satellite and in situ data is slightly more severe in the RO37 data than in the RO139 data. At the same time, the temporal evolution is generally well described in the satellite data: The impact of the presence and absence of precipitation can be seen in increasing and decreasing SM conditions, in satellite as well as in situ data.

Differences in performance can be observed for different field conditions. Some examples are highlighted in Fig. 4.4. In periods highlighted in green (Fig. 4.4a, b, c, e), the S1 SM estimates follow the in situ temporal dynamics rather well. The photos taken in the field during these periods show that soils were bare or covered with only minimal amounts of vegetation. Moreover, the meteorological conditions were moderately wet and moderately warm, with temperatures rarely dropping below 2°C. A bias in the results still persists, albeit less so in October 2020 (Fig. 4.4b). In that period, temperatures stayed above 5 °C and precipitation occurred almost daily.

In contrast, January 2021 (Fig. 4.4d) showed especially challenging conditions for SM retrieval. Air temperatures were very low (<2°C) for the first half of the month. This led to frozen soils in mid January, when satellite estimates of SM dropped to values of around 0.1, a clear underestimation of actual moisture conditions. At the end of the month, frozen soils made way for standing water on the field. This caused specular reflection that decreased the backscatter intensity and again led to an underestimation of SM conditions.

In April–May 2021 (Fig. 4.4f), vegetation hampered accurate SM retrievals. S1 SM estimates dropped to extremely low values rapidly before in situ conditions reflected this drop. S1 SM estimates did also not reflect the expected signal after precipitation in the beginning of May. The reduction in estimation accuracy in this period coincides with a period of large uncertainty in roughness estimates (Fig. 4.2), that are suddenly extremely low starting from mid April 2021, likely due to the presence of vegetation. The vegetation attenuates the σ^0 signal, and the algorithm is unable to distinguish this attenuation from surface scattering. Hence, the backscatter is low not because of low SM, but because of the small part of the signal that reaches the surface in the first place.

Based on this analysis, several conditions that affect the performance of S1 SM retrieval were filtered out before computing the temporal metrics:

- days where air temperatures dropped below 2°C;
- days where standing water was observed; and
- days during the height of the growing season (after 2021-04-15).

After filtering, 22 days with TDR measurements remained, 12 for the RO37 data and 10 for RO139.

The temporal metrics for the two different orbits are visualised in Fig. 4.5a. The smaller amount of in situ data for RO139 leads to non-significant correlations more often than for RO37: only at resolutions lower than 80 m, the majority of pixels has a significant Pearson correlation ($P<0.05$). For the RO37 data, this is already the case at 40 m. The temporal r (Fig. 4.5a) is higher in the RO37 data for high spatial resolutions, but for low spatial resolutions, the RO139 data perform better. The RO37 20 m resolution has a spatially averaged temporal r with the in situ data of 0.39 (or 0.66 for significant pixels). At 40 m resolution, the average correlation already improves to 0.59 (or 0.68). The improvement in r stagnates after 60 m with a value of 0.67 (0.69) and does not get higher than 0.69 at a 100 m resolution. In the RO139 data, r improves until a lower resolution, peaking at 0.76 at a 100 m resolution. Comparing the different pixels within each resolution, spatial variation is limited for the RO37, except on the 20 m resolution. For the 139 orbit, a higher spatial variation exists, with higher correlations occurring in the northern part of the field.

The temporal ubRMSE gives an indication how different the S1 SM estimates are from the in situ SM observations (Fig. 4.5b). At lower spatial resolutions, the value decreases slightly from 0.09 to 0.05 (RO37) or 0.04 (RO139). Spatial variation in the ubRMSE is especially apparent in the 20 m resolution images and is more pronounced in the 139 than the 37 orbit. In both cases, spatial variability decreases as spatial resolution decreases.

4.4.3 Spatial metrics

Spatial metrics were computed for the entire field campaign, hence including the days that were characterised by unfavourable retrieval conditions. They are shown in Fig. 4.6 for each day on which field data were collected, together with their averages over the entire time period. To distinguish between favourable and less favourable conditions, temperature and vegetation conditions are indicated in different shapes and colours in the plot, respectively. Spatial metrics could not be computed for the 120 m resolution because there was only one pixel at this size that had more than 50% of its area located in the field (see Fig. 4.5). It should also be noted that at lower spatial resolutions, fewer pixels can be analysed and so the chances of finding a significant correlation decrease.

The average spatial r (printed in grey in Fig. 4.6) over the field is low. In the case of RO37 (upper panels), r increases as the spatial resolution decreases, with its maximum at 0.232 at 100 m resolution. For RO139 (lower panels), no clear trend exists between the average r and spatial resolution. The highest r does occur at the lowest spatial resolution, with a value of 0.062. In contrast, the average ubRMSE clearly improves with increasing spatial resolution for both orbits. For both orbits ubRMSE drops below 0.04 at 60 m resolution, further decreasing to their respective minima at 100 m (RO139: 0.016; RO37: 0.017). Differences in performance between the orbits are mostly visible at high resolutions (up to 60 m), where RO37 outperforms RO139.

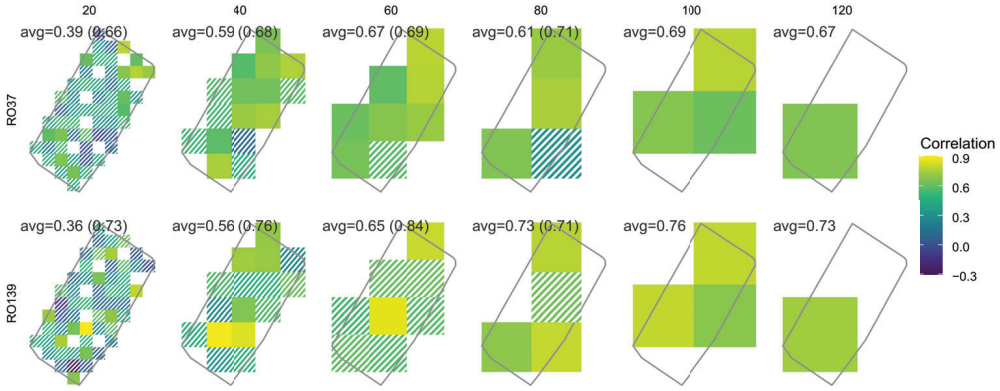

(**a**) Pearson correlation per pixel.

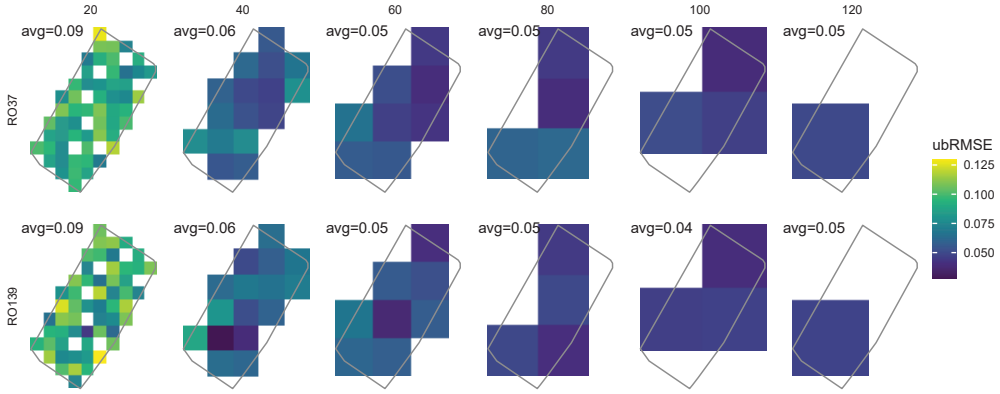

(**b**) Unbiased root mean square error per pixel.

Figure 4.5: Temporal performance metrics between S1 SM and in situ data, for all six different spatial resolutions studied here. Pixels with non-significant correlation values are dashed. The grey text shows the metric averaged over the entire field, and the correlation for the significant correlations only are given between brackets. Data were removed from the analysis when temperatures were below 2°C, when standing water was observed on the field and when vegetation hampered the SM retrieval (Section 4.4.2).

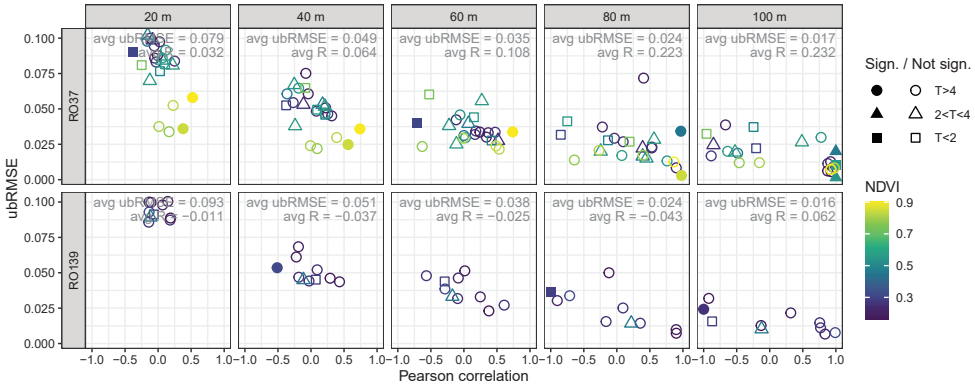

Figure 4.6: Spatial correlation and unbiased RMSE on each day of the field campaign, for different spatial resolutions (m). Colours show the value for field-averaged NDVI on that measurement day. Filled shapes indicate that the correlation was significant (P<0.05) and shapes indicate the temperature range at the time of overpass. The text in grey shows the average *r* and ubRMSE. At a 120 m resolution, only one pixel is present in the field, so no values for spatial correlation exist and ubRMSE equals zero by definition.

The separate shapes in Fig. 4.6 show the spatial performance metrics for each day on which data were collected. The low average *r* discussed earlier is clearly not caused by outliers, since on most days the correlation is rather low, especially at high spatial resolutions. Moreover, in only a handful of cases the correlation was found to be significant (P<0.05), shown by the filled shapes. In RO37, a significant correlation was found on only two or three days for all studied spatial resolutions. In most cases, these significant correlations were found to be positive. Negative significant correlations only occur for temperatures below 2°C, as shown by squares in the figure. For the RO139 on the other hand, in all cases where correlation is significant, it is negative. Both orbits show an increasing variability of *r* at decreasing spatial resolutions, shown by the spreading of values over the x-axis. Interestingly, the ubRMSE shows an opposite trend in RO37: spread in the y-direction decreases at lower resolutions. This trend is not visible in RO139. For both orbits, the ubRMSE is lower than 0.05 for most days in 60, 80 and 100 m resolutions, but generally higher in 20 and 40 m resolutions.

Only one clear high ubRMSE outlier in the data exists at the 80 m resolution for orbit 37. Low outliers are visible in the 20 and 40 m resolutions at RO37, interestingly on days with high NDVI values. Judging from the temporal analysis in Section 4.4.2, this seems to be a coincidence rather than a result with a physical basis: both increased vegetation and decreasing water content result in the same change in backscatter and occurred simultaneously in the early summer of 2021. In terms of temperature, correlations are often negative when temperatures were below 2°C (squares in Fig. 4.6). No substantial

difference was found between the spatial metrics on days where temperature was between 2 and 4°C (triangles) and days where temperature was higher than 4°C (circles).

4.4.4 Case study

Both the temporal and spatial analysis indicated that differences in retrieval accuracy exist between individual days. Even though spatial correlations are generally low due to the low variability in the field, we expect that under favourable field conditions, MULESME is able to capture temporal dynamics at a high spatial resolution. In this case study, we zoom in to a period with favourable field conditions and a clear temporal variation in SM (Fig. 4.4): February–March 2021. This analysis is performed for the RO37 data only, since higher performances were found at higher spatial resolutions compared to the RO139 data.

Fig. 4.7 shows that the first two studied days are drier than the last two days. The biggest change in SM is observed between the 5th and the 11th of March. Temporal in situ SM trends are accurately represented in S1 SM conditions: wetter in situ conditions correspond with wetter S1 SM conditions and vice versa. This is not true for all spatial resolutions. At a 20 m resolution, the satellite retrieval shows spatially varying SM in the field that is not present in the in situ data. At lower spatial resolutions, the agreement between different pixels in space improves, and patterns in in situ data are better represented in the satellite data. However, the earlier identified bias is still visible.

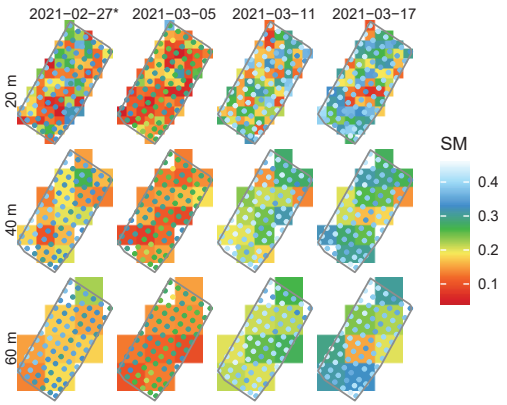

Figure 4.7: Spatiotemporal SM dynamics in the field in February–March, 2021 at a 20, 40, and 60 m spatial resolution. The S1 SM is shown as pixels in the back and the TDR measurements are plotted as points on top. *Due to a lack of TDR data on 2021-02-27, TDR data from 2021-02-26 are shown.

To further test whether temporal trends are accurately represented in the MULESME output, we plotted the temporal variation in SM content in the field for the 20, 40, and 60 m resolution (Fig. 4.8). The satellite data does bear a distinct resemblance to the in situ data.

The daily variations show that trends found in spatially aggregated in situ data are well visible in satellite data with high a spatial resolution. This is especially true for the centre date pair, when SM levels increased substantially. At comparatively stable SM conditions, such as in the March 17th–11th pair, the satellite retrieval is less accurate. Even at the 60 m resolution, large S1 SM changes are visible on the studied field whereas no substantial change showed in the in situ data.

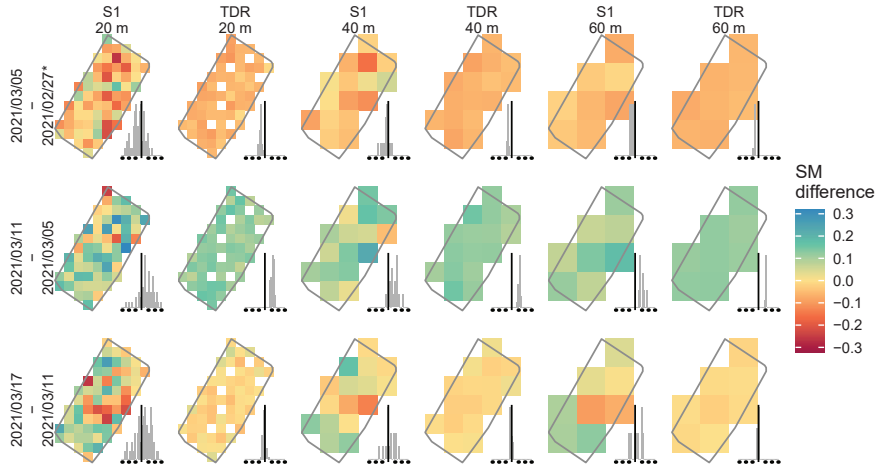

Figure 4.8: Temporal difference between SM on subsequent field days in February and March 2021, at 20 m, 40 m, and 60 m resolution. Histograms show the distribution of values, with a vertical line at zero and tick marks at every 0.1. *Due to a lack of in situ data on 2021-02-27, in situ data from 2021-02-26 are shown.

4.4.5 Copernicus data

To be able to put the MULESME analysis into context, we include an analysis of the CSM dataset over our field (Fig. 4.9). The CSM dataset has a spatial resolution of 1×1 km. Since our S1 retrieved SM data has a higher spatial resolution, we spatially aggregated the MULESME dataset to the same resolution and normalised them both to their minimum and maximum values. The top part of Fig. 4.9 shows the agreement between the two datasets in the 1×1 km pixel overlaying the field. This shows a good agreement and a strong temporal correlation (0.803) between both datasets. The bottom part of Fig. 4.9 shows the agreement between the Copernicus SM and the field average in situ SM measurements. These also showed a good agreement, with a temporal correlation of 0.778, compared to 0.583 between the 1×1 km MULESME and the field average. This is lower than the MULESME estimates at higher resolutions (Fig. 4.5a), indicating that further multilooking the data to lower resolutions reduces retrieval accuracies.

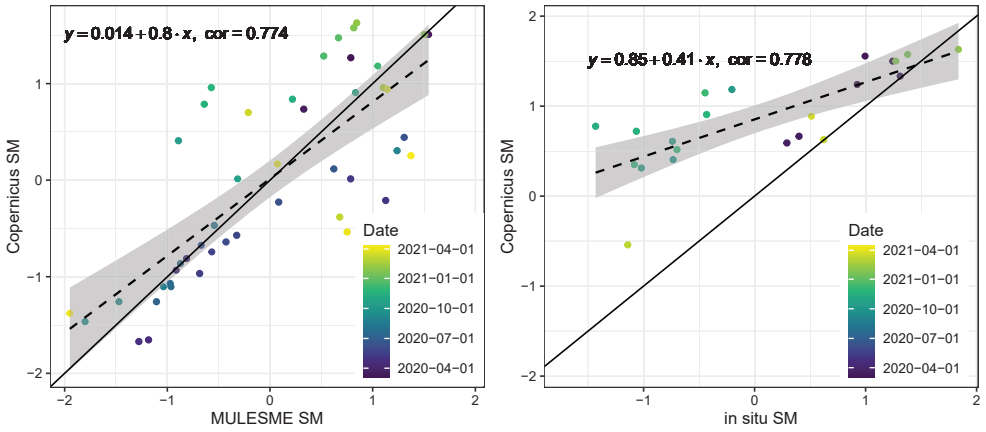

Figure 4.9: A comparison between MULESME RO37 and Copernicus SM data at a 1×1 km scale (left) and in situ and Copernicus SM data (right) over the field.

4.5 Discussion

We compared a SM dataset retrieved from S1 data with a high spatial resolution with a high spatial resolution field dataset with extended temporal coverage. This comparison showed that temporal SM variability was well reflected in the satellite data, although performance increased with decreasing spatial resolution (Fig. 4.5). Spatial performance behaved similarly, but r was generally low and ubRMSE was generally high (Fig. 4.6). Taking into account differences in performance dependent on field conditions, the optimal retrieval accuracy was finally identified at a 60 m resolution using the RO37 data (i.e. the equivalent of 36 looks of native S1 data). At that resolution, a good average temporal correlation (0.67, or 0.69 only taking into account significant r values) was found and sub-field SM variation could still be distinguished.

Performance of the satellite dataset depended on the satellite orbit and on field conditions (Fig. 4.4), most notably on temperature, vegetation and wetness. The performance difference between the orbits could be caused by their different incidence angles (Palmisano et al., 2021). Frozen soils caused negative spatial correlation (Fig. 4.6) due to the inverse relationship between backscatter and SM under these conditions as compared to "normal" conditions (Hallikainen et al., 1985; de Rosnay et al., 2006). The presence of vegetation increased the bias of the S1 SM retrievals (Fig. 4.4), as previously found by for instance Bindlish and Barros (2001), Yadav et al. (2020), and Zhang et al. (2021). However, the spatial correlation was barely affected by increased NDVI values, and the ubRMSE was even lower at higher NDVI values (Fig. 4.6). Based on the sudden decrease in estimated roughness during the same period (Fig. 4.2), it seems that the increase in performance is coincidental. Wheat attenuates backscatter especially at high incidence angles due to its

geometry (Mattia et al., 2003), as does a decreasing moisture content that occurs simultaneously. Decreasing backscatter and hence decreasing moisture estimates are therefore likely caused by vegetation growth rather than decreasing moisture conditions, indicating that S1 SM estimates were unreliable in that period.

The case study showed that temporal variability could be described better when clear variations in SM existed. Unfortunately, since the study area was not irrigated, spatial variation in SM was limited (Fig. 4.3). Meanwhile, a large spatial variability existed in S1 SM, especially in images with a high spatial resolution. This indicates that the sub-field variation in SM is smaller than the spatial variation in the backscatter data. This high spatial variation is not caused by the retrieval algorithm, because the algorithm is pixel-based and so SM values do not depend on neighbouring pixels. The spatial variations in S1 SM were thus caused by speckle, indicating that at high spatial resolutions, the spatial signal is smaller than the noise. Speckle introduces spatially uncorrelated fluctuation, whereas it is quite correlated in time due to the small orbital tube of S1 (Torres et al., 2012). Hence, temporal variation in speckle is limited. This explains why temporal performance was better than the spatial performance. High spatial resolution S1 data thus contain information on temporal variability of SM that could be further exploited.

While speckle did influence SM retrievals at a high spatial resolution, a correlation with reference data as high as 1 is near to impossible because in situ data have their own uncertainties. Uncertainties in SM observations are a common issue: due to small-scale variations in SM caused by for instance local topography, heterogeneous soil properties and plant water uptake, point scale SM can be different from gridded SM (e.g. Babaeian et al., 2019; Famiglietti et al., 2008; Teuling et al., 2006b; Vereecken et al., 2008; Western and Bloschl, 1999). The uncertainty of in situ SM observations makes it difficult to relate the in situ SM to the ground truth. Therefore the uncertainty was limited as much as possible by taking five measurements at each sampling location and by calibrating the data with volumetric soil samples.

The MULESME algorithm assumes that roughness in each pixel remains constant over the five considered backscatter images. The assumption of constant roughness always is a major part of a multitemporal algorithm, but the way this assumption is handled depends on the algorithm. Results from a second multitemporal algorithm (TU Wien) were therefore also compared to the in situ data. This analysis showed that the TU Wien algorithm results in higher temporal correlations than the MULESME dataset. At the same time, the MULESME dataset was able to accurately depict temporal SM variations at a much higher spatial resolution. In light of the high temporal correlation between the two products at a 1×1 km resolution, we believe that the use of a different SM retrieval algorithm for the present study would not have considerably affected the results.

The measurements presented in this paper were made in a moderate climate under varying moisture, meteorological and vegetation conditions. Since the entire range of valid SM

conditions was observed, the chosen location for the field campaign had sufficient seasonality in moisture conditions, as well as sufficient different meteorological conditions and vegetation states. Finally, the studied field is a "normal" agricultural field by European standards in terms of size, slope and soil type. Because of these wide ranging conditions, conclusions from this study are expected to be valid under most conditions and perhaps even in other climatic zones.

4.6 Conclusion and outlook

A high spatial resolution SM dataset resulting from S1 backscatter data was used to explore the limits in spatial resolution of active microwave SM measurements. The performance of this six-day dataset was evaluated with a closely spaced in situ SM data that was collected in a dedicated field campaign in Southeastern Luxembourg. This comparison showed that the optimal retrieval accuracy could be found at a 60 m resolution, equivalent to 36 looks at a native S1 spatial resolution: a good average temporal correlation was found and spatial variation could still be distinguished. Spatial correlation, on the other hand, was low, likely due to the limited spatial variability over the field. A case study under favourable field conditions did show that short-term SM variability could be captured at a 60 m resolution regardless of the low spatial correlation.

Though high spatial resolution SM data have been presented before, to the best of our knowledge, this is the first time that they were compared to an extensive in situ dataset whose spacing matches the S1 native spatial resolution. We demonstrated that high resolution backscatter intensity images can contain temporal information on SM at a spatial scale smaller than the field scale, and future research should focus on further exploiting this merit. Another path to explore would be an analysis on a larger scale, with larger spatial variability in SM, thereby also including other land cover types, soil types and soil textures. It would be interesting to study how large scale SM monitoring on high resolutions would compare to a similar analysis on lower resolutions. Sub-field variations might be of significant importance for the evolution of SM droughts and can thus be of interest for the drought community, as well as for precision agriculture applications.


5

Chapter 5

Satellite soil moisture for high resolution drought monitoring

This chapter is based on:

T. C. van Hateren, M. Chini, P. Matgen, J. Zhao, and A. J. Teuling (2023b). 'Evaluating C-band satellite soil moisture observations for high resolution drought monitoring'. In preparation for Geophysical Research Letters.

Abstract

Recent advances in satellite soil moisture retrievals now allow for satellite soil moisture retrievals at sub-field scale. Their relevance for drought monitoring remains to be studied. We take the opportunity of the unique availability of three high resolution (60 m, 100 m, 1 km) soil moisture datasets over Luxembourg for an intercomparison between drought data. Monthly anomalies of satellite retrieved soil moisture were evaluated with those of reference in situ soil moisture and precipitation (SPI). An analysis on the national scale showed that the 1 km data most often correctly identifies a drought observed in the in situ data. Compared to SPI, the 60 m dataset also performs well, while the 100 m data shows a poorer performance. On smaller scales, both the 1 km and 100 m datasets show little spatial variability in their soil moisture anomalies. Only the 60 m dataset is able to distinguish between local variations in soil moisture. Hence, while 1 km data allowed for soil moisture drought monitoring on the national scale, higher resolution data is needed to adequately monitor droughts on (sub-)field scales.

5.1 Introduction

A drought is, in principal, a natural phenomenon that is defined as a period with below-normal water availability (Tallaksen and van Lanen, 2004), that can occur in any part of the water cycle. A soil moisture deficit can thus be called a soil moisture drought when levels are considered to be below-normal. To monitor the biophysical, climate and socio-economic impact of soil moisture droughts, remotely sensed soil moisture at coarse spatial resolutions (i.e. 0.25°) plays an increasingly important role (Denissen et al., 2020; Miralles et al., 2014; Nicolai-Shaw et al., 2017; Vroege et al., 2021). However, these coarse resolutions do not provide relevant information on the agricultural field scale. Hence, for drought management and agricultural purposes higher spatial resolutions (i.e. 1 km and finer) are required. At spatial resolutions of 100 m and smaller, soil moisture data could even help improve irrigation efficiency to optimise water use (Corbari and Mancini, 2023) and, in turn, alleviate drought impacts.

Accurate soil moisture drought monitoring at sub-field scales comes with challenges: in situ soil moisture data are sparsely and irregularly spaced point data and thus do not provide the required support, spacing and extent (Crow et al., 2022; Western and Bloschl, 1999). Models can provide high resolution soil moisture estimates at a large extent (Vergopolan et al., 2022; Vergopolan et al., 2021), but these estimates are often based on simplified assumptions such as hydrological similarity. Satellite observations of soil moisture are a more direct estimate of hydrological conditions in the field and could provide soil moisture data anywhere, including data-sparse regions (West et al., 2019).

At spatial resolutions of 1 km and larger, satellite soil moisture data have already been used successfully for drought monitoring (Fang et al., 2021; Liu et al., 2019; Vroege et al., 2021). At higher spatial resolutions, these techniques have not yet reached the same maturity. However, recent advances in satellite soil moisture retrievals now allow for soil moisture retrievals at sub-field scales (De Jeu et al., 2017, Chapters 3 and 4). The availability of such high resolution soil moisture datasets enables an assessment of the use of high resolution soil moisture data for drought monitoring.

We take the opportunity of the unique availability three high (60 m, 100 m, 1 km) resolution soil moisture datasets over Luxembourg, a region where various in situ soil moisture datasets are also available. These datasets together represent the academic and commercial state-of-the-art and allow for an intercomparison between drought data retrieved from three soil moisture products at different high resolutions. This analysis is supplemented by a comparison with reference in situ datasets of soil moisture and precipitation to test the accuracy of the different products in drought monitoring on monthly timescales. We then discuss the advantages and disadvantages of the use of these products.

5.2 Data and methods

5.2.1 Data

The data used for this study consisted of satellite datasets of soil moisture and in situ datasets of soil moisture and precipitation. They are summarised in Table 5.1. The individual in situ datasets were combined in one large dataset with 162 unique locations within the borders of Luxembourg (Fig. 5.1). Because the temporal coverage differed per in situ dataset, the amount of locations with data in any given month ranged from 2 to 85. The satellite datasets MULESME surface soil moisture (MUL), vanderSat surface soil moisture (VDS) and Copernicus Global Land service Surface Soil Moisture (CSM) were each processed separately, because of their different spatial resolutions.

The MULESME dataset is largely the same as the dataset used in Chapter 4, although some slight changes were made to the processing chain. To obtain cloud-free estimates of NDVI over the entire territory of Luxembourg, a monthly cloud-free S2 NDVI composite was computed with Google Earth Engine. This composite was used to perform the vegetation correction in the MULESME algorithm (Pulvirenti et al., 2018). Moreover, an exclusion map where soil moisture could not be retrieved accurately was created for the backscatter images following Zhao et al. (2021). This was used to mask pixels prior to soil moisture retrieval in MULESME. The other two satellite datasets were readily available online and did not require additional preprocessing other than that discussed in Section 5.2.2.

Table 5.1: Overview of the data used in this study.

		Spatial / temporal resolution		Coverage	Satellite	Algorithm	Citations	URL	Units
In situ precipitation	LIST, ASTA, MeteoLux	point	daily	01-01-2002 31-12-2022			LIST-HOST, 2022 ASTA, 2022 MeteoLux, 2022	https://envdata.private.list.lu/	[mm]
In situ soil moisture	LIST, ASTA	point	daily	30-04-2012 17-11-2022			LIST-HOST, 2022 ASTA, 2022	https://envdata.private.list.lu/	[m3/m3]
	van Hateren	point[1]	6-daily	04-03-2020 03-06-2021			van Hateren et al., 2023a		[m3/m3]
	Foets	point[1]	monthly	05-12-2017 21-11-2018			Foets et al., 2020		[m3/m3]
	Blume & Weiler	point	daily	01-03-2012 25-04-2018					[m3/m3]
Satellite soil moisture	MULESME	60 m	6-daily	01-01-2016 31-12-2022	Sentinel-1	MULESME	Pulvirenti et al., 2018 van Hateren et al., 2023a		[m3/m3]
	VanderSat's C-band soil moisture	100 m	daily	15-06-2002 05-09-2022	AMSR-E, AMSR2	Planet		https://data.public.lu/en/datasets/soil-humidity-in-luxembourg-2002-2022/	[m3/m3]
	Copernicus	1 km	daily	10-2014 present	Sentinel-1	TU Wien	Bauer-Marschallinger et al., 2018	https://land.copernicus.eu/global/products/ssm	[% sat.]

5.2.2 Preprocessing

The VDS data contained some images with unrealistic patterns of soil moisture, where for instance half of Luxembourg was covered with a value of 0 m^3/m^3. Those images were removed from the analysis, since they had a large impact on the monthly average

[1] average of multiple independent samples

soil moisture values. Then, all satellite data were filtered spatially to only consider pixels where at least 80% of the underlying land was covered by agricultural area according to the vectorised CCI land cover 2018 dataset (https://data.public.lu/en/datasets/corine-land-cover-2018/). The remaining data were converted to monthly mean soil moisture and monthly precipitation sums. Missing values were ignored so that monthly values were obtained when at least one of the days of that month had data. Monthly soil moisture anomalies (SMA) were computed using Eq. 2.1 (e.g. Cammalleri et al., 2015), using a reference period from 2015 to 2022. Monthly precipitation sums were standardised using the SPI (McKee et al., 1993). Similar to soil moisture, SPI was computed on a one-month timescale (SPI1).

To allow for a comparison with gridded satellite datasets, the point-scale in situ data were also converted to gridded data. Precipitation is spatially rather homogeneous compared to soil moisture. Available precipitation data were therefore considered to be representative for the entire country. To convert these precipitation point data into gridded data, they were first interpolated to values for the entire study area with Thiessen polygons. These polygons were then rasterised to a gridded dataset with a 10 km spatial resolution, to obtain a total of 58 pixels over the study area, similar to the number of precipitation stations (Fig. 5.1).

Soil moisture is more heterogeneous in nature than precipitation and was converted to gridded data differently. For each pixel in the satellite SM datasets, the available in situ SM was spatially averaged. A correlation between satellite and in situ SM therefore indicates how well satellite data can describe soil moisture dynamics on a pixel scale, rather than on a point scale.

The satellite soil moisture datasets were resampled to all of the other spatial resolutions that were studied. For instance, the CSM dataset (1 km) was resampled to the spatial resolutions of the MUL (60 m) and VDS (100 m) datasets using the nearest neighbour method, and spatially averaged to the resolution of the precipitation dataset (10 km).

5.2.3 Analysis

After preprocessing the available data, the satellite soil moisture datasets were compared to each other, as well as to the reference datasets consisting of in situ soil moisture and precipitation data. Soil moisture data were compared at each spatial resolution. For example, 60 m resolution MUL data were compared to the 1 km resolution CSM data at a 60 m, 100 m, 1 km and 10 km spatial resolution. The Pearson correlation (r) was used as the performance metric, and only computed when a minimum of four pairs of observations were present. Temporal correlations were computed for the SMA to test their performance during anomalous conditions. Spatial correlations, on the other hand, were computed for monthly SM averages.

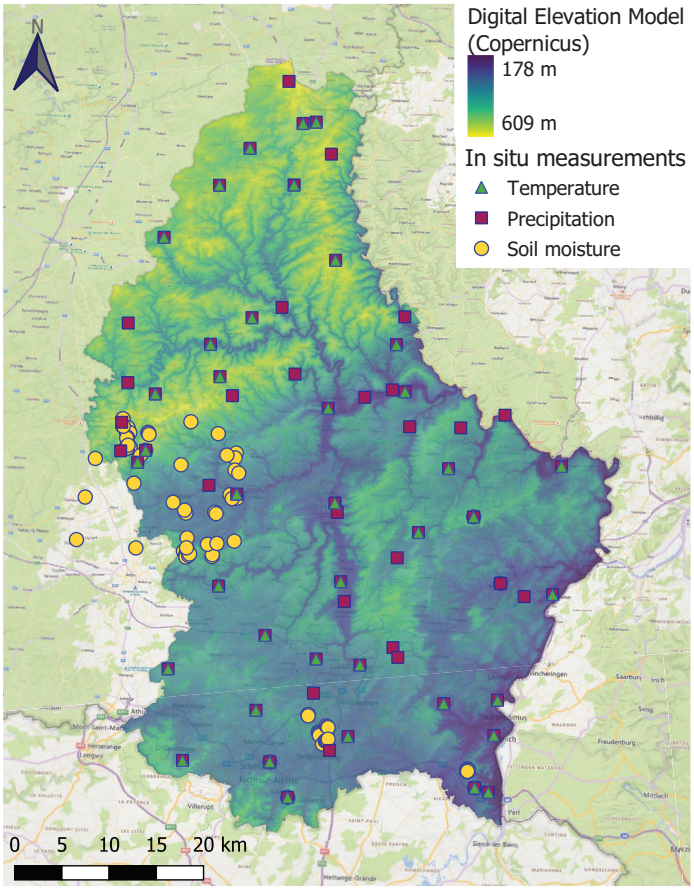

Figure 5.1: Map of the study region and location of in situ stations.

The second part of the analysis focused solely on drought conditions. Drought years were identified in the SPI1 data and the most recent drought over Luxembourg, 2022, was chosen to compare spatial and temporal accuracy of the different soil moisture datasets. Droughts were identified starting when average SPI1 values dropped below −1 and ending when they returned to positive values (e.g. Brito et al., 2018; McKee et al., 1993; Spinoni et al., 2014). This way, drought onset, duration and intensity, as well as hit rates and misses, could be determined for all the different datasets and compared to those of the reference data, even though the characteristics of drought in surface soil moisture might differ slightly from the meteorological drought as reflected in SPI1.

5.3 Results

5.3.1 Temporal variation

Fig. 5.2 shows time series of satellite and in situ SMA and SPI1. The SPI1 and in situ SMA are taken to be the reference value for drought conditions. The SPI1 shows that the longest drought in the studied period occurred from Dec 2016 up until Jun 2017. This was also the period with the highest spatially averaged drought intensity in SPI1: −2.3 in April 2017. All other droughts identified in the SPI1 data were short-lived, with a maximum duration of two months. The In Situ (IS) data had fewer droughts over the entire studied period, although they were longer in duration. Three droughts were identified, of which the longest took place between Oct 2016 and Jul 2017. The most intense drought in IS was in Nov 2018 with an intensity of −1.6.

The MUL SMA data only identified one drought, from Oct to Dec 2018, with a minimum of −1.4 in Oct. The drought in 2022 that was identified in other datasets was only just not severe enough in the MUL data (−0.98) to become part of the analysis. Four droughts were identified in the VDS data, of which the longest took place in 2021–2022, lasting a full year between Sep 2021 and Aug 2022. The most intense drought month was in Nov 2020, as part of a four-month drought in winter. The CSM SMA dataset showed seven droughts over the studied period, of which the longest took place in 2022, between March and August. The most intense drought was in Dec 2016, with a minimum of −2.0.

When identified droughts in satellite SMA data are compared to those in the reference data in Fig. 5.2, it seems that the CSM most often correctly identifies a drought. The hit- and false alarm rates in the data (Tab. D1) confirm the good performance of the CSM data on this national scale. This dataset has the highest hit rate for both the SPI and the IS reference data. The CSM does have higher false alarm rates than the MUL data, due to the low number of identified droughts in the MUL data. The VDS data has higher false alarm rates than hit rates for both reference datasets.

Of course, the timeseries in Fig. 5.2 only identify a drought when the average values in the country do so. In datasets with more spatial variation (indicated by the shaded area), the mean value drops below −1 less often. The MUL dataset indeed only identifies a drought on this national scale in three months during the entire studied period. It is possible that a drought could in fact have been identified in a smaller spatial subset, even though the national SMA average is not low enough for this timeseries analysis to show a drought. For this reason, we discuss smaller spatial subsets in Section 5.3.3.

5.3.2 Spatial and temporal correlation

After a general comparison of temporal variation in the different datasets, here we add quantitative detail on their agreement. Fig. 5.3 shows the temporal (top, monthly anoma-

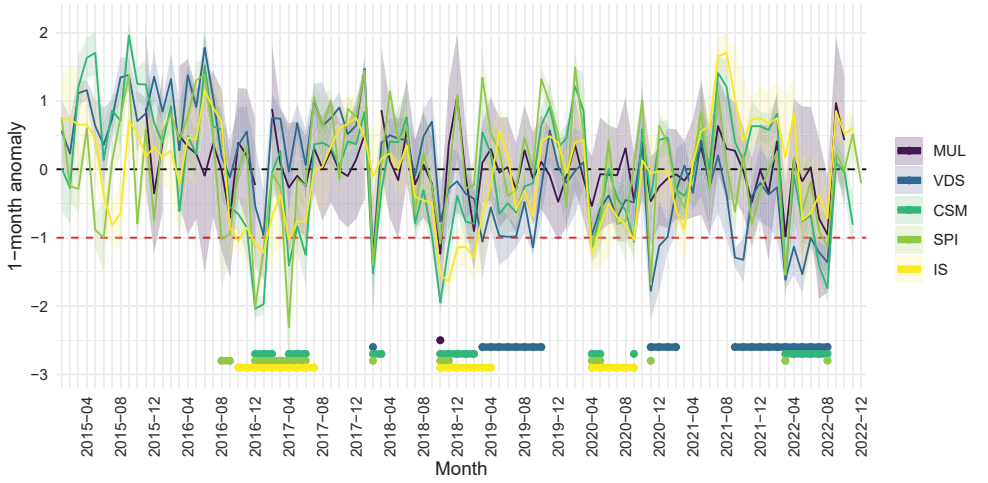

Figure 5.2: Temporal evolution of standardised drought indices. Monthly anomaly timeseries of the satellite SM datasets (MUL, VDS, CSM), precipitation (SPI), and in situ SM dataset (IS). Lines and shaded areas show the spatial average and spatial standard deviation over Luxembourg. The horizontal lines at the bottom indicate whether or not a drought was identified in each dataset.

lies) and spatial (bottom, monthly averages) correlation between the different satellite soil moisture and reference datasets.

Fig. 5.3 a and d indicate the correlation between the monthly satellite and in situ SM datasets. The temporal r with in situ data improves for all the datasets with a coarser spatial resolution, except for the VDS dataset that shows its highest r at the 1 km resolution (median of 0.42). The highest temporal correlations are found for the CSM dataset at the 10 km resolution, with a median r of 0.67. That is also the dataset with the smallest spread in temporal correlations. Unlike the temporal correlations, the spatial correlations of monthly average SM with in situ data are lowest at the 10 km resolution. The dataset with the highest spatial r is the VDS SM dataset at a 1 km resolution, with a median of 0.45.

The middle panels in Fig. 5.3 compare the different satellite SMA (b) and SM (e) datasets to the SPI1 reference dataset. The patterns are similar in the temporal and the spatial correlation: both the MUL and CSM dataset show comparably high correlations (0.49 and 0.56, respectively) and the VDS dataset has a lower median correlation (0.36).

Finally, panels c and f show a comparison between the different satellite soil moisture datasets. The temporal correlation between VDS and CSM SMA is constant moving from fine to coarse resolutions with a median ranging between 0.49 and 0.50. The other two pairs show higher temporal correlations at coarser resolutions than at fine resolutions. The highest temporal correlations were found between the CSM and VDS SMA datasets

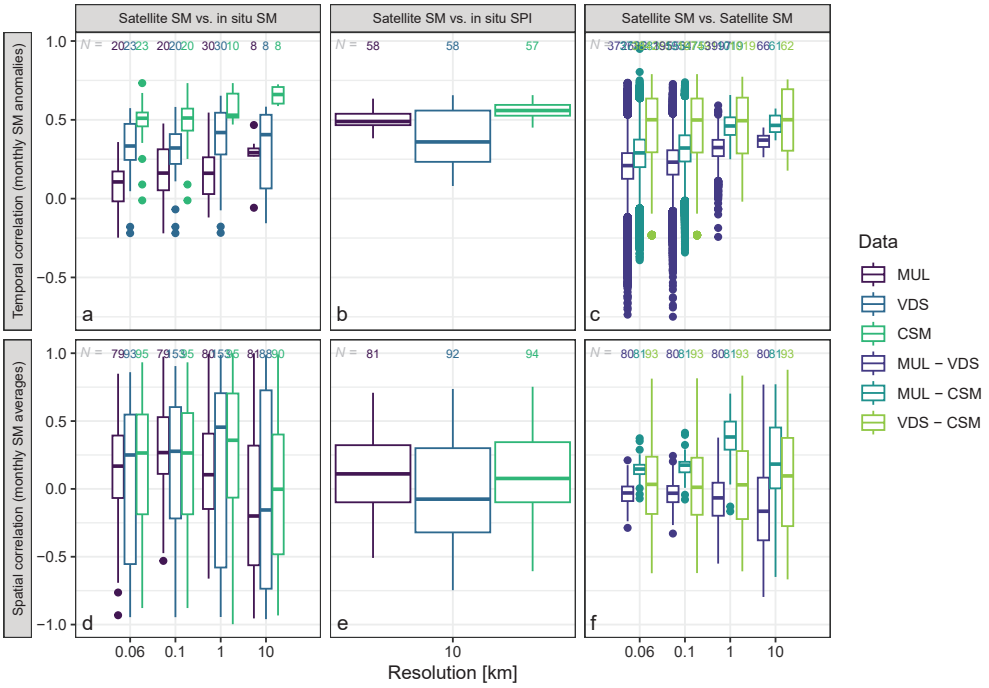

Figure 5.3: Comparison between the various datasets over the study area. Temporal correlations are shown for monthly satellite soil moisture anomalies (SMA, a,b,c) and spatial correlations for monthly soil moisture averages (SM, d,e,f). Soil moisture datasets were compared to in situ soil moisture (a,d), SPI1 (b,e) and other soil moisture datasets (c,f).

at a 10 km resolution (0.50), and the lowest temporal correlations between the MUL and VDS SMA datasets at a 60 m resolution (0.21).

For the spatial correlation, again the VDS–CSM comparison shows a rather constant trend with coarsening resolution. The correlation between monthly SM averages in MUL and CSM increases to a median of 0.38 at a 1 km resolution and is lower again at a 10 km resolution. Interestingly, the correlation between MUL and VDS decreases with coarsening resolution. Highest spatial correlations are found between MUL and CSM at a 1 km resolution, and lowest between MUL and VDS at a 10 km resolution (−0.16).

5.3.3 Spatial subsets

Although the time series and the performance metrics give an adequate view on the average performance over the entirety of the study area, they do not show how drought conditions vary in space. Here, we focus on three spatial subregions during the summer of 2022, when two out of three satellite SMA datasets identified a drought on a national scale (Fig. 5.2). Our

focus here is on a summer drought, rather than a winter drought, since these droughts have a more direct and severe impact on agricultural vegetation (Stagge et al., 2015). The three regions (Fig. 5.4) for this analysis were chosen because of their differences in geology and land use. The northern subset is located in the Eisleck region that is characterised by schists. The eastern subset on the other hand is located in Gutland, characterised by sandstones. The western subset is located on the border between the two geological regions and contains one of the in situ stations that had data over this summer.

Fig. 5.4 shows the three spatial subsets, with their respective timeseries of SMA and SPI during the summer of 2022. Differences between the regions are identified in both the drought duration and the drought intensity. Some similarities are also visible in the different regions: all of them have their minima in March and August, and experienced a wet month in September. Moreover, even though on a national scale the 2022 drought was identified in only two of the satellite soil moisture datasets, on a local scale, throughout the three locations, a drought was identified in all of them.

In the western subregion (left column in Fig. 5.4), SMA in the MUL dataset has an almost identical temporal variation as SPI, but the in situ SMA are considerably different from both the satellite SMA and the SPI, especially in the beginning of the growing season. In the eastern subregion (right column) it is CSM that follows SPI most closely. In the northern subregion (central column), both CSM and MUL SMA follow the reference SPI rather well. Together, these images show that it depends on the region which satellite soil moisture dataset most accurately describes drought conditions. This is confirmed in the hit- and false alarm rates (Table D1) and in Figs. D1 and D2, that show for each 10 km pixel during the 2022 growing season which satellite SMA dataset has the highest temporal correlation with in situ and SPI data, respectively. Figs. D3 and D4 show the same analysis, but for the full time period (2015–2022).

The spatial images in Fig. 5.4 depict local spatial variation in drought conditions in August 2022. Both CSM and VDS show a spatially constant SMA. These smooth appearances are also visible in the low values for spatial standard deviation in the timeseries of Figs. 5.2 and 5.4. The MUL dataset, on the other hand, shows more spatial variation and even contains pixels with a wet soil moisture anomaly. For the western and northern region, these wet pixels are concentrated around the borders of more vegetated regions visible in the RGB image, which could indicate that the influence of vegetation is not sufficiently masked out. It could also indicate that these transition zones are in fact less impacted by drought conditions. These transition zone are more shaded and sheltered than agricultural fields and hence have lower temperatures and less evaporation, directly impacting surface soil moisture. The southeastern region does not seem to be impacted by these transition zones: wet pixels are more spatially distributed over the image.

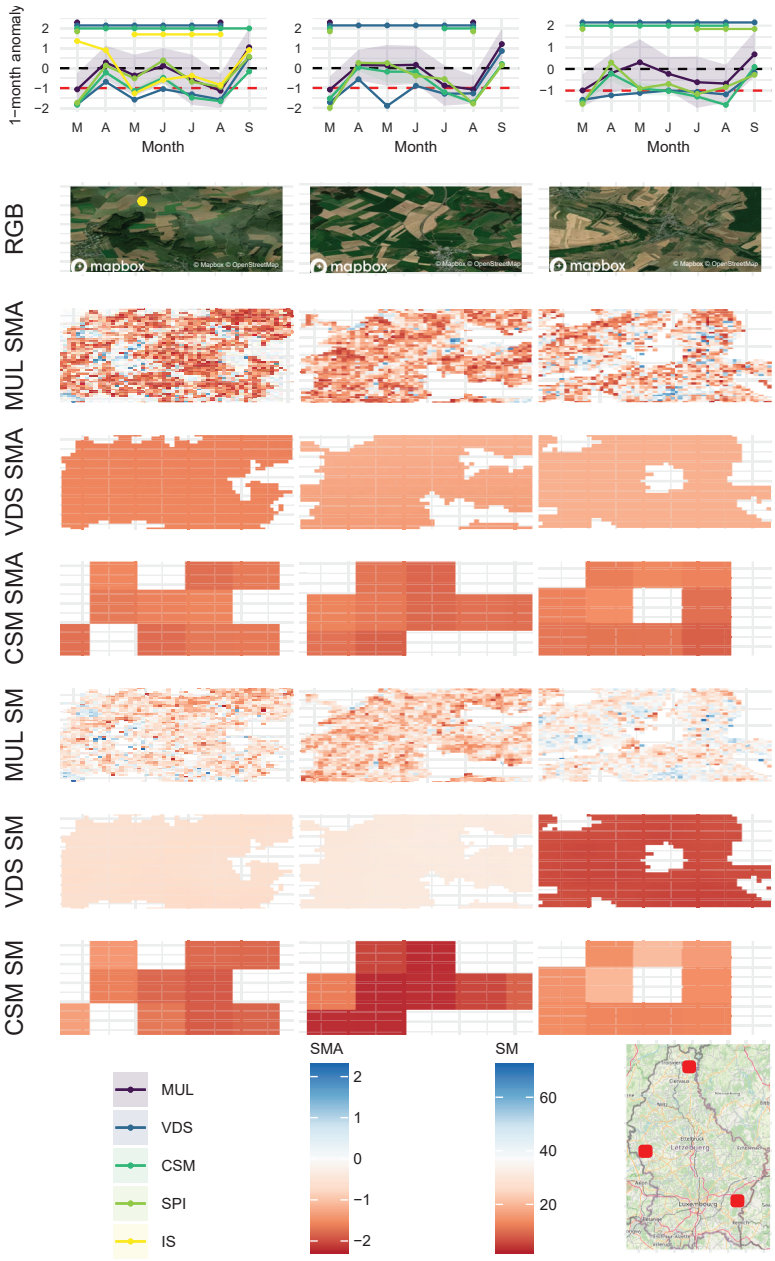

Figure 5.4: Illustration of spatial variation in satellite SMA and SM during the summer of 2022 for three subregions. The timeseries show spatial mean and standard deviation over the three regions shown in the map at the bottom of the figure. Horizontal lines in the timeseries show whether or not a drought was identified in each of the datasets. Spatial plots are shown the western (left), northern (middle) and eastern (right) subset for August, the driest month of that summer for most satellite SMA (middle) and SM (bottom) datasets. RGB images are cloudless composites and thus do not necessarily provide information on field conditions in August 2022.

5.4 Discussion

In our analysis, we showed the performance of different hyper- and high resolution surface soil moisture datasets in depicting drought conditions. We compared monthly values and monthly anomalies to those of in situ soil moisture and precipitation reference datasets.

A temporal analysis (Fig. 5.2) showed that, on a national scale, the Copernicus surface soil moisture (CSM) dataset most accurately identified droughts that occurred in the reference datasets. The vanderSat (VDS) dataset had the most false alarms, and the MULESME (MUL) dataset had a high hit rate but at the same time missed most droughts that were identified in the reference datasets. The CSM dataset also showed highest temporal correlations with in situ soil moisture data (Fig. 5.3). Compared with the SPI, both the CSM and MUL datasets had a higher temporal and spatial correlation than the VDS dataset. A spatial analysis on a regional scale showed a high performance of both MUL and CSM compared to SPI data. Droughts in the in situ reference data were not always adequately represented in the different satellite datasets. Out of the three satellite soil moisture anomaly datasets, the MUL data showed the largest spatial variation. The VDS data, even though it had a high spatial resolution, only showed a limited spatial variation. Variation was larger in the CSM data, despite its coarser spatial resolution.

A comparison between the different soil moisture datasets showed that temporal correlations between VDS and CSM were the highest. That is interesting, because CSM and MUL are both based on S1 data, whereas VDS is based on Advanced Microwave Scanning Radiometer (AMSR)2 data. The comparatively low correlation between two datasets based on the same satellite data is likely related to the difference in their respective correction for frozen soils. While CSM data are flagged and removed for extremely low values, likely relating to frozen soils, MUL data were removed whenever temperatures dropped below 2°C, as in Chapter 4. This results in a smaller range of SM values to compute correlations, hence reducing the correlation value. Fig. D5 shows a comparison between the datasets where MUL data hasn't been filtered for temperatures, and does indicate a higher correlation for the two datasets that are based on S1 data.

Although this analysis showed that the higher spatial resolution of MUL and VDS data do currently not lead to higher temporal or spatial correlations than data at coarser resolutions (Fig. 5.2), these fine resolution data can show added value at local scales in depicting local variations in soil moisture drought (Fig. 5.4). In fact, at a 10 km spatial resolution, the MUL data shows similar temporal and higher spatial correlations as the CSM data, that had the highest performance at its own spatial resolution. That means that the MUL data does accurately reflect soil moisture conditions on the large scale. A reason that these good performances at large scales do not translate to those at smaller scales could be that small scale variations in soil moisture are not accurately reflected in reference data.

In most cases, the satellite soil moisture data reflected the SPI reference data more accurately than the in situ reference data. Two factors play a role here. First, in situ data were collected at depths of 5 and 10 cm, deeper than the penetration depth of the satellite signal. This means that there is some lagging and dampening of the soil moisture temporal variation in the in situ data as compared to satellite soil moisture, which describes surface soil moisture only. For a more accurate reflection of soil moisture variations deeper in the soil, a longer satellite wavelength and/or a coupling with land surface model is required (Liu et al., 2016). Second, the in situ data are point measurements, that could be different from the gridded soil moisture data that are presented by the satellite products (e.g. Babaeian et al., 2019; Chen et al., 2019). The SPI data reflect precipitation, which has a smaller spatial variability than soil moisture, especially on the fine resolutions studied here, possibly explaining the higher correlation with the gridded satellite soil moisture products.

In this study, we computed soil moisture anomalies based on a short reference period (i.e., 8 years), because only the VDS dataset had a record longer than this: the Sentinel-1 data that underlies the CSM and MUL datasets was available from 2015 onwards. As recommended by the World Meteorological Organization (WMO), droughts are generally identified based on a reference period of 30 years. Such a long record of satellite soil moisture data does exist, for instance in the 0.25° CCI soil moisture data. Unfortunately, that spatial resolution does not allow for an analysis on high resolutions. The droughts identified in our data have however also been identified in studies where reference data with a larger time span was used (e.g. Bakke et al., 2020; García-Herrera et al., 2019; Rakovec et al., 2022; Toreti et al., 2022).

5.5 Conclusion

Making use of three satellite soil moisture datasets with spatial resolutions ranging from 60 m to 1 km, we showed how these can be used to monitor droughts on local as well as national scales. At large scales, the Copernicus soil moisture dataset at a 1 km resolution showed highest drought monitoring accuracies compared to in situ soil moisture data as well as in situ precipitation data. At smaller scales, the Copernicus dataset still performed well, but local variations in drought conditions could not be distinguished. For some regions, the high resolution (i.e. 60 m, MULESME) soil moisture dataset performed better in comparison with the reference drought dataset. A spatial analysis of the best performing datasets per 10 km pixel did not reveal what caused this difference in performance. Future research should focus on analysing the causes of this discrepancy so that the most suitable soil moisture dataset could be chosen based on local conditions, taking into account that high resolution data could provide more information on the sub-field scale.


6

Chapter 6
Synthesis

6.1 This thesis

Under future warming and increased pressure on the hydrological system, accurate drought monitoring systems are needed to limit the negative impacts of these drought events. Large scale drought monitoring systems should include accurate soil moisture observations, because soil moisture plays a central role in the water cycle (Fig. 1.1). Although large scale soil moisture data exist, they are limited by their coarse resolution. At high resolutions, soil moisture data can additionally be used to alleviate drought impacts on a local scale. That is why this thesis discussed soil moisture drought monitoring on both low and high resolutions, and the impacts of soil moisture droughts on vegetation. Here I synthesise the main findings of this thesis, interpret their combined strengths and weaknesses, and put the conclusions into context of scientific challenges and opportunities.

6.2 Main findings

Soil moisture droughts are often referred to as agricultural droughts because of their large impact on vegetation. However, drought impacts on vegetation are not always negative because these drought events often coincide with increased solar energy. Hence, the term *agricultural drought* could be ambiguous. Chapter 2 compared soil moisture and vegetation patterns during major European drought events in the past two decades to test the ambiguity of the term agricultural drought. A clear asynchrony was found between the surface soil moisture drought and the impact of these droughts on vegetation. This was especially true in energy-limited regions, such as mountain ranges and high latitude regions. In general, negative anomalies in vegetation occurred with a delay compared to negative anomalies in soil moisture. Occasionally, soil moisture droughts coincided with positive anomalies in vegetation. Negative vegetation anomalies were also found in some of the events, even though no soil moisture drought was observed. Overforecasting, i.e., when more droughts are forecasted using soil moisture than there are droughts observed in vegetation, generally occurred in the beginning of the growing season, whereas underforecasting occurred near the end of the growing season.

For the monitoring of small-scale variations in soil moisture droughts, high resolution soil moisture data are needed. The next two chapters therefore focused on retrieving high resolution soil moisture data and on testing their potential over an agricultural field in southeastern Luxembourg. Chapter 3 discussed two strategies for retrieving high resolution soil moisture data from native Sentinel-1 backscatter data: the Calculate-then-Average (CtA) and Average-then-Calculate (AtC) strategies. Both were tested in a synthetic and a field experiment with spatial resolutions ranging from 20 to 120 m, to determine the strategy with the most accurate results. The CtA strategy applied to native resolution (20 m) Sentinel-1 data led to a higher performance on all tested target resolutions (20–120 m). CtA

works especially well when the difference between source resolution and target resolution increases, and performance peaks at the lowest target resolution. With an increasing spatial variability in the data, the performance variations between the different strategies increased. This indicated that when more information is contained in the backscatter data, more information relevant to soil moisture retrieval is lost during the averaging.

In Chapter 4 the CtA strategy was applied in a field experiment to explore the limits in spatial resolution of active microwave soil moisture retrievals. Under bare soil conditions, in situ soil moisture variability was captured well by the satellite estimates, albeit with a bias. During periods with substantial vegetation, frozen soils, or standing water on the field, the performance of satellite estimates was much lower. At a 60 m resolution, an average temporal correlation of 0.67 was found and spatial variation could still be distinguished. Spatial correlation remained low, likely due to the limited spatial variability over the field. A case study under favourable field conditions did show that short-term soil moisture variability could be captured at a 60 m resolution regardless of the low spatial correlation.

This 60 m resolution satellite soil moisture dataset was then used in Chapter 5 for a study over a larger scale. The aim was to determine the value of high resolution soil moisture data for drought monitoring. The 60 m dataset was used together with two other high spatial resolution datasets (100 m, 1 km). These three satellite datasets were compared to in situ soil moisture and precipitation anomalies on local and regional scales. Local scale monitoring allows for drought monitoring on the agricultural field scale, while regional scale monitoring can provide a general quantification of drought conditions that can be relevant for policy makers. At both these scales, the 1 km resolution soil moisture data showed the highest drought monitoring accuracy compared to reference drought data. At local scales, the added benefit of higher resolution data became clear. Those data allowed for monitoring local scale soil moisture drought variations, whereas the 1 km resolution data did not show local variations in drought conditions.

6.3 Conclusions

This thesis had two main objectives. First, to obtain accurate satellite soil moisture observations at a high resolution (Chapters 3 and 4), and second, to determine the relevance of state-of-the-art soil moisture data for drought monitoring (Chapters 2 and 5). Together, these objectives enabled the answering of the research questions posed in Chapter 1.

What is the value of state-of-the-art satellite soil moisture products for drought monitoring?

Based on the asynchrony between soil moisture droughts and vegetation droughts derived from state-of-the-art Earth observation data, it was suggested to move away from the com-

bined term *agricultural drought*, which can lead to confusion between soil moisture and vegetation effects. Instead, it was recommended to use two separate terms: soil moisture drought and vegetation drought, each with their own indices and use in drought monitoring and forecasting. This can prevent false drought alarms, and may benefit accurate drought monitoring and prediction. State-of-the-art satellite soil moisture products can thus not be used for vegetation drought monitoring, but they can be used for soil moisture drought monitoring on large scales. That means that, at their present state, soil moisture products are useful for policy makers to derive large scale strategies. They can however not yet be used to provide information on the (sub-)plot scale to inform farmers on water-saving or yield-saving strategies.

What is the highest spatial resolution at which soil moisture can be accurately retrieved from satellite data?

Important information on soil moisture conditions is lost when the AtC strategy is applied on high resolution data. Using the CtA strategy can retain this information and results in higher retrieval performance. Hence, retrieving soil moisture at fine resolutions prior to multilooking, results in higher retrieval performance at both fine and coarse target resolutions. This CtA strategy was applied on native backscatter data to retrieve soil moisture at six different resolutions ranging from 20 to 120 m. The coarsest of these resolutions did not allow for an analysis of sub-field soil moisture variability, while the finest did not result in sufficiently high retrieval performance. The highest spatial resolution at which soil moisture could be accurately retrieved was found to be 60 m.

Can high resolution satellite soil moisture data be used for large scale drought monitoring?

On large scales, state-of-the-art soil moisture products of 1 km currently perform better than products with a higher spatial resolution, compared to in situ and precipitation reference drought data. However, based on the results from chapters 4 and 5, high resolution soil moisture data do show promising results for drought monitoring at higher spatial resolutions. To further improve performance of the high resolution soil moisture products, retrieval limitations will need to be addressed in future research.

6.4 Limitations of satellite soil moisture observations

The relatively low performance of the high resolution satellite soil moisture dataset presented here does not stand on its own. Previous comparisons between satellite and in situ data have also not always led to high correlations. For instance Zheng et al. (2022) compared 24 active, passive and merged satellite as well as modelled soil moisture datasets with an in situ dataset. Spatial resolutions ranged from 0.1° to 36 km, and the highest

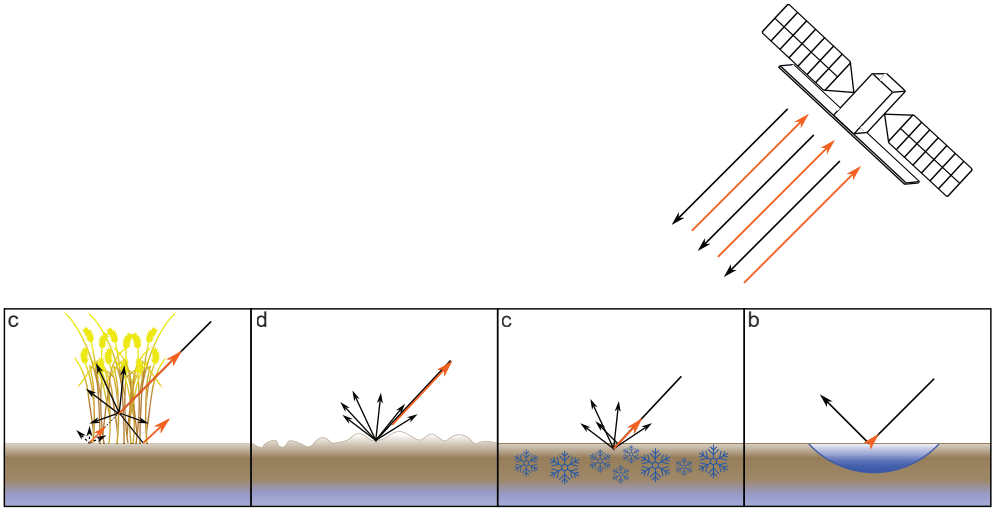

Figure 6.1: Factors influencing the backscatter signal: vegetation (a), roughness (b), frost and snow (c) and standing water (d).

correlation with in situ data was found to be 0.666 for a modelled soil moisture product. This is very similar to the correlation that was found with the 60 m satellite soil moisture dataset over the field in southeastern Luxembourg (0.67).

Considering the limited correlation found in this thesis, the accuracy of satellite soil moisture products (and especially that of high resolution products) should be improved. Uncertainties from three sources need to be addressed: the backscatter signal, the retrieval algorithm, and the in situ observations.

Backscatter signal

The backscatter signal is influenced not only by soil moisture, but also by speckle (Chapter 5) and field conditions such as dense vegetation, soil roughness, frozen soils, or standing water (Fig. 6.1, Baghdadi et al., 2018). These limitations in field conditions were confirmed by the results in Chapter 4, where they played a substantial role in the experimental field (Fig. 4.4).

Vegetation

Vegetation influences the backscatter signal, via the water contained in the plant as well as plant structure (Ulaby and Long, 2014). That makes it difficult to distinguish which part of the backscatter signal is caused by vegetation and which part is caused by variations in soil moisture. The MULESME algorithm, that was used in this thesis to derive soil moisture content, only corrects for plant water content, not plant structure. This could be one of

the reasons why the influence of vegetation on both the backscatter and the soil moisture signal were still visible in Chapter 4. Ideally, field conditions are used to interpret the data, so that uncertainties can be flagged where necessary. This is easier on small scales, where local knowledge on field conditions can be used. On larger scales this is more difficult. Field conditions then have to be derived from other types of available data such as optical data that can provide information on vegetation greenness, photosynthetic activity, or leaf area as an indicator for vegetation water content. These data do however still not provide any information on plant structure.

Crop type information can be useful to derive plant structure, which in turn can be used for improved correction of the backscatter signal. Moreover, different crops go through growth stages in different climates and at different times of the year, and with it, the crop's sensitivity to drought (Stagge et al., 2015). It is vital that especially at the vegetation's most sensitive growth stages, soil moisture is measured accurately. In that case, drought mitigation measures can be taken at the right time and place to most efficiently reduce drought impact on the crops.

Roughness

Soil roughness influences the backscatter signal because the soil scatters the signal (Fig. 6.1). However, compared to soil moisture, it varies only slowly. In multitemporal retrieval algorithms roughness is therefore often assumed to be constant, reducing the ill-posedness of the retrieval. The same is done in MULESME, where roughness is estimated together with soil moisture. At the same time, while soil roughness varies more slowly than soil moisture, it still varies as a result of precipitation and farming activity. Ideally, similarly to vegetation, local knowledge is used to flag such conditions, as was done in Chapter 4. On large scales this, again, is not possible. Unfortunately, unlike vegetation, no large scale roughness products exist to help account for this uncertainty.

While the roughness interference with the microwave signal is inherent to the SAR signal, the signal's sensitivity to roughness does depend on the polarisation: VV is often found to be less sensitive than VH and HH (Baghdadi et al., 2008). This is the polarisation that was used in this thesis to retrieve soil moisture. Since soil roughness depends on soil type as well as environmental variables, perhaps global soil type datasets could be used in soil moisture retrieval algorithms to predict the fraction of the backscatter signal that is caused by roughness to allow for a better soil moisture estimation.

Speckle

Image speckle has a large influence on the backscatter signal, especially at high resolution approaches. To reduce speckle, the backscatter signal is generally multilooked before the signal is transformed to soil moisture data. This leads to an information loss, that can be minimised by retrieving soil moisture prior to the spatial average. The same concept

holds in other speckle filters, and so the CtA strategy could be applied in combination with other types of speckle filters to further improve soil moisture retrieval accuracy. Whether this works should still be studied in future scientific work.

Retrieval algorithm

Differences between soil moisture retrieval algorithms lead to differences in soil moisture products (Chapters 4 and 5). In this thesis, a comparison was performed between MULESME and the TU Wien algorithm. Both use Sentinel-1 data as input. Differences were found in spatial and temporal correlations for the experimental field as well as on larger scales. These differences in performance can only result from differences in the retrieval strategy, because both the MULESME and the TU Wien algorithm use the same input data and because their respective outputs were compared to the same reference data.

There are several reasons why the results can differ between the two algorithms. First, the retrieval approach is different: MULESME is a multitemporal algorithm while the TU Wien algorithm is a change detection algorithm. This results in absolute soil moisture values for the MULESME algorithm, and relative values for the TU Wien algorithm. Secondly, while vegetation and roughness are corrected for in both algorithms, their methods are different. Thirdly, the model parameters in the TU Wien algorithm are calibrated for each pixel using a multi-year backscatter dataset while parameters in the MULESME algorithm are empirical and do not require such a pixel-based calibration. It is difficult to say which of these could have caused the difference in performance, but it is possible that both have their merits under different conditions and at different locations (Fig. D2).

To further improve the algorithm, vegetation correction could be improved based on a more direct vegetation water content estimation, rather than an empirical conversion from NDVI to this water content, and an inclusion of vegetation structure. An automated temperature flagging could be added, so that frozen soils can be masked out automatically, rather than in the postprocessing phase. Chapter 5 also showed that the different tested datasets (and hence algorithms) showed a spatial distribution in terms of which datasets performed best. Ideally, I envision a high resolution soil moisture dataset where soil moisture is retrieved from backscatter data with the algorithm that works best in that specific location, under those specific conditions, and dependent on the needs and requirements of the end users.

In situ data

Finally, uncertainties also exist in in situ observations, especially the spatial resolutions relevant for satellite retrievals (Gruber et al., 2020). Since soil moisture has a large local variability, individual in situ point observations are likely to be different from gridded soil moisture (Babaeian et al., 2019; Famiglietti et al., 2008; Vereecken et al., 2008; Western and Bloschl, 1999). In theory, this could mean that the satellites observe soil moisture

accurately, but the in situ data does not adequately capture small-scale variations in soil moisture, leading to low correlations between the two observations.

Once an accurate gridded in situ observation of soil moisture has been made, the next challenge is to relate this to the satellite signal. The penetration depth of the SAR signal depends on the signal wavelength, as well as on moisture conditions in the field (Baghdadi et al., 2008; Ulaby and Long, 2014). C-band SAR signals have a penetration depth of about 1.5–3.5 cm. This is shallower than most in situ data, that are generally collected deeper in the soil, because of the higher uncertainty in shallower measurements.

Using a retrieval algorithm, the C-band satellite signal can be transformed to a surface soil moisture estimate. Ideally, the root zone soil moisture could be retrieved. That would allow us to more accurately predict soil moisture drought impacts, and to directly compare the data with less uncertain in situ soil moisture estimates. Because satellites can not measure soil moisture at those depths, root zone soil moisture is often estimated by combining satellite soil moisture data with a land surface model (e.g. Reichle et al., 2022; Tobin et al., 2019). These are however not direct observations of field conditions, and this additional conceptualisation comes with additional uncertainties.

6.5 Opportunities and outlook

Although the present state of high resolution satellite soil moisture retrieval for drought monitoring still has its limitations, this thesis showed the potential of Sentinel-1 for drought monitoring on the sub-field scale. The data can already be useful on bare soil fields for drought monitoring and mitigation. Continued efforts to improve the data and future microwave missions can make remotely sensed soil moisture data useful for a larger range of field and climatic conditions.

Drought monitoring

Chapter 5 showed the applicability of high resolution satellite soil moisture for plot scale drought monitoring. The data could follow temporal variations in soil moisture well on the pixel scale. In regions with larger spatial variation in soil moisture, such as regions with irrigated agriculture, spatial patterns might also be adequately captured. These regions can also benefit most from accurate drought monitoring systems, because of a larger pressure on the hydrological system.

Drought mitigation

Since the soil moisture data is available on the sub-field scale, it can be used for precision agriculture purposes. Farmers could adapt their irrigation systems so that only dry pixels in the field are irrigated. This leads to drought mitigation as well as drought prevention: on

the one hand, drought conditions in the field are alleviated by irrigation, and on the other hand, water use is restrained because only areas limited by water content are irrigated. This is especially useful when soil moisture data is combined with other types of (remote sensing) data that can provide information on vegetation functioning. For an efficient drought mitigation strategy, all these data do have to be available to farmers in near-real time.

Outlook

Future work can focus on further improving the signal filtering and data processing to increase the accuracy of high resolution soil moisture products and to make the data useful for a larger range of field and climatic conditions. Improved data can further help local drought mitigation and alleviation strategies as well as regional to national water management strategies. Besides, future satellite missions can have a large impact on data quality and availability. These will in time replace the current satellites and sensors in orbit and so influence future large scale soil moisture products.

The Sentinel-1 satellite constellation will be continued in the future by ESA. The C-satellite is scheduled for launch at the end of 2023, and the fourth in the series (D) in 2024. While the C-satellite will mostly replace the B-satellite that failed at the end of 2021, the D-satellite could possible further improve the temporal resolution of the constellation, dependent on the lifespan of Sentinel-1A. Such an improvement in temporal resolution would not only directly improve the temporal resolution of soil moisture datasets, but also likely improve their accuracy in two ways. Either the assumption of roughness is more valid: the five used images are retrieved over a shorter window of time, or more images are used for the retrieval, thereby decreasing the ill-posedness of the retrieval algorithm. A continuation of the Sentinel-1 constellation will also help drought monitoring because a longer data availability allows for a more accurate drought quantification: The 8 year time span used in this thesis is somewhat short of the 30 year time span recommended by WMO for climatic comparisons.

At L-band, ESA is currently planning the ROSE-L mission, of which the first satellite is scheduled to launch in 2028 (Davidson et al., 2019). With a similar set-up as the Sentinel-1 mission, its aim is to complement Sentinel-1 C-band data. Due to its longer wavelength, L-band data has two main advantages compared to C-band data: an increased accuracy under vegetation cover, and a larger soil penetration depth. This will be extremely helpful in increasing sensing accuracy during the growing season, as well as performing measurements towards the root zone depth, thereby increasing the measurement's relevance for plant functioning.

The increasing number of private satellites could be an opportunity for drought monitoring as well, dependent on the amount of openly available data that results from these efforts. Currently, the large scale monitoring efforts by the large space agencies are still more

interesting because of their longer time span and stricter acquisition schedules. Non-open data lead to limited scientific and end-user usability of the data, who rely on governments to buy these data. Not only open data availability important, but also its availability in near-real time. While data with a longer latency can be useful for scientific purposes, i.e. improving retrieval algorithms, for drought management and water management in general, it is imperative that the data are made available shortly after they are retrieved so that they can be used for drought mitigation and drought alleviation. In the end, scientific findings need to be available to the public for its impact on society to be largest.

Appendices

A Appendices to Chapter 2

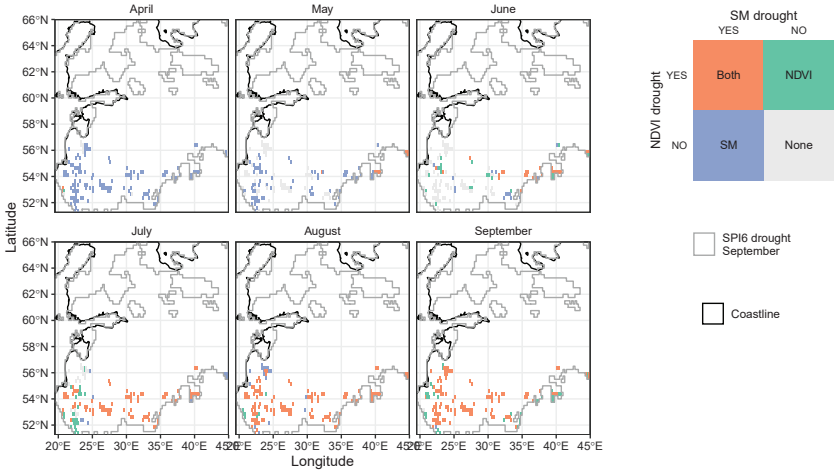

Figure A1: Soil moisture and vegetation anomalies during the 2002 growing season, produced in the same way as Figure 2.3.

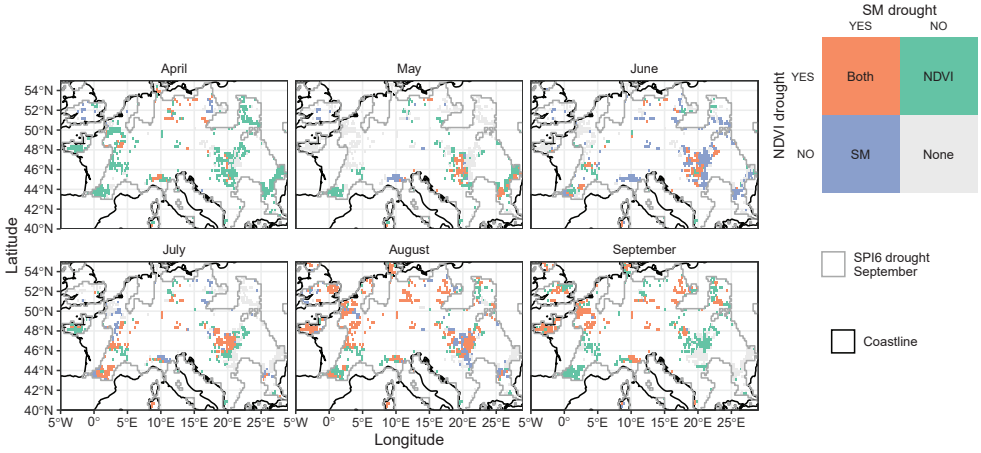

Figure A2: Soil moisture and vegetation anomalies during the 2003 growing season, produced in the same way as Figure 2.3.

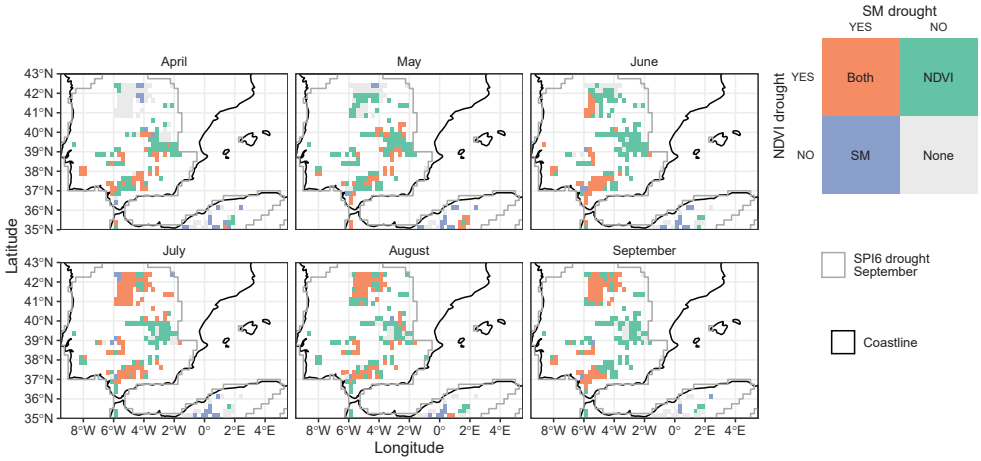

Figure A3: Soil moisture and vegetation anomalies during the 2005 growing season, produced in the same way as Figure 2.3.

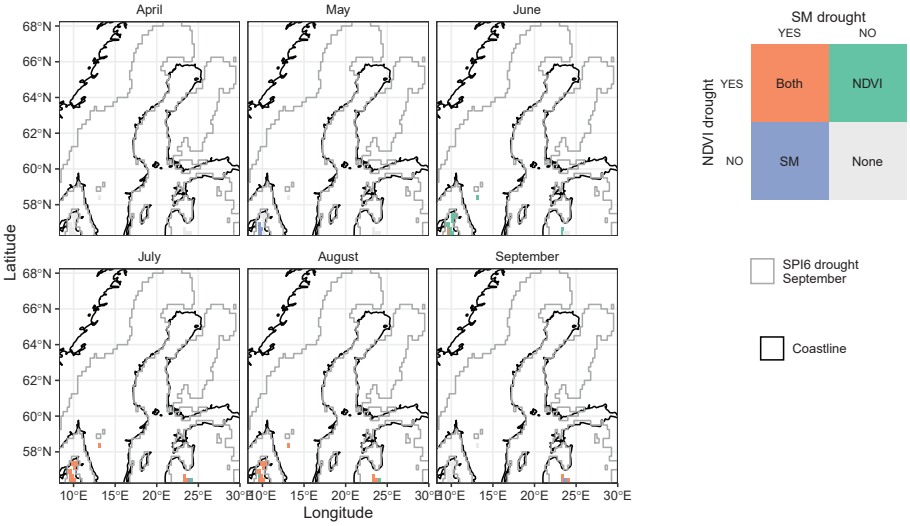

Figure A4: Soil moisture and vegetation anomalies during the 2018 growing season (northern part of drought event), produced in the same way as Figure 2.3.

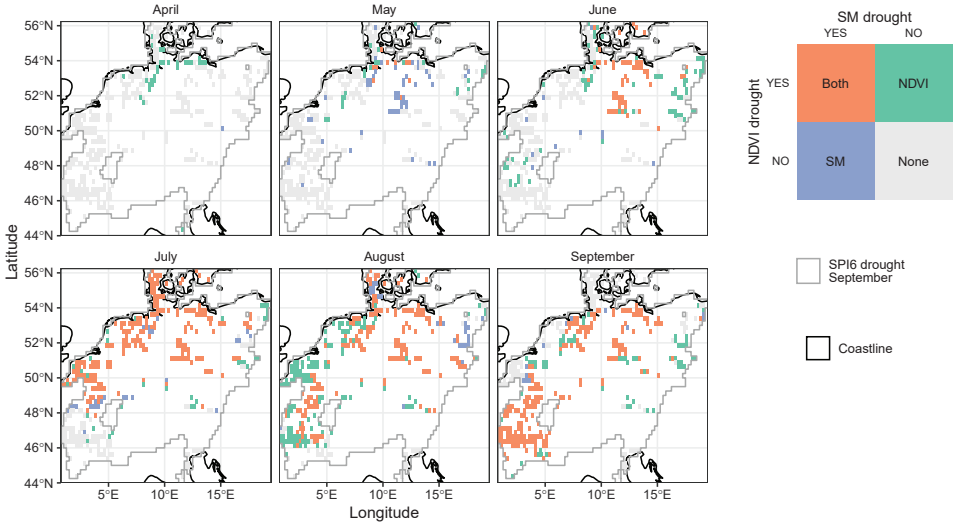

Figure A5: Soil moisture and vegetation anomalies during the 2018 growing season (southern part of drought event), produced in the same way as Figure 2.3.

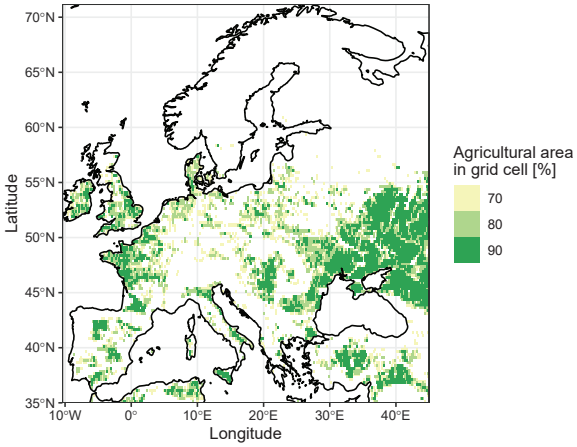

Figure A6: Percentages of agricultural area in the 0.25° grid cells in the study area. We opted to use the 80% mask in the analysis to balance the number of used grid cells and an accurate representation of the area.

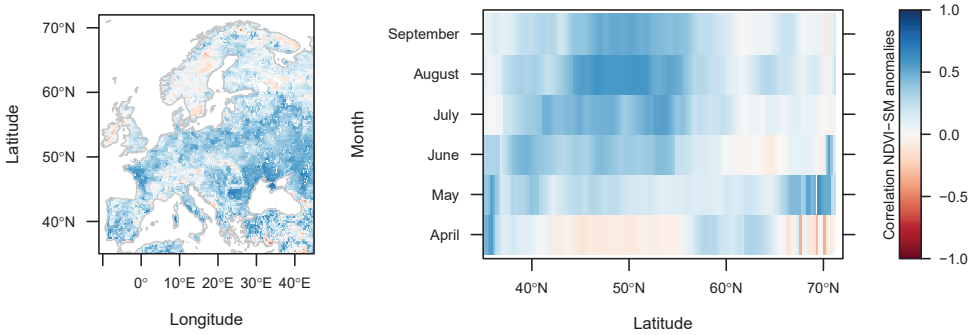

Figure A7: Correlation between soil moisture and NDVI, in space (left), and zonal averages throughout the growing season (right).

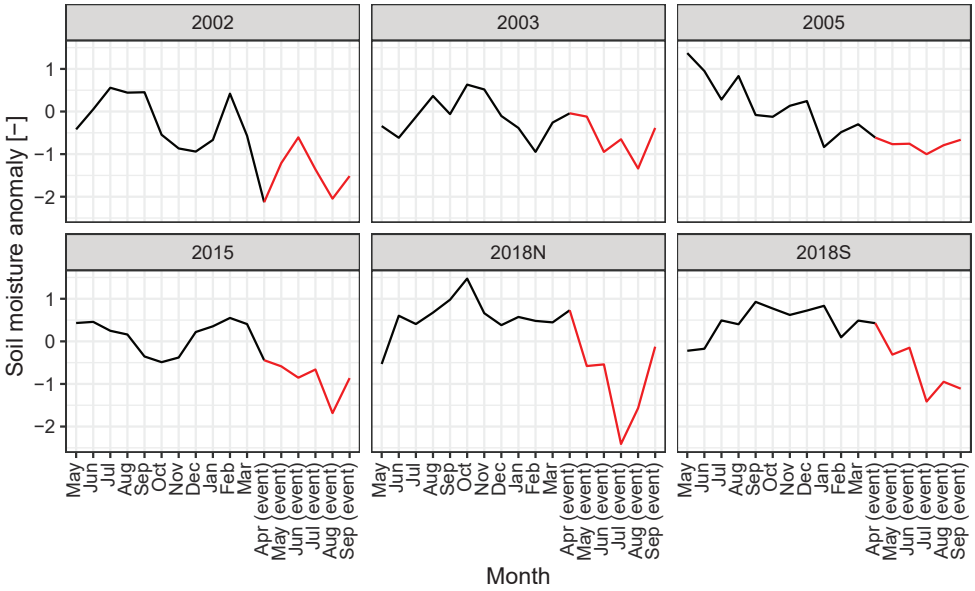

Figure A8: Average soil moisture anomalies in event areas prior to (black) and during (red) each event.

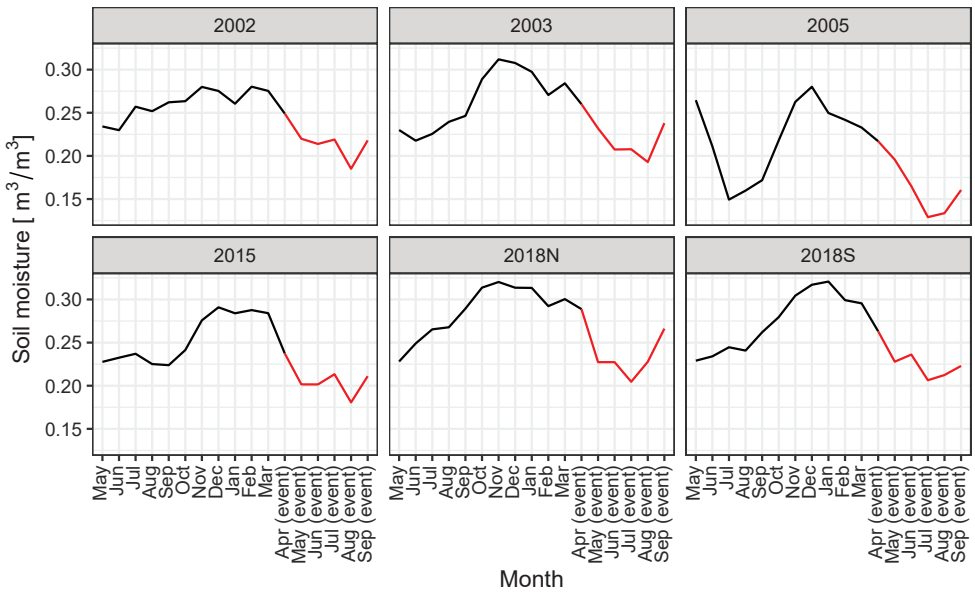

Figure A9: Average soil moisture in event areas prior to (black) and during (red) each event.

Figure A10: Average NDVI anomalies in event areas prior to (black) and during (red) each event.

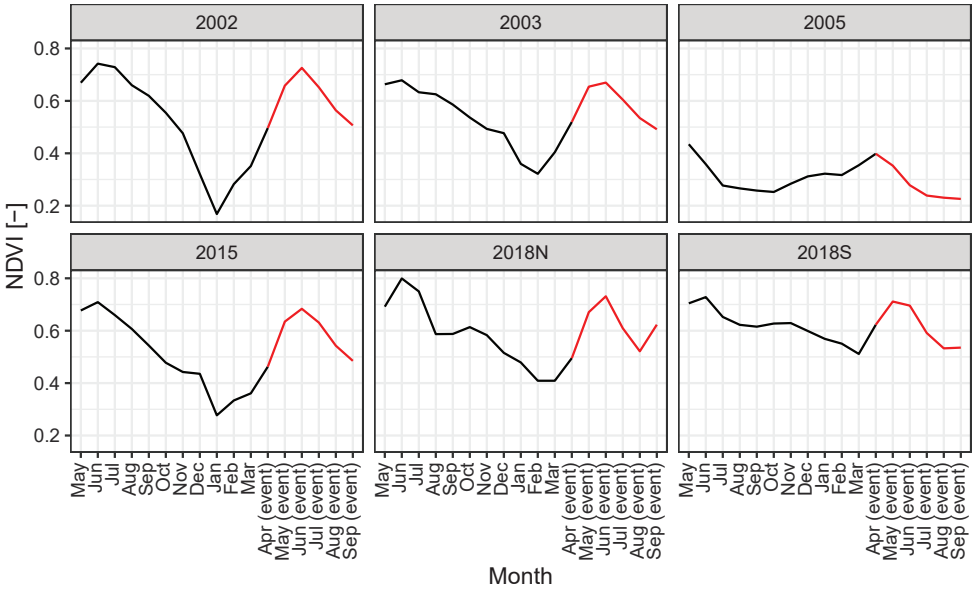

Figure A11: Average NDVI in event areas prior to (black) and during (red) each event.

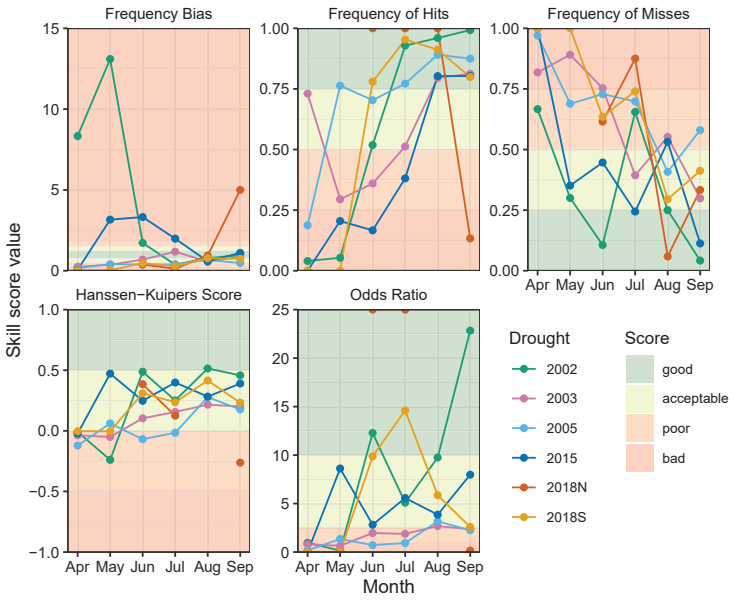

Figure A12: Skill scores for soil moisture drought as a proxy for vegetation drought, with a 1 month lag between soil moisture and vegetation. Background colours indicate the quality of the skill scores (see Methods for their description), and the lines show different drought events. The Odds Ratios for June and July in the 2018N event are both infinity, due to zero False Alarms in both cases, and are plotted at the top of the graph.

B Appendices to Chapter 3

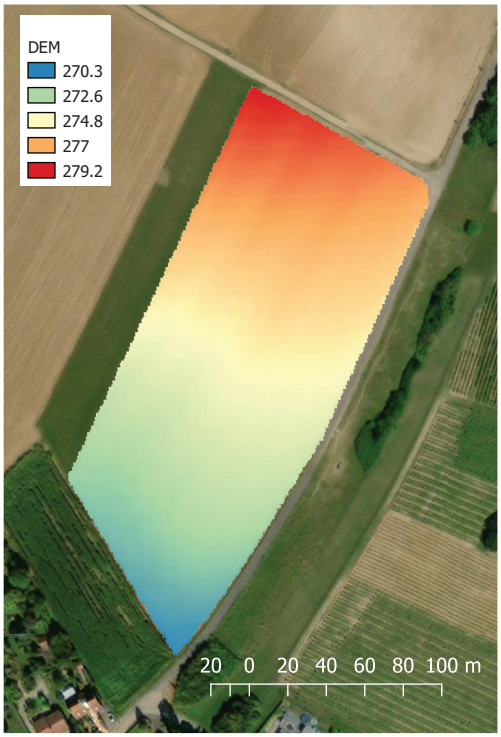

Figure B1: DEM over the studied agricultural field, slowing a mild slope over the field.

C Appendices to Chapter 4

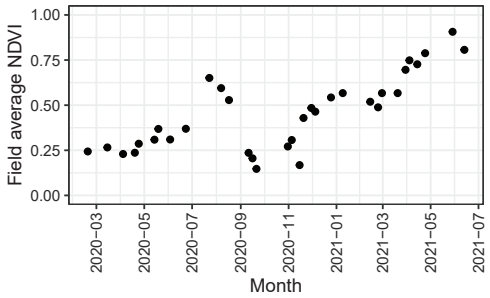

Figure C1: Time series of average NDVI in the studied agricultural field, where maize was grown in the first growing season, and winter wheat in the second.

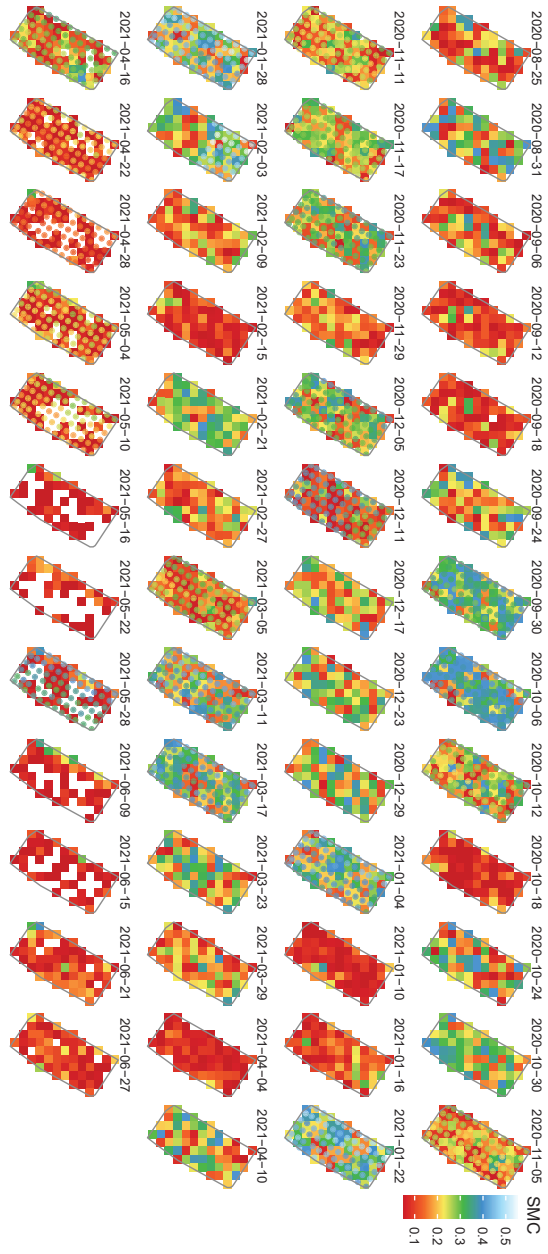

Figure C2: All RO37 SM retrievals at 20 m resolution, overlain with in situ TDR data

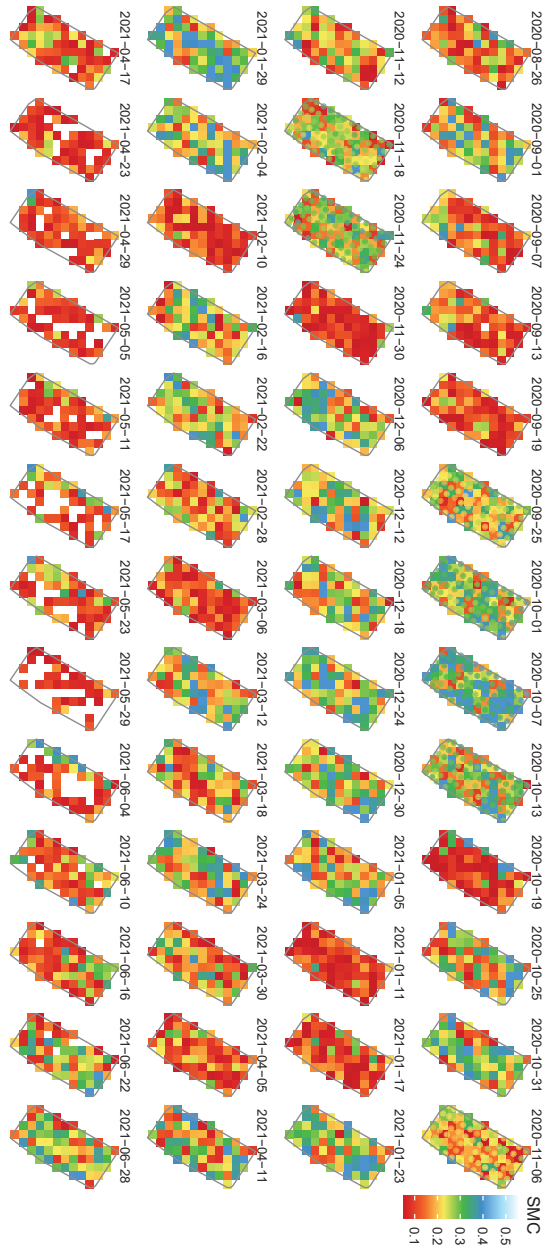

Figure C3: All RO139 SM retrievals at 20 m resolution, overlain with in situ TDR data

D Appendices to Chapter 5

Table D1: Hit rates (HR = H/(H+M)) and False Alarm rates (FA/(FA+CR)) for the spatial and temporal extents described in Chapter 5. The subsets refer to the regions shown in Fig. 5.4.

Time period		Full		Mar - Sep 2022					
Extent		Luxembourg		Western subset		Central subset		Eastern subset	
ref. data	SM data	HR	FAR	HR	FAR	HR	FAR	HR	FAR
SPI	MUL	0.06	0.00	1	0.17	1	0	0	0
	VDS	0.24	0.28	1	0.83	1	0.80	1	1
	CSM	0.76	0.12	1	1	1	0.20	0.75	1
IS	MUL	0.04	0	1	1				
	VDS	0.09	0.33	1	0.67				
	CSM	0.61	0.11	0.25	0.33				

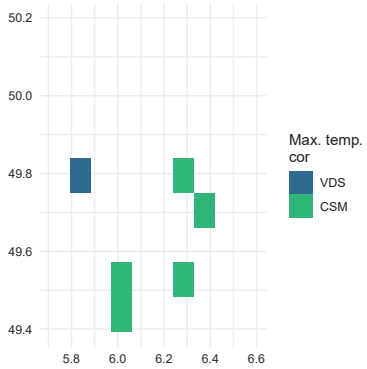

Figure D1: Illustration showing which of the satellite soil moisture anomaly datasets have the highest maximum temporal correlation with **in situ** data in each of the 10 km pixels in the period between March and September 2022 (the same period as the one illustrated in Fig. 5.4

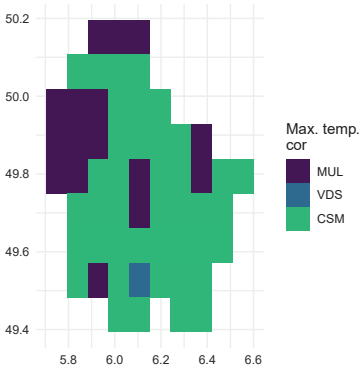

Figure D2: Illustration showing which of the satellite soil moisture anomaly datasets have the highest maximum temporal correlation with **SPI** data in each of the 10 km pixels in the period between March and September 2022 (the same period as the one illustrated in Fig. 5.4).

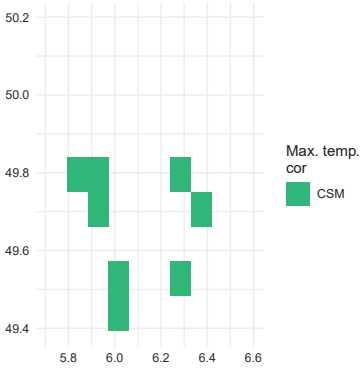

Figure D3: Illustration showing which of the satellite soil moisture anomaly datasets have the highest maximum temporal correlation with **in situ** data in each of the 10 km pixels in the full time period (2015–2022).

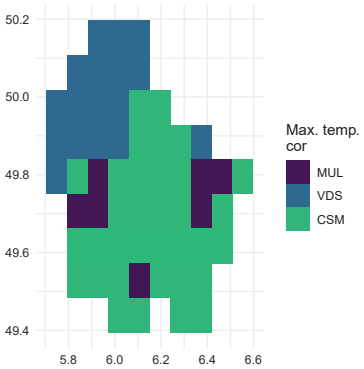

Figure D4: Illustration showing which of the satellite soil moisture anomaly datasets have the highest maximum temporal correlation with **SPI** data in each of the 10 km pixels in the full time period (2015–2022).

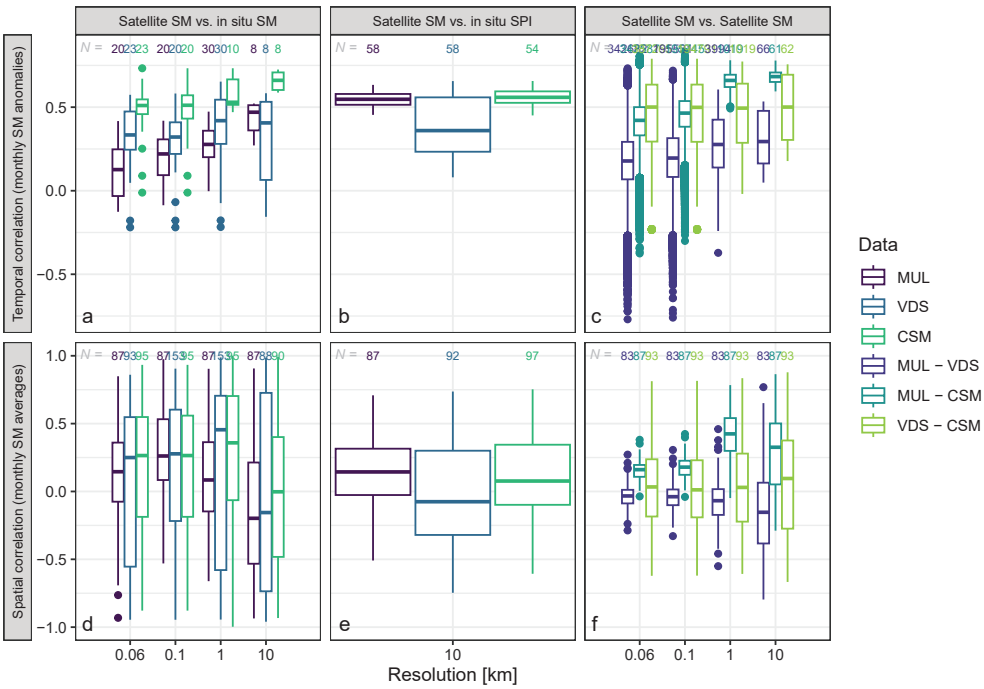

Figure D5: Comparison between the various datasets over the study area. The figure shows results as in Fig. 5.3, but without the temperature filtering applied to the MUL dataset. Temporal correlations are shown for monthly satellite soil moisture anomalies (SMA, a,b,c) and spatial correlations for monthly soil moisture averages (SM, d,e,f). Soil moisture datasets were compared to in situ soil moisture (a,d), SPI1 (b,e) and other soil moisture datasets (c,f).

Acronyms

r	Pearson correlation
AMSR	Advanced Microwave Scanning Radiometer
ASCAT	Advanced SCATterometer
AtC	Average-then-Calculate
CCI	Climate Change Initiative
CLC	Corine Land Cover
CR	Correct Rejections
CSM	Copernicus Global Land service Surface Soil Moisture
CtA	Calculate-then-Average
DEM	Digital Elevation Model
ESA	European Space Agency
FA	False Alarms
FB	Frequency Bias
FOH	Frequency of Hits
FOM	Frequency of Misses
GRD	ground-range detected
H	Hits
HK	Hanssen–Kuipers score

IS In Situ

ISMN International Soil Moisture Network

IW Interferometric Wide swath

LIA Local Incidence Angle

LUT Look Up Table

M Misses

MODIS Moderate-resolution Imaging Spectroradiometer

MUL MULESME surface soil moisture

MULESME MUltitemporal LEast Square Moisture Estimator

NASA National Aeronautics and Space Administration

NDVI Normalized Difference Vegetation Index

NDVIA anomalies in NDVI

OR Odds Ratio

PDSI Palmer Drought Severity Index

PWC Plant Water Content

S1 Sentinel-1

S2 Sentinel-2

SAR Synthetic Aperture Radar

SM soil moisture

SMA anomalies in SM

SNAP Sentinel Application Platform

SPI Standardized Precipitation Index

SRTM Shuttle Radar Topography Mission

TDR Time Domain Reflectivity

ubRMSE unbiased Root Mean Square Error

USDA United States Department of Agriculture

VDS vanderSat surface soil moisture

WMO World Meteorological Organization

References

Abbe, C. (1894). "Drought". *Monthly weather review* 22, 323.

Anyamba, A. and C. J. Tucker (2012). "Historical Perspectives on AVHRR NDVI and Vegetation Drought Monitoring". In: *Remote Sensing of Drought: Innovative Monitoring Approaches*. Ed. by B. D. Wardlow, M. C. Anderson, and J. P. Verdin. CRC Press, 23.

ASTA (2022). *Administration des Services Techniques de l'Agriculture* (*ASTA*) *Precipitation, soil moisture data*. (Visited on 2022).

Attarzadeh, R., J. Amini, C. Notarnicola, and F. Greifeneder (2018). "Synergetic Use of Sentinel-1 and Sentinel-2 Data for Soil Moisture Mapping at Plot Scale". *Remote Sensing* 10.8, 1285. DOI: 10.3390/rs10081285.

Attema, E. P. W. and F. T. Ulaby (1978). "Vegetation modeled as a water cloud". *Radio Science* 13.2, 357. DOI: 10.1029/RS013i002p00357.

Babaeian, E., M. Sadeghi, S. B. Jones, C. Montzka, H. Vereecken, and M. Tuller (2019). "Ground, Proximal, and Satellite Remote Sensing of Soil Moisture". *Reviews of Geophysics* 57.2, 530. DOI: 10.1029/2018RG000618.

Baghdadi, N., H. Bazzi, M. El Hajj, and M. Zribi (2018). "Detection of Frozen Soil Using Sentinel-1 SAR Data". *Remote Sensing* 10.8, 1182. DOI: 10.3390/rs10081182.

Baghdadi, N., O. Cerdan, M. Zribi, V. Auzet, F. Darboux, M. El Hajj, and R. B. Kheir (2008). "Operational performance of current synthetic aperture radar sensors in mapping soil surface characteristics in agricultural environments: application to hydrological and erosion modelling". *Hydrological Processes* 22.1, 9. DOI: 10.1002/hyp.6609.

Bakke, S. J., M. Ionita, and L. M. Tallaksen (2020). "The 2018 northern European hydrological drought and its drivers in a historical perspective". *Hydrology and Earth System Sciences* 24.11, 5621. DOI: 10.5194/hess-24-5621-2020.

Balenzano, A., F. Mattia, G. Satalino, F. P. Lovergine, D. Palmisano, J. Peng, P. Marzahn, U. Wegmuller, O. Cartus, K. Dabrowska-Zielinska, J. P. Musial, M. W. J. Davidson, V. R. N. Pauwels, M. H. Cosh, H. McNairn, J. T. Johnson, J. P. Walker, S. H. Yueh, D. Entekhabi, Y. H. Kerr, and T. J. Jackson (2021). "Sentinel-1 soil moisture at 1 km resolution: a validation study". *Remote Sensing of Environment* 263, 112554. DOI: 10.1016/j.rse.2021.112554.

Balenzano, A., F. Mattia, G. Satalino, and M. W. J. Davidson (2011). "Dense Temporal Series of C- and L-band SAR Data for Soil Moisture Retrieval Over Agricultural Crops". *IEEE Journal of Selected Topics in Applied Earth Observations and Remote Sensing* 4.2. DOI: 10.1109/JSTARS.2010.2052916.

Bastos, A., R. Orth, M. Reichstein, P. Ciais, N. Viovy, S. Zaehle, P. Anthoni, A. Arneth, P. Gentine, E. Joetzjer, S. Lienert, T. Loughran, P. C. McGuire, S. O, J. Pongratz, and S. Sitch (2021). "Vulnerability of European ecosystems to two compound dry and hot summers in 2018 and 2019". *Earth System Dynamics* 12.4, 1015. DOI: 10.5194/esd-12-1015-2021.

Bauer-Marschallinger, B., V. Freeman, S. Cao, C. Paulik, S. Schaufler, T. Stachl, S. Modanesi, C. Massari, L. Ciabatta, L. Brocca, and W. Wagner (2019). "Toward Global Soil Moisture Monitoring With Sentinel-1: Harnessing Assets and Overcoming Obstacles". *IEEE Transactions on Geoscience and Remote Sensing* 57.1, 520. DOI: 10.1109/TGRS.2018.2858004.

Bauer-Marschallinger, B., C. Paulik, S. Hochstoger, T. Mistelbauer, S. Modanesi, L. Ciabatta, C. Massari, L. Brocca, and W. Wagner (2018). "Soil Moisture from Fusion of Scatterometer and SAR: Closing the Scale Gap with Temporal Filtering". *Remote Sensing* 10.7, 1030. DOI: 10.3390/rs10071030.

Beaudoing, H., M. Rodell, A. Getirana, and B. Li (2017). *Groundwater and Soil Moisture Conditions from GRACE Data Assimilation L4 7-days 0.125 x 0.125 degree V2.0*. DOI: 10.5067/ASNKR4DD9AMW.

Beck, H. E., M. Pan, D. G. Miralles, R. H. Reichle, W. A. Dorigo, S. Hahn, J. Sheffield, L. Karthikeyan, G. Balsamo, R. M. Parinussa, A. I. J. M. van Dijk, J. Du, J. S. Kimball, N. Vergopolan, and E. F. Wood (2021). "Evaluation of 18 satellite- and model-based soil moisture products using in situ measurements from 826 sensors". *Hydrology and Earth System Sciences* 25.1, 17. DOI: 10.5194/hess-25-17-2021.

Benedict, I., C. C. van Heerwaarden, E. C. van der Linden, A. H. Weerts, and W. Hazeleger (2021). "Anomalous moisture sources of the Rhine basin during the extremely dry summers of 2003 and 2018". *Weather and Climate Extremes* 31, 100302. DOI: 10.1016/j.wace.2020.100302.

Beniston, M. and M. Stoffel (2014). "Assessing the impacts of climatic change on mountain water resources". *Science of The Total Environment* 493, 1129. DOI: 10.1016/j.scitotenv.2013.11.122.

Berg, A., K. Findell, B. Lintner, A. Giannini, S. I. Seneviratne, B. van den Hurk, R. Lorenz, A. Pitman, S. Hagemann, A. Meier, F. Cheruy, A. Ducharne, S. Malyshev, and P. C. D. Milly (2016). "Land–atmosphere feedbacks amplify aridity increase over land under global warming". *Nature Climate Change* 6.9, 869. DOI: 10.1038/nclimate3029.

Berg, A. and J. Sheffield (2018). "Climate Change and Drought: the Soil Moisture Perspective". *Current Climate Change Reports* 4.2, 180. DOI: 10.1007/s40641-018-0095-0.

Bierkens, M. F. P., V. A. Bell, P. Burek, N. Chaney, L. E. Condon, C. H. David, A. de Roo, P. Doll, N. Drost, J. S. Famiglietti, M. Florke, D. J. Gochis, P. Houser, R. Hut, J. Keune, S.

Kollet, R. M. Maxwell, J. T. Reager, L. Samaniego, E. Sudicky, E. H. Sutanudjaja, N. van de Giesen, H. Winsemius, and E. F. Wood (2015). "Hyper-resolution global hydrological modelling: what is next?" *Hydrological Processes* 29.2, 310. DOI: 10.1002/hyp.10391.

Bindlish, R. and A. P. Barros (2001). "Parameterization of vegetation backscatter in radar-based, soil moisture estimation". *Remote Sensing of Environment* 76.1, 130. DOI: 10.1016/S0034-4257(00)00200-5.

Bolten, J. D., W. T. Crow, X. Zhan, T. J. Jackson, and C. A. Reynolds (2010). "Evaluating the Utility of Remotely Sensed Soil Moisture Retrievals for Operational Agricultural Drought Monitoring". *IEEE Journal of Selected Topics in Applied Earth Observations and Remote Sensing* 3.1, 57. DOI: 10.1109/JSTARS.2009.2037163.

Bousbih, S., M. Zribi, Z. Lili-Chabaane, N. Baghdadi, M. El Hajj, Q. Gao, and B. Mougenot (2017). "Potential of Sentinel-1 Radar Data for the Assessment of Soil and Cereal Cover Parameters". *Sensors* 17.11, 2617. DOI: 10.3390/s17112617.

Brier, G. W. and R. A. Allen (1951). "Verification of Weather Forecasts". In: *Compendium of Meteorology: Prepared under the Direction of the Committee on the Compendium of Meteorology*. Ed. by H. R. Byers, H. E. Landsberg, H. Wexler, B. Haurwitz, A. F. Spilhaus, H. C. Willett, H. G. Houghton, and T. F. Malone. Boston, MA: American Meteorological Society, 841. DOI: 10.1007/978-1-940033-70-9_68.

Briffa, K. R., P. D. Jones, and M. Hulme (1994). "Summer moisture variability across Europe, 1892–1991: An analysis based on the palmer drought severity index". *International Journal of Climatology* 14.5, 475. DOI: https://doi.org/10.1002/joc.3370140502.

Brito, S. S. B., A. P. M. A. Cunha, C. C. Cunningham, R. C. Alvalá, J. A. Marengo, and M. A. Carvalho (2018). "Frequency, duration and severity of drought in the Semiarid Northeast Brazil region". *International Journal of Climatology* 38.2, 517. DOI: 10.1002/joc.5225.

Brocca, L., L. Ciabatta, C. Massari, S. Camici, and A. Tarpanelli (2017). "Soil Moisture for Hydrological Applications: Open Questions and New Opportunities". *Water* 9.2, 140. DOI: 10.3390/w9020140.

Brocca, L., F. Melone, T. Moramarco, and R. Morbidelli (2010). "Spatial-temporal variability of soil moisture and its estimation across scales". *Water Resources Research* 46.2. DOI: 10.1029/2009WR008016.

Buitink, J., T. C. van Hateren, and A. J. Teuling (2021). "Hydrological System Complexity Induces a Drought Frequency Paradox". *Frontiers in Water* 3. DOI: 10.3389/frwa.2021.640976.

Buitink, J., A. M. Swank, M. van der Ploeg, N. E. Smith, H.-J. F. Benninga, F. van der Bolt, C. D. U. Carranza, G. Koren, R. van der Velde, and A. J. Teuling (2020). "Anatomy of the 2018 agricultural drought in the Netherlands using in situ soil moisture and satellite vegetation indices". *Hydrology and Earth System Sciences* 24.12, 6021. DOI: 10.5194/hess-24-6021-2020.

Buitink, J., R. Uijlenhoet, and A. J. Teuling (2019). "Evaluating seasonal hydrological extremes in mesoscale (pre-)Alpine basins at coarse 0.5° and fine hyperresolution". *Hydrology and Earth System Sciences* 23.3, 1593. DOI: 10.5194/hess-23-1593-2019.

Buras, A., A. Rammig, and C. S. Zang (2020). "Quantifying impacts of the 2018 drought on European ecosystems in comparison to 2003". *Biogeosciences* 17.6, 1655. DOI: 10.5194/bg-17-1655-2020.

Cammalleri, C., F. Micale, and J. Vogt (2015). "On the value of combining different modelled soil moisture products for European drought monitoring". *Journal of Hydrology* 525, 547. DOI: 10.1016/j.jhydrol.2015.04.021.

Cammalleri, C., G. Naumann, L. Mentaschi, B. Bisselink, E. Gelati, A. De Roo, and L. Feyen (2020). "Diverging hydrological drought traits over Europe with global warming". *Hydrology and Earth System Sciences* 24.12, 5919. DOI: 10.5194/hess-24-5919-2020.

Cao, Y., S. Chen, L. Wang, B. Zhu, T. Lu, and Y. Yu (2019). "An Agricultural Drought Index for Assessing Droughts Using a Water Balance Method: A Case Study in Jilin Province, Northeast China". *Remote Sensing* 11.9, 1066. DOI: 10.3390/rs11091066.

Carrão, H., S. Russo, G. Sepulcre-Canto, and P. Barbosa (2016). "An empirical standardized soil moisture index for agricultural drought assessment from remotely sensed data". *International Journal of Applied Earth Observation and Geoinformation* 48, 74. DOI: 10.1016/j.jag.2015.06.011.

Carvalho-Santos, C., A. T. Monteiro, J. C. Azevedo, J. P. Honrado, and J. P. Nunes (2017). "Climate Change Impacts on Water Resources and Reservoir Management: Uncertainty and Adaptation for a Mountain Catchment in Northeast Portugal". *Water Resources Management* 31.11, 3355. DOI: 10.1007/s11269-017-1672-z.

Chakrabarti, S., T. Bongiovanni, J. Judge, L. Zotarelli, and C. Bayer (2014). "Assimilation of SMOS Soil Moisture for Quantifying Drought Impacts on Crop Yield in Agricultural Regions". *IEEE Journal of Selected Topics in Applied Earth Observations and Remote Sensing* 7.9, 3867. DOI: 10.1109/JSTARS.2014.2315999.

Chan, S., R. Hunt, R. Bindlish, E. Njoku, J. Kimball, and T. Jackson (2011). *Ancillary Data Report for Vegetation Water Content*. Tech. rep. SMAP project document #D53061. JPL.

Chen, F., W. T. Crow, M. H. Cosh, A. Colliander, J. Asanuma, A. Berg, D. D. Bosch, T. G. Caldwell, C. H. Collins, K. H. Jensen, J. Martínez-Fernández, H. McNairn, P. J. Starks, Z. Su, and J. P. Walker (2019). "Uncertainty of Reference Pixel Soil Moisture Averages Sampled at SMAP Core Validation Sites". *Journal of Hydrometeorology* 20.8, 1553. DOI: 10.1175/JHM-D-19-0049.1.

Chen, T., R. de Jeu, Y. Liu, G. van der Werf, and A. Dolman (2014). "Using satellite based soil moisture to quantify the water driven variability in NDVI: A case study over mainland Australia". *Remote Sensing of Environment* 140, 330. DOI: 10.1016/j.rse.2013.08.022.

Choker, M., N. Baghdadi, M. Zribi, M. El Hajj, S. Paloscia, N. E. C. Verhoest, H. Lievens, and F. Mattia (2017). "Evaluation of the Oh, Dubois and IEM Backscatter Models Using a Large Dataset of SAR Data and Experimental Soil Measurements". *Water* 9.1, 38. DOI: 10.3390/w9010038.

Christian, J. I., E. R. Martin, J. B. Basara, J. C. Furtado, J. A. Otkin, L. E. L. Lowman, E. D. Hunt, V. Mishra, and X. Xiao (2023). "Global projections of flash drought show increased risk in a warming climate". *Communications Earth & Environment* 4.1, 1. DOI: 10.1038/s43247-023-00826-1.

Colliander, A., T. J. Jackson, R. Bindlish, S. Chan, N. Das, S. B. Kim, M. H. Cosh, R. S. Dunbar, L. Dang, L. Pashaian, J. Asanuma, K. Aida, A. Berg, T. Rowlandson, D. Bosch, T. Caldwell, K. Caylor, D. Goodrich, H. al Jassar, E. Lopez-Baeza, J. Martínez-Fernández, A. González-Zamora, S. Livingston, H. McNairn, A. Pacheco, M. Moghaddam, C. Montzka, C. Notarnicola, G. Niedrist, T. Pellarin, J. Prueger, J. Pulliainen, K. Rautiainen, J. Ramos, M. Seyfried, P. Starks, Z. Su, Y. Zeng, R. van der Velde, M. Thibeault, W. Dorigo, M. Vreugdenhil, J. P. Walker, X. Wu, A. Monerris, P. E. O'Neill, D. Entekhabi, E. G. Njoku, and S. Yueh (2017). "Validation of SMAP surface soil moisture products with core validation sites". *Remote Sensing of Environment* 191, 215. DOI: 10.1016/j.rse.2017.01.021.

Colliander, A., M. H. Cosh, S. Misra, T. J. Jackson, W. T. Crow, J. Powers, H. McNairn, P. Bullock, A. Berg, R. Magagi, Y. Gao, R. Bindlish, R. Williamson, I. Ramos, B. Latham, P. O'Neill, and S. Yueh (2019). "Comparison of high-resolution airborne soil moisture retrievals to SMAP soil moisture during the SMAP validation experiment 2016 (SMAPVEX16)". *Remote Sensing of Environment* 227, 137. DOI: 10.1016/j.rse.2019.04.004.

Colliander, A., T. Jackson, H. McNairn, S. Chazanoff, S. Dinardo, B. Latham, I. O'Dwyer, W. Chun, S. Yueh, and E. Njoku (2015). "Comparison of Airborne Passive and Active L-Band System (PALS) Brightness Temperature Measurements to SMOS Observations During the SMAP Validation Experiment 2012 (SMAPVEX12)". *IEEE Geoscience and Remote Sensing Letters* 12.4, 801. DOI: 10.1109/LGRS.2014.2362889.

COPA-COGECA (2003). *Assessment of the impact of the heat wave and drought of the summer 2003 on agriculture and forestry*. Tech. rep. Brussels: Committee of Agricultural Organisations in the European Union.

Corbari, C. and M. Mancini (2023). "Irrigation efficiency optimization at multiple stakeholders' levels based on remote sensing data and energy water balance modelling". *Irrigation Science* 41.1, 121. DOI: 10.1007/s00271-022-00780-4.

Crow, W. T., S. V. Kumar, and J. D. Bolten (2012a). "On the utility of land surface models for agricultural drought monitoring". *Hydrology and Earth System Sciences* 16.9, 3451. DOI: 10.5194/hess-16-3451-2012.

Crow, W., F. Chen, and A. Colliander (2022). "Benchmarking downscaled satellite-based soil moisture products using sparse, point-scale ground observations". *Remote Sensing of Environment* 283, 113300. DOI: 10.1016/j.rse.2022.113300.

Crow, W. (2012). *AMSR-E/Aqua root zone soil moisture (LPRM) L3 1 day 25 km x 25 km descending and 2-Layer Palmer Water Balance Model V001*.

Crow, W. and K. Tobin (2018). *GES DISC Dataset: Smerge-Noah-CCI root zone soil moisture 0-40 cm L4 daily 0.125 x 0.125 degree V2.0 (SMERGE_RZSM0_40CM 2.0)*. (Visited on 2020).

Crow, W. T., A. A. Berg, M. H. Cosh, A. Loew, B. P. Mohanty, R. Panciera, P. de Rosnay, D. Ryu, and J. P. Walker (2012b). "Upscaling sparse ground-based soil moisture observations for the validation of coarse-resolution satellite soil moisture products". *Reviews of Geophysics* 50.2. DOI: 10.1029/2011RG000372.

Das, N. N., D. Entekhabi, R. S. Dunbar, M. J. Chaubell, A. Colliander, S. Yueh, T. Jagdhuber, F. Chen, W. Crow, P. E. O'Neill, J. P. Walker, A. Berg, D. D. Bosch, T. Caldwell, M. H. Cosh, C. H. Collins, E. Lopez-Baeza, and M. Thibeault (2019). "The SMAP and Copernicus Sentinel 1A/B microwave active-passive high resolution surface soil moisture product". *Remote Sensing of Environment* 233, 111380. DOI: 10.1016/j.rse.2019.111380.

Davidson, M., M. Chini, W. Dierking, S. Djavidnia, J. Haarpaintner, G. Hajduch, G. V. Laurin, M. Lavalle, C. Lopez Martinez, T. Nagler, N. Pierdicca, and B. Su (2019). *Copernicus L-band SAR Mission Requirements Document*. Mission Requirements Document (MRD) ESA-EOPSM-CLIS-MRD-3371 2.0. European Space Agency.

De Jeu, R. A. M. D., A. H. A. De Nijs, and M. H. W. Van Klink (2017). "Method and system for improving the resolution of sensor data". WO2017216186A1.

Del Frate, F., P. Ferrazzoli, and G. Schiavon (2003). "Retrieving soil moisture and agricultural variables by microwave radiometry using neural networks". *Remote Sensing of Environment* 84.2, 174. DOI: 10.1016/S0034-4257(02)00105-0.

Denissen, J. M. C., A. J. Teuling, M. Reichstein, and R. Orth (2020). "Critical Soil Moisture Derived From Satellite Observations Over Europe". *Journal of Geophysical Research: Atmospheres* 125.6. DOI: 10.1029/2019JD031672.

Didan, K. (2015). *MOD13C2 MODIS/Terra Vegetation Indices Monthly L3 Global 0.05Deg CMG V006 [Data set]*. doi: 10.5067/MODIS/MOD13C2.006.

Dorigo, W., I. Himmelbauer, D. Aberer, L. Schremmer, I. Petrakovic, L. Zappa, W. Preimesberger, A. Xaver, F. Annor, J. Ardo, D. Baldocchi, M. Bitelli, G. Bloschl, H. Bogena, L. Brocca, J.-C. Calvet, J. J. Camarero, G. Capello, M. Choi, M. C. Cosh, N. van de Giesen, I. Hajdu, J. Ikonen, K. H. Jensen, K. D. Kanniah, I. de Kat, G. Kirchengast, P. Kumar Rai, J. Kyrouac, K. Larson, S. Liu, A. Loew, M. Moghaddam, J. Martínez Fernández, C. Mattar Bader, R. Morbidelli, J. P. Musial, E. Osenga, M. A. Palecki, T. Pellarin, G. P. Petropoulos, I. Pfeil, J. Powers, A. Robock, C. Rudiger, U. Rummel, M. Strobel, Z. Su, R. Sullivan, T. Tagesson, A. Varlagin, M. Vreugdenhil, J. Walker, J. Wen, F. Wenger, J. P. Wigneron,

M. Woods, K. Yang, Y. Zeng, X. Zhang, M. Zreda, S. Dietrich, A. Gruber, P. van Oevelen, W. Wagner, K. Scipal, M. Drusch, and R. Sabia (2021). "The International Soil Moisture Network: serving Earth system science for over a decade". *Hydrology and Earth System Sciences* 25.11, 5749. DOI: 10.5194/hess-25-5749-2021.

Dorigo, W., W. Wagner, C. Albergel, F. Albrecht, G. Balsamo, L. Brocca, D. Chung, M. Ertl, M. Forkel, A. Gruber, E. Haas, P. D. Hamer, M. Hirschi, J. Ikonen, R. de Jeu, R. Kidd, W. Lahoz, Y. Y. Liu, D. Miralles, T. Mistelbauer, N. Nicolai-Shaw, R. Parinussa, C. Pratola, C. Reimer, R. van der Schalie, S. I. Seneviratne, T. Smolander, and P. Lecomte (2017). "ESA CCI Soil Moisture for improved Earth system understanding: State-of-the art and future directions". *Remote Sensing of Environment*. Earth Observation of Essential Climate Variables 203, 185. DOI: 10.1016/j.rse.2017.07.001.

El Hajj, M., N. Baghdadi, M. Zribi, and H. Bazzi (2017). "Synergic Use of Sentinel-1 and Sentinel-2 Images for Operational Soil Moisture Mapping at High Spatial Resolution over Agricultural Areas". *Remote Sensing* 9.12, 1292. DOI: 10.3390/rs9121292.

Elshorbagy, A. and K. Parasuraman (2008). "On the relevance of using artificial neural networks for estimating soil moisture content". *Journal of Hydrology* 362.1, 1. DOI: 10.1016/j.jhydrol.2008.08.012.

Entekhabi, D., R. H. Reichle, R. D. Koster, and W. T. Crow (2010). "Performance Metrics for Soil Moisture Retrievals and Application Requirements". *Journal of Hydrometeorology* 11.3, 832. DOI: 10.1175/2010JHM1223.1.

Erda, L., X. Wei, J. Hui, X. Yinlong, L. Yue, B. Liping, and X. Liyong (2005). "Climate change impacts on crop yield and quality with CO2 fertilization in China". *Philosophical Transactions of the Royal Society B: Biological Sciences* 360.1463, 2149. DOI: 10.1098/rstb.2005.1743.

EROS (2017). *Shuttle Radar Topography Mission* (*SRTM*) *1 Arc-Second Global*. Medium: tiff Type: dataset. DOI: 10.5066/F7PR7TFT. (Visited on 2022).

ESA (2017). *Land Cover CCI Product User Guide Version 2*. Tech. rep. European Space Agency.

ESA Sentinel Online, . (2023). *IW GRD Resolutions - Sentinel-1 SAR Technical Guide*. (Visited on 2023).

European Commission, . (2007). *COMMUNICATION FROM THE COMMISSION TO THE EUROPEAN PARLIAMENT AND THE COUNCIL - Addressing the challenge of water scarcity and droughts in the European Union*. Tech. rep. SEC(2007) 993; SEC(2007) 996. Koninklijke Brill NV. DOI: 10.1163/2210-7975_HRD-4679-0058. (Visited on 2023).

Ezzahar, J., N. Ouaadi, M. Zribi, J. Elfarkh, G. Aouade, S. Khabba, S. Er-Raki, A. Chehbouni, and L. Jarlan (2020). "Evaluation of Backscattering Models and Support Vector Machine for the Retrieval of Bare Soil Moisture from Sentinel-1 Data". *Remote Sensing* 12.1, 72. DOI: 10.3390/rs12010072.

Famiglietti, J. S., D. Ryu, A. A. Berg, M. Rodell, and T. J. Jackson (2008). "Field observations of soil moisture variability across scales". *Water Resources Research* 44.1. DOI: 10.1029/2006WR005804.

Fang, B., P. Kansara, C. Dandridge, and V. Lakshmi (2021). "Drought monitoring using high spatial resolution soil moisture data over Australia in 2015–2019". *Journal of Hydrology* 594, 125960. DOI: 10.1016/j.jhydrol.2021.125960.

Foets, J., C. E. Wetzel, A. J. Teuling, and L. Pfister (2020). "Temporal and spatial variability of terrestrial diatoms at the catchment scale: controls on productivity and comparison with other soil algae". *PeerJ* 8, e9198. DOI: 10.7717/peerj.9198.

Ford, T. W. and S. M. Quiring (2019). "Comparison of Contemporary In Situ, Model, and Satellite Remote Sensing Soil Moisture With a Focus on Drought Monitoring". *Water Resources Research* 55.2, 1565. DOI: 10.1029/2018WR024039.

Fung, A., Z. Li, and K. Chen (1992). "Backscattering from a randomly rough dielectric surface". *IEEE Transactions on Geoscience and Remote Sensing* 30.2, 356. DOI: 10.1109/36.134085.

García-Herrera, R., J. M. Garrido-Perez, D. Barriopedro, C. Ordóñez, S. M. Vicente-Serrano, R. Nieto, L. Gimeno, R. Sorí, and P. Yiou (2019). "The European 2016/17 Drought". *Journal of Climate* 32.11, 3169. DOI: 10.1175/JCLI-D-18-0331.1.

Grillakis, M. G., A. G. Koutroulis, J. Komma, I. K. Tsanis, W. Wagner, and G. Bloschl (2016). "Initial soil moisture effects on flash flood generation – A comparison between basins of contrasting hydro-climatic conditions". *Journal of Hydrology*. Flash floods, hydrogeomorphic response and risk management 541, 206. DOI: 10.1016/j.jhydrol.2016.03.007.

Gruber, A., G. De Lannoy, C. Albergel, A. Al-Yaari, L. Brocca, J. C. Calvet, A. Colliander, M. Cosh, W. Crow, W. Dorigo, C. Draper, M. Hirschi, Y. Kerr, A. Konings, W. Lahoz, K. McColl, C. Montzka, J. Muñoz-Sabater, J. Peng, R. Reichle, P. Richaume, C. Rudiger, T. Scanlon, R. van der Schalie, J. P. Wigneron, and W. Wagner (2020). "Validation practices for satellite soil moisture retrievals: What are (the) errors?" *Remote Sensing of Environment* 244, 111806. DOI: 10.1016/j.rse.2020.111806.

Gruber, A., W. A. Dorigo, W. Crow, and W. Wagner (2017). "Triple Collocation-Based Merging of Satellite Soil Moisture Retrievals". *IEEE Transactions on Geoscience and Remote Sensing* 55.12, 6780. DOI: 10.1109/TGRS.2017.2734070.

Gruber, A., T. Scanlon, R. v. d. Schalie, W. Wagner, and W. Dorigo (2019). "Evolution of the ESA CCI Soil Moisture climate data records and their underlying merging methodology". *Earth System Science Data* 11.2, 717. DOI: 10.5194/essd-11-717-2019.

Hachani, A., M. Ouessar, S. Paloscia, E. Santi, and S. Pettinato (2019). "Soil moisture retrieval from Sentinel-1 acquisitions in an arid environment in Tunisia: application of Artificial Neural Networks techniques". *International Journal of Remote Sensing* 40.24, 9159. DOI: 10.1080/01431161.2019.1629503.

Hallikainen, M. T., F. T. Ulaby, M. C. Dobson, M. A. El-rayes, and L.-k. Wu (1985). "Microwave Dielectric Behavior of Wet Soil-Part 1: Empirical Models and Experimental Observations". *IEEE Transactions on Geoscience and Remote Sensing* GE-23.1, 25. DOI: 10.1109/TGRS.1985.289497.

Hanel, M., O. Rakovec, Y. Markonis, P. Máca, L. Samaniego, J. Kyselý, and R. Kumar (2018). "Revisiting the recent European droughts from a long-term perspective". *Scientific Reports* 8.1, 9499. DOI: 10.1038/s41598-018-27464-4.

Hanssen, A. W. and W. J. A. Kuipers (1965). *On the relationship between the frequency of rain and various meteorological parameters*. Tech. rep. 81. Koninklijk Nederlands Meteorologisch Instituut.

Hao, Z. and A. AghaKouchak (2013). "Multivariate Standardized Drought Index: A parametric multi-index model". *Advances in Water Resources* 57, 12. DOI: 10.1016/j.advwatres.2013.03.009.

Hari, V., O. Rakovec, Y. Markonis, M. Hanel, and R. Kumar (2020). "Increased future occurrences of the exceptional 2018–2019 Central European drought under global warming". *Scientific Reports* 10.1, 12207. DOI: 10.1038/s41598-020-68872-9.

Hateren, T. C. van, M. Chini, P. Matgen, L. Pulvirenti, N. Pierdicca, and A. J. Teuling (2023a). "On the potential of Sentinel-1 for sub-field scale soil moisture monitoring". *International Journal of Applied Earth Observation and Geoinformation* 120, 103342. DOI: 10.1016/j.jag.2023.103342.

Hateren, T. C. van, M. Chini, P. Matgen, and A. J. Teuling (2021). "Ambiguous Agricultural Drought: Characterising Soil Moisture and Vegetation Droughts in Europe from Earth Observation". *Remote Sensing* 13.10, 1990. DOI: 10.3390/rs13101990.

Hateren, T. C. van, M. Chini, P. Matgen, J. Zhao, and A. J. Teuling (2023b). "Evaluating C-band satellite soil moisture observations for high resolution drought monitoring". *In preparation for Geophysical Research Letters*.

Hateren, T. C. van, M. Chini, P. Matgen, L. Pulvirenti, N. Pierdicca, and A. J. Teuling (2023c). "On the Use of Native Resolution Backscatter Intensity Data for Optimal Soil Moisture Retrieval". *IEEE Geoscience and Remote Sensing Letters* 20, 1. DOI: 10.1109/LGRS.2023.3264732.

Hateren, T. C. van, H. J. Jongen, H. Al-Zawaidah, J. G. Beemster, J. Boekee, L. Bogerd, S. Gao, C. Kannen, I. van Meerveld, S. I. de Lange, F. Linke, R. B. Pinto, J. O. Remmers, J. Ruijsch, S. R. Rusli, R. C. van de Vijsel, J. P. Aerts, S. M. Agoungbome, M. Anys, S. Blanco Ramírez, T. van Emmerik, L. Gallitelli, G. Chiquito Gesualdo, W. Gonzalez Otero, S. Hanus, Z. He, S. Hoffmeister, R. O. Imhoff, T. Kerlin, S. M. Meshram, J. Meyer, A. Meyer Oliveira, A. C. Muller, R. Nijzink, M. Scheller, L. Schreyers, D. Sehgal, P. F. Tasseron, A. J. Teuling, M. Trevisson, K. Waldschlager, B. Walraven, C. Wannasin, J. Wienhofer, M. J. Zander, S. Zhang, J. Zhou, J. Y. Zomer, and B. W. Zwartendijk (2023d). "Where should hydrology go?

An early-career perspective on the next IAHS Scientific Decade: 2023–2032". *Hydrological Sciences Journal* 68.4, 529. DOI: 10.1080/02626667.2023.2170754.

Hayes, M., M. Svoboda, N. Wall, and M. Widhalm (2011). "The Lincoln Declaration on Drought Indices: Universal Meteorological Drought Index Recommended". *Bulletin of the American Meteorological Society* 92.4, 485. DOI: 10.1175/2010BAMS3103.1.

Heim Jr., R. R. (2002). "A Review of Twentieth- Century Drought Indices Used in the United States", 17.

Hogan, R. J. and I. B. Mason (2011). "Deterministic forecasts of binary events". In: *Forecast Verification: A practitioner's guide in atmospheric science*. Ed. by I. T. Joliffe and D. B. Stephenson. 2nd ed. John Wiley & Sons, Ltd.

Hostache, R., D. Rains, K. Mallick, M. Chini, R. Pelich, H. Lievens, F. Fenicia, G. Corato, N. E. C. Verhoest, and P. Matgen (2020). "Assimilation of Soil Moisture and Ocean Salinity (SMOS) brightness temperature into a large-scale distributed conceptual hydrological model to improve soil moisture predictions: the Murray–Darling basin in Australia as a test case". *Hydrology and Earth System Sciences* 24.10, 4793. DOI: 10.5194/hess-24-4793-2020.

Houborg, R., M. Rodell, B. Li, R. Reichle, and B. Zaitchik (2012). "Drought indicators based on model assimilated GRACE terrestrial water storage observations". *Water Resources Research* 48.W07525. DOI: 10.1029/2011WR011291.

Hu, X., H. Ren, K. Tansey, Y. Zheng, D. Ghent, X. Liu, and L. Yan (2019). "Agricultural drought monitoring using European Space Agency Sentinel 3A land surface temperature and normalized difference vegetation index imageries". *Agricultural and Forest Meteorology* 279, 107707. DOI: 10.1016/j.agrformet.2019.107707.

Huffman, G. J., D. T. Bolvin, D. Braithwaite, K. Hsu, R. Joyce, C. Kidd, E. J. Nelkin, S. Sorooshian, J. Tan, and P. Xie (2020). *Algorithm Theoretical Basis Document (ATBD) Version 06 NASA Global Precipitation Measurement (GPM) Integrated Multi-satellitE Retrievals for GPM (IMERG)*. Tech. rep. National Aeronautics and Space Administration (NASA).

Huffman, G. J., E. F. Stocker, D. T. Bolvin, E. J. Nelkin, and J. Tan (2019). *GES DISC Dataset: GPM IMERG Final Precipitation L3 1 month 0.1 degree x 0.1 degree V06 (GPM_3IMERGM 06)*. doi: 10.5067/GPM/IMERG/3B-MONTH/06. (Visited on 2020).

Ionita, M. and V. Nagavciuc (2021). "Changes in drought features at the European level over the last 120 years". *Natural Hazards and Earth System Sciences* 21.5, 1685. DOI: 10.5194/nhess-21-1685-2021.

Ionita, M., L. Tallaksen, D. Kingston, J. Stagge, G. Laaha, H. Van Lanen, P. Scholz, S. Chelcea, and K. Haslinger (2017). "The European 2015 drought from a climatological perspective". *Hydrology and Earth System Sciences* 21, 1397. DOI: 10.5194/hess-21-1397-2017.

IPCC (2012). "Glossary of terms". In: *Managing the Risks of Extreme Events and Disasters to Advance Climate Change Adaptation. A Special Report of Working Groups I and II of*

the Intergovernmental Panel on Climate Change (*IPCC*). Ed. by C. B. Field, V. Barros, T. F. Stocker, D. Qin, D. J. Dokken, K. L. Ebi, M. D. Mastrandrea, K. J. Mach, G.-K. Plattner, S. Allen, and M. Tignor. Cambridge University Press, Cambridge, UK, and New York, NY, USA, 555.

——(2023). *Synthesis report of the IPCC sixth assessment report* (*AR6*). Tech. rep. (Visited on 2023).

Ji, L. and A. J. Peters (2003). "Assessing vegetation response to drought in the northern Great Plains using vegetation and drought indices". *Remote Sensing of Environment* 87.1, 85. DOI: 10.1016/S0034-4257(03)00174-3.

Jolly, W. M., M. Dobbertin, N. E. Zimmermann, and M. Reichstein (2005). "Divergent vegetation growth responses to the 2003 heat wave in the Swiss Alps". *Geophysical Research Letters* 32.18. DOI: 10.1029/2005GL023252.

Kim, K. B., H.-H. Kwon, and D. Han (2018). "Exploration of warm-up period in conceptual hydrological modelling". *Journal of Hydrology* 556, 194. DOI: 10.1016/j.jhydrol.2017.11.015.

Kim, S.-B., M. Moghaddam, L. Tsang, M. Burgin, X. Xu, and E. G. Njoku (2014). "Models of L-Band Radar Backscattering Coefficients Over Global Terrain for Soil Moisture Retrieval". *IEEE Transactions on Geoscience and Remote Sensing* 52.2, 1381. DOI: 10.1109/TGRS.2013.2250980.

Kim, Y. and G. Wang (2007). "Impact of Vegetation Feedback on the Response of Precipitation to Antecedent Soil Moisture Anomalies over North America". *Journal of Hydrometeorology* 8.3, 534. DOI: 10.1175/JHM612.1.

Kogan, F. N. (1990). "Remote sensing of weather impacts on vegetation in non-homogeneous areas". *International Journal of Remote Sensing* 11.8, 1405. DOI: 10.1080/01431169008955102.

Kowalska, N., L. Šigut, M. Stojanović, M. Fischer, I. Kyselova, and M. Pavelka (2020). "Analysis of floodplain forest sensitivity to drought". *Philosophical Transactions of the Royal Society B: Biological Sciences* 375.1810, 20190518. DOI: 10.1098/rstb.2019.0518.

Kumar, R., J. L. Musuuza, A. F. Van Loon, A. J. Teuling, R. Barthel, J. Ten Broek, J. Mai, L. Samaniego, and S. Attinger (2016). "Multiscale evaluation of the Standardized Precipitation Index as a groundwater drought indicator". *Hydrology and Earth System Sciences* 20.3, 1117. DOI: 10.5194/hess-20-1117-2016.

Kundzewicz, Z. (2008). "Climate change impacts on the hydrological cycle". *Ecohydrology and Hydrobiology* 8, 195. DOI: 10.2478/v10104-009-0015-y.

Laaha, G., T. Gauster, L. M. Tallaksen, J.-P. Vidal, K. Stahl, C. Prudhomme, B. Heudorfer, R. Vlnas, M. Ionita, H. A. J. Van Lanen, M.-J. Adler, L. Caillouet, C. Delus, M. Fendekova, S. Gailliez, J. Hannaford, D. Kingston, A. F. Van Loon, L. Mediero, M. Osuch, R. Romanowicz, E. Sauquet, J. H. Stagge, and W. K. Wong (2017). "The European 2015 drought from a

hydrological perspective". *Hydrology and Earth System Sciences* 21.6, 3001. DOI: 10.5194/hess-21-3001-2017.

Lagasio, M., A. Parodi, L. Pulvirenti, A. N. Meroni, G. Boni, N. Pierdicca, F. S. Marzano, L. Luini, G. Venuti, E. Realini, A. Gatti, G. Tagliaferro, S. Barindelli, A. Monti Guarnieri, K. Goga, O. Terzo, A. Rucci, E. Passera, D. Kranzlmueller, and B. Rommen (2019a). "A Synergistic Use of a High-Resolution Numerical Weather Prediction Model and High-Resolution Earth Observation Products to Improve Precipitation Forecast". *Remote Sensing* 11.20, 2387. DOI: 10.3390/rs11202387.

Lagasio, M., L. Pulvirenti, A. Parodi, G. Boni, N. Pierdicca, G. Venuti, E. Realini, G. Tagliaferro, S. Barindelli, and B. Rommen (2019b). "Effect of the ingestion in the WRF model of different Sentinel-derived and GNSS-derived products: analysis of the forecasts of a high impact weather event". *European Journal of Remote Sensing* 52.sup4, 16. DOI: 10.1080/22797254.2019.1642799.

Lahoz, W., J. Blyverket, and P. Hamer (2018). *ESA Climate Change Initiative Phase II Soil Moisture - Product Validation and Intercomparison Report (PVIR) Revision 3*. Tech. rep. 2.6. Earth Observation Data Centre for Water Resources Monitoring (EODC) GmbH, 93.

Lange, M., B. Dechant, C. Rebmann, M. Vohland, M. Cuntz, and D. Doktor (2017). "Validating MODIS and Sentinel-2 NDVI Products at a Temperate Deciduous Forest Site Using Two Independent Ground-Based Sensors". *Sensors* 17.8, 1855. DOI: 10.3390/s17081855.

Lee, J.-S. (1986). "Speckle Suppression And Analysis For Synthetic Aperture Radar Images". *Optical Engineering* 25.5, 636. DOI: 10.1117/12.7973877.

Lee, J. H., S. Budhathoki, and K.-E. Lindenschmidt (2021). "Stochastic bias correction for RADARSAT-2 soil moisture retrieved over vegetated areas". *Geocarto International* 0.0, 1. DOI: 10.1080/10106049.2021.2017009.

Li, Z.-L., P. Leng, C. Zhou, K.-S. Chen, F.-C. Zhou, and G.-F. Shang (2021). "Soil moisture retrieval from remote sensing measurements: Current knowledge and directions for the future". *Earth-Science Reviews* 218, 103673. DOI: 10.1016/j.earscirev.2021.103673.

Liang, M. and X. Yuan (2021). "Critical Role of Soil Moisture Memory in Predicting the 2012 Central United States Flash Drought". *Frontiers in Earth Science* 9. DOI: 10.3389/feart.2021.615969.

LIST-HOST (2022). *Luxembourg Institute of Science and Technology (LIST) Hydro-Climatological Observation network (HOST) Precipitation, soil moisture data*. (Visited on 2022).

Liu, X., X. Zhu, Y. Pan, S. Li, Y. Liu, and Y. Ma (2016). "Agricultural drought monitoring: Progress, challenges, and prospects". *Journal of Geographical Sciences* 26.6, 750. DOI: 10.1007/s11442-016-1297-9.

Liu, Y., Y. Liu, and W. Wang (2019). "Inter-comparison of satellite-retrieved and Global Land Data Assimilation System-simulated soil moisture datasets for global drought analysis". *Remote Sensing of Environment* 220, 1. DOI: 10.1016/j.rse.2018.10.026.

Lloyd-Hughes, B. and M. A. Saunders (2002). "A drought climatology for Europe". *International Journal of Climatology* 22.13, 1571. DOI: https://doi.org/10.1002/joc.846.

Loon, A. F. van (2015). "Hydrological drought explained". *WIREs Water* 2.4, 359. DOI: 10.1002/wat2.1085.

Ma, C., X. Li, and M. F. McCabe (2020). "Retrieval of High-Resolution Soil Moisture through Combination of Sentinel-1 and Sentinel-2 Data". *Remote Sensing* 12.14, 2303. DOI: 10.3390/rs12142303.

Madakumbura, G. D., H. Kim, N. Utsumi, H. Shiogama, E. M. Fischer, Ø. Seland, J. F. Scinocca, D. M. Mitchell, Y. Hirabayashi, and T. Oki (2019). "Event-to-event intensification of the hydrologic cycle from 1.5 °C to a 2 °C warmer world". *Scientific Reports* 9.1, 3483. DOI: 10.1038/s41598-019-39936-2.

Mansourpour, M., M. Rajabi, and J. Blais (2006). "Effects and performance of speckle noise reduction filters on active radar and SAR images". In: *Proceedings of the ISPRS*. Vol. 36. 1. Ankara, Turkey, W41.

Martínez-Fernández, J., A. González-Zamora, N. Sánchez, and A. Gumuzzio (2015). "A soil water based index as a suitable agricultural drought indicator". *Journal of Hydrology* 522, 265. DOI: 10.1016/j.jhydrol.2014.12.051.

Martínez-Fernández, J., A. González-Zamora, N. Sánchez, A. Gumuzzio, and C. M. Herrero-Jiménez (2016). "Satellite soil moisture for agricultural drought monitoring: Assessment of the SMOS derived Soil Water Deficit Index". *Remote Sensing of Environment* 177, 277. DOI: 10.1016/j.rse.2016.02.064.

Marx, A., R. Kumar, S. Thober, O. Rakovec, N. Wanders, M. Zink, E. F. Wood, M. Pan, J. Sheffield, and L. Samaniego (2018). "Climate change alters low flows in Europe under global warming of 1.5, 2, and 3 °C". *Hydrology and Earth System Sciences* 22.2, 1017. DOI: 10.5194/hess-22-1017-2018.

Mastrotheodoros, T., C. Pappas, P. Molnar, P. Burlando, G. Manoli, J. Parajka, R. Rigon, B. Szeles, M. Bottazzi, P. Hadjidoukas, and S. Fatichi (2020). "More green and less blue water in the Alps during warmer summers". *Nature Climate Change* 10.2, 155. DOI: 10.1038/s41558-019-0676-5.

Matgen, P., S. Heitz, S. Hasenauer, C. Hissler, L. Brocca, L. Hoffmann, W. Wagner, and H. H. G. Savenije (2012). "On the potential of MetOp ASCAT-derived soil wetness indices as a new aperture for hydrological monitoring and prediction: a field evaluation over Luxembourg". *Hydrological Processes* 26.15, 2346. DOI: 10.1002/hyp.8316.

Mattia, F., T. Le Toan, G. Picard, F. Posa, A. D'Alessio, C. Notarnicola, A. Gatti, M. Rinaldi, G. Satalino, and G. Pasquariello (2003). "Multitemporal C-band radar measurements

on wheat fields". *IEEE Transactions on Geoscience and Remote Sensing* 41.7, 1551. DOI: 10.1109/TGRS.2003.813531.

Mattia, F., G. Satalino, V. R. N. Pauwels, and A. Loew (2009). "Soil moisture retrieval through a merging of multi-temporal L-band SAR data and hydrologic modelling". *Hydrology and Earth System Sciences* 13.3, 343. DOI: 10.5194/hess-13-343-2009.

McKee, T. B., N. J. Doesken, and J. Kleist (1993). "The relationship of drought frequency and duration to time scales". In: *Eighth Conference on Applied Climatology*. Anaheim, California.

MeteoLux (2022). *MeteoLux precipitation data*. (Visited on 2023).

Miralles, D. G., P. Gentine, S. I. Seneviratne, and A. J. Teuling (2019). "Land–atmospheric feedbacks during droughts and heatwaves: state of the science and current challenges". *Annals of the New York Academy of Sciences* 1436.1, 19. DOI: 10.1111/nyas.13912.

Miralles, D. G., A. J. Teuling, C. C. van Heerwaarden, and J. Vilà-Guerau de Arellano (2014). "Mega-heatwave temperatures due to combined soil desiccation and atmospheric heat accumulation". *Nature Geoscience* 7.5, 345. DOI: 10.1038/ngeo2141.

Mittelbach, H., F. Casini, I. Lehner, A. J. Teuling, and S. I. Seneviratne (2011). "Soil moisture monitoring for climate research: Evaluation of a low-cost sensor in the framework of the Swiss Soil Moisture Experiment (SwissSMEX) campaign". *Journal of Geophysical Research: Atmospheres* 116.D5. DOI: 10.1029/2010JD014907.

Mozny, M., M. Trnka, Z. Zalud, P. Hlavinka, J. Nekovar, V. Potop, and M. Virag (2012). "Use of a soil moisture network for drought monitoring in the Czech Republic". *Theoretical and Applied Climatology* 107.1, 99. DOI: 10.1007/s00704-011-0460-6.

Murphy, A. H. and E. S. Epstein (1989). "Skill Scores and Correlation Coefficients in Model Verification". *Monthly Weather Review* 117.3, 572. DOI: 10.1175/1520-0493(1989)117⟨0572:SSACCI⟩2.0.CO;2.

Narasimhan, B. and R. Srinivasan (2005). "Development and evaluation of Soil Moisture Deficit Index (SMDI) and Evapotranspiration Deficit Index (ETDI) for agricultural drought monitoring". *Agricultural and Forest Meteorology* 133.1, 69. DOI: 10.1016/j.agrformet.2005.07.012.

Naumann, G., C. Cammalleri, L. Mentaschi, and L. Feyen (2021). "Increased economic drought impacts in Europe with anthropogenic warming". *Nature Climate Change* 11.6, 485. DOI: 10.1038/s41558-021-01044-3.

Navarro, A., E. García-Ortega, A. Merino, J. L. Sánchez, C. Kummerow, and F. J. Tapiador (2019). "Assessment of IMERG Precipitation Estimates over Europe". *Remote Sensing* 11.21, 2470. DOI: 10.3390/rs11212470.

Nicolai-Shaw, N., J. Zscheischler, M. Hirschi, L. Gudmundsson, and S. I. Seneviratne (2017). "A drought event composite analysis using satellite remote-sensing based soil moisture".

Remote Sensing of Environment. Earth Observation of Essential Climate Variables 203, 216. DOI: 10.1016/j.rse.2017.06.014.

Nilson, E. (2014). *Auswirkungen des Klimawandels auf das Abflussgeschehen und die Binnenschifffahrt in Deutschland : Schlussbericht KLIWAS-Projekt 4.01*. Tech. rep. KLIWAS-Schriftenreihe / BfG – KLIWAS-43/2014. Bundesanstalt fur Gewasserkunde, Koblenz. DOI: 10.5675/KLIWAS_43/2014_4.01.

Oh, Y. (2004). "Quantitative retrieval of soil moisture content and surface roughness from multipolarized radar observations of bare soil surfaces". *IEEE Transactions on Geoscience and Remote Sensing* 42.3, 596. DOI: 10.1109/TGRS.2003.821065.

Owe, M., R. A. M. De Jeu, and T. Holmes (2008). "Multisensor historical climatology of satellite-derived global land surface moisture". *Journal of Geophysical Research* F01002. DOI: 10.1029/2007JF000769.

Palmer, W. C. (1965). *Meteorological Drought*. U.S. Department of Commerce, Weather Bureau.

Palmisano, D., F. Mattia, A. Balenzano, G. Satalino, N. Pierdicca, and A. V. M. Guarnieri (2021). "Sentinel-1 Sensitivity to Soil Moisture at High Incidence Angle and the Impact on Retrieval Over Seasonal Crops". *IEEE Transactions on Geoscience and Remote Sensing*, 1. DOI: 10.1109/TGRS.2020.3033887.

Panu, U. S. and T. C. Sharma (2002). "Challenges in drought research: some perspectives and future directions". *Hydrological Sciences Journal* 47.sup1, S19. DOI: 10.1080/02626660209493019.

Papagiannopoulou, C., D. G. Miralles, W. A. Dorigo, N. E. C. Verhoest, M. Depoorter, and W. Waegeman (2017). "Vegetation anomalies caused by antecedent precipitation in most of the world". *Environmental Research Letters* 12.7, 074016. DOI: 10.1088/1748-9326/aa7145.

Peled, E., E. Dutra, P. Viterbo, and A. Angert (2010). "Technical Note: Comparing and ranking soil drought indices performance over Europe, through remote-sensing of vegetation". *Hydrology and Earth System Sciences* 14.2, 271. DOI: 10.5194/hess-14-271-2010.

Peleg, N., F. Marra, S. Fatichi, P. Molnar, E. Morin, A. Sharma, and P. Burlando (2018). "Intensification of Convective Rain Cells at Warmer Temperatures Observed from High-Resolution Weather Radar Data". *Journal of Hydrometeorology* 19.4, 715. DOI: 10.1175/JHM-D-17-0158.1.

Peng, J., C. Albergel, A. Balenzano, L. Brocca, O. Cartus, M. H. Cosh, W. T. Crow, K. Dabrowska-Zielinska, S. Dadson, M. W. J. Davidson, P. de Rosnay, W. Dorigo, A. Gruber, S. Hagemann, M. Hirschi, Y. H. Kerr, F. Lovergine, M. D. Mahecha, P. Marzahn, F. Mattia, J. P. Musial, S. Preuschmann, R. H. Reichle, G. Satalino, M. Silgram, P. M. van Bodegom, N. E. C. Verhoest, W. Wagner, J. P. Walker, U. Wegmuller, and A. Loew (2021). "A roadmap for high-resolution satellite soil moisture applications – confronting product

characteristics with user requirements". *Remote Sensing of Environment* 252, 112162. DOI: 10.1016/j.rse.2020.112162.

Petropoulos, G. P., G. Ireland, and B. Barrett (2015). "Surface soil moisture retrievals from remote sensing: Current status, products & future trends". *Physics and Chemistry of the Earth, Parts A/B/C*. Emerging science and applications with microwave remote sensing data 83-84, 36. DOI: 10.1016/j.pce.2015.02.009.

Pierdicca, N., L. Pulvirenti, and G. Pace (2014). "A Prototype Software Package to Retrieve Soil Moisture From Sentinel-1 Data by Using a Bayesian Multitemporal Algorithm". *IEEE Journal of Selected Topics in Applied Earth Observations and Remote Sensing* 7.1, 153. DOI: 10.1109/JSTARS.2013.2257698.

Portail Open Data, . (2017). *Orthophoto officielle du Grand-Duché de Luxembourg, édition 2016 - Portail Open Data*. (Visited on 2023).

Pulvirenti, L., G. Squicciarino, L. Cenci, G. Boni, N. Pierdicca, M. Chini, C. Versace, and P. Campanella (2018). "A surface soil moisture mapping service at national (Italian) scale based on Sentinel-1 data". *Environmental Modelling & Software* 102, 13. DOI: 10.1016/j.envsoft.2017.12.022.

Raible, C. C., O. Barenbold, and J. J. Gómez-navarro (2017). "Drought indices revisited – improving and testing of drought indices in a simulation of the last two millennia for Europe". *Tellus A: Dynamic Meteorology and Oceanography* 69.1, 1287492. DOI: 10.1080/16000870.2017.1296226.

Rakovec, O., L. Samaniego, V. Hari, Y. Markonis, V. Moravec, S. Thober, M. Hanel, and R. Kumar (2022). "The 2018–2020 Multi-Year Drought Sets a New Benchmark in Europe". *Earth's Future* 10.3, e2021EF002394. DOI: 10.1029/2021EF002394.

Rasmijn, L. M., G. van der Schrier, R. Bintanja, J. Barkmeijer, A. Sterl, and W. Hazeleger (2018). "Future equivalent of 2010 Russian heatwave intensified by weakening soil moisture constraints". *Nature Climate Change* 8.5, 381. DOI: 10.1038/s41558-018-0114-0.

Reichle, R., G. De Lannoy, R. Koster, W. Crow, J. Kimball, Q. Liu, and M. Bechtold (2022). *SMAP L4 Global 3-hourly 9 km EASE-Grid Surface and Root Zone Soil Moisture Geophysical Data, Version 7*. DOI: 10.5067/EVKPQZ4AFC4D.

Reichle, R. H., R. D. Koster, P. Liu, S. P. P. Mahanama, E. G. Njoku, and M. Owe (2007). "Comparison and assimilation of global soil moisture retrievals from the Advanced Microwave Scanning Radiometer for the Earth Observing System (AMSR-E) and the Scanning Multichannel Microwave Radiometer (SMMR)". *Journal of Geophysical Research: Atmospheres* 112.D9. DOI: 10.1029/2006JD008033.

Reinhart, V., C. C. Fonte, P. Hoffmann, B. Bechtel, D. Rechid, and J. Boehner (2021). "Comparison of ESA climate change initiative land cover to CORINE land cover over Eastern Europe and the Baltic States from a regional climate modeling perspective". *International Journal of Applied Earth Observation and Geoinformation* 94, 102221. DOI: 10.1016/j.jag.2020.102221.

Rimkus, E., E. Stonevicius, J. Kilpys, V. Maciulyte, and D. Valiukas (2017). "Drought identification in the eastern Baltic region using NDVI". *Earth System Dynamics* 8.3, 627. DOI: 10.5194/esd-8-627-2017.

Rosnay, P. de, J.-C. Calvet, Y. Kerr, J.-P. Wigneron, F. Lemaitre, M. J. Escorihuela, J. M. Sabater, K. Saleh, J. Barrié, G. Bouhours, L. Coret, G. Cherel, G. Dedieu, R. Durbe, N. E. D. Fritz, F. Froissard, J. Hoedjes, A. Kruszewski, F. Lavenu, D. Suquia, and P. Waldteufel (2006). "SMOSREX: A long term field campaign experiment for soil moisture and land surface processes remote sensing". *Remote Sensing of Environment* 102.3, 377. DOI: 10.1016/j.rse.2006.02.021.

Rotzoll, K. and C. H. Fletcher (2013). "Assessment of groundwater inundation as a consequence of sea-level rise". *Nature Climate Change* 3.5, 477. DOI: 10.1038/nclimate1725.

Samaniego, L., S. Thober, R. Kumar, N. Wanders, O. Rakovec, M. Pan, M. Zink, J. Sheffield, E. F. Wood, and A. Marx (2018). "Anthropogenic warming exacerbates European soil moisture droughts". *Nature Climate Change* 8.5, 421. DOI: 10.1038/s41558-018-0138-5.

Satalino, G., G. Pasquariello, F. Mattia, and L. Dente (2004). "On the accuracy of soil moisture content retrieved at pixel, segment or field scale, from advanced-SAR data: a simulation study". In: *2004 IEEE IGARSS*. Vol. 5, 3532. DOI: 10.1109/IGARSS.2004.1370472.

Scanlon, T., A. Pasik, W. Dorigo, R. A. M. De Jeu, S. Hahn, R. van der Schalie, W. Wagner, R. Kidd, A. Gruber, L. Moesinger, and W. Preimesberger (2020). *ESA Climate Change Initiative Plus-Soil Moisture. Algorithm Theoretical Baseline Document* (*ATBD*). Tech. rep. D2.1 Version 04.7. Austria: Earth Observation Data Centre for Water Resources Monitoring (EODC) GmbH. (Visited on 2020).

Schonbrodt-Stitt, S., N. Ahmadian, M. Kurtenbach, C. Conrad, N. Romano, H. R. Bogena, H. Vereecken, and P. Nasta (2021). "Statistical Exploration of Sentinel-1 Data, Terrain Parameters, and in-situ Data for Estimating the Near-Surface Soil Moisture in a Mediterranean Agroecosystem". *Frontiers in Water* 3, 75. DOI: 10.3389/frwa.2021.655837.

Schumacher, D. L., J. Keune, C. C. van Heerwaarden, J. Vilà-Guerau de Arellano, A. J. Teuling, and D. G. Miralles (2019). "Amplification of mega-heatwaves through heat torrents fuelled by upwind drought". *Nature Geoscience* 12.9, 712. DOI: 10.1038/s41561-019-0431-6.

Seneviratne, S. I., T. Corti, E. L. Davin, M. Hirschi, E. B. Jaeger, I. Lehner, B. Orlowsky, and A. J. Teuling (2010). "Investigating soil moisture–spinclimate interactions in a changing climate: A review". *Earth-Science Reviews* 99.3, 125. DOI: 10.1016/j.earscirev.2010.02.004.

Seneviratne, S. I., N. Nicholls, D. Easterling, C. M. Goodess, S. Kanae, J. Kossin, Y. Luo, J. Marengo, K. McInnes, M. Rahimi, M. Reichstein, A. Sorteberg, C. Vera, X. Zhang, M. Rusticucci, V. Semenov, L. V. Alexander, S. Allen, G. Benito, T. Cavazos, J. Clague, D. Conway, P. M. Della-Marta, M. Gerber, S. Gong, B. N. Goswami, M. Hemer, C. Huggel, B. van den Hurk, V. V. Kharin, A. Kitoh, A. M. K. Tank, G. Li, S. Mason, W. McGuire, G. J. van

Oldenborgh, B. Orlowsky, S. Smith, W. Thiaw, A. Velegrakis, P. Yiou, T. Zhang, T. Zhou, and F. W. Zwiers (2012). "Changes in Climate Extremes and their Impacts on the Natural Physical Environment". In: *Managing the Risks of Extreme Events and Disasters to Advance Climate Change Adaptation*. Ed. by C. B. Field, V. Barros, T. F. Stocker, and Q. Dahe. Cambridge: Cambridge University Press, 109. DOI: 10.1017/CBO9781139177245.006.

Sepulcre-Canto, G., S. Horion, A. Singleton, H. Carrao, and J. Vogt (2012). "Development of a Combined Drought Indicator to detect agricultural drought in Europe". *Natural Hazards and Earth System Sciences* 12.11, 3519. DOI: 10.5194/nhess-12-3519-2012.

Shukla, S. and A. W. Wood (2008). "Use of a standardized runoff index for characterizing hydrologic drought". *Geophysical Research Letters* 35.2. DOI: 10.1029/2007GL032487.

Sivakumar, M. V. K., R. Stone, P. Cesar Sentelhas, M. Svoboda, P. Omondi, J. Sarkar, and B. Wardlow (2010). "Agricultural drought indices: Summary and Recommendations". In: *Agricultural Drought Indices. Proceedings of an expert meeting*. Ed. by M. V. K. Sivakumar, R. P. Motha, D. A. Wilhite, and D. A. Wood. Murcia, Spain: WMO, 172.

Spinoni, J., G. Naumann, H. Carrao, P. Barbosa, and J. Vogt (2014). "World drought frequency, duration, and severity for 1951–2010". *International Journal of Climatology* 34.8, 2792. DOI: 10.1002/joc.3875.

Sridhar, V., K. G. Hubbard, J. You, and E. D. Hunt (2008). "Development of the Soil Moisture Index to Quantify Agricultural Drought and Its "User Friendliness" in Severity-Area-Duration Assessment". *Journal of Hydrometeorology* 9.4, 660. DOI: 10.1175/2007JHM892.1.

Stagge, J. H., D. G. Kingston, L. M. Tallaksen, and D. M. Hannah (2017). "Observed drought indices show increasing divergence across Europe". *Scientific Reports* 7.1, 14045. DOI: 10.1038/s41598-017-14283-2.

Stagge, J. H., I. Kohn, L. M. Tallaksen, and K. Stahl (2015). "Modeling drought impact occurrence based on meteorological drought indices in Europe". *Journal of Hydrology* 530, 37. DOI: 10.1016/j.jhydrol.2015.09.039.

Stahl, K., I. Kohn, V. Blauhut, J. Urquijo, L. De Stefano, V. Acácio, S. Dias, J. H. Stagge, L. M. Tallaksen, E. Kampragou, A. F. Van Loon, L. J. Barker, L. A. Melsen, C. Bifulco, D. Musolino, A. de Carli, A. Massarutto, D. Assimacopoulos, and H. A. J. Van Lanen (2016). "Impacts of European drought events: insights from an international database of text-based reports". *Natural Hazards and Earth System Sciences* 16.3, 801. DOI: 10.5194/nhess-16-801-2016.

Stephenson, D. B. (2000). "Use of the "Odds Ratio" for Diagnosing Forecast Skill". *Weather and Forecasting* 15.2, 221. DOI: 10.1175/1520-0434(2000)015⟨0221:UOTORF⟩2.0.CO;2.

Szczypta, C., J.-C. Calvet, F. Maignan, W. Dorigo, F. Baret, and P. Ciais (2014). "Suitability of modelled and remotely sensed essential climate variables for monitoring Euro-Mediterranean droughts". *Geoscientific Model Development* 7.3, 931. DOI: 10.5194/gmd-7-931-2014.

Tallaksen, L. M. and H. A. J. van Lanen, eds. (2004). *Hydrological Drought – 1st Edition*. Vol. 84. Developments in water science. Elsevier.

Teuling, A. J., S. I. Seneviratne, C. Williams, and P. A. Troch (2006a). "Observed timescales of evapotranspiration response to soil moisture". *Geophysical Research Letters* 33.23. DOI: 10.1029/2006GL028178.

Teuling, A. J. and P. A. Troch (2005). "Improved understanding of soil moisture variability dynamics". *Geophysical Research Letters* 32.5, L05404. DOI: 10.1029/2004GL021935.

Teuling, A. J., R. Uijlenhoet, F. Hupet, E. E. van Loon, and P. A. Troch (2006b). "Estimating spatial mean root-zone soil moisture from point-scale observations". *Hydrology and Earth System Sciences* 10.5, 755. DOI: 10.5194/hess-10-755-2006.

Teuling, A. J. (2018). "A hot future for European droughts". *Nature Climate Change* 8.5, 364. DOI: 10.1038/s41558-018-0154-5.

Teuling, A. J., A. F. V. Loon, S. I. Seneviratne, I. Lehner, M. Aubinet, B. Heinesch, C. Bernhofer, T. Grunwald, H. Prasse, and U. Spank (2013). "Evapotranspiration amplifies European summer drought". *Geophysical Research Letters* 40.10, 2071. DOI: 10.1002/grl.50495.

Teuling, A. J., R. Uijlenhoet, F. Hupet, and P. A. Troch (2006c). "Impact of plant water uptake strategy on soil moisture and evapotranspiration dynamics during drydown". *Geophysical Research Letters* 33.3. DOI: 10.1029/2005GL025019.

Teuling, A. J., R. Uijlenhoet, and P. A. Troch (2005). "On bimodality in warm season soil moisture observations". *Geophysical Research Letters* 32.13. DOI: 10.1029/2005GL023223.

Tobin, K. J., W. T. Crow, J. Dong, and M. E. Bennett (2019). "Validation of a New Root-Zone Soil Moisture Product: Soil MERGE". *IEEE Journal of Selected Topics in Applied Earth Observations and Remote Sensing* 12.9. Conference Name: IEEE Journal of Selected Topics in Applied Earth Observations and Remote Sensing, 3351. DOI: 10.1109/JSTARS.2019.2930946.

Toreti, A., D. Bavera, J. Acosta Navarro, C. Cammalleri, A. de Jager, C. Di Ciollo, A. Hrast Essenfelder, W. Maetens, D. Magni, D. Masante, M. Mazzeschi, S. Niemeyer, and J. Spinoni (2022). *Drought in Europe: August 2022 : GDO analytical report*. Tech. rep. JRC130493. LU: Publications Office of the European Union. DOI: 10.2760/264241.

Torres, R., P. Snoeij, D. Geudtner, D. Bibby, M. Davidson, E. Attema, P. Potin, B. Rommen, N. Floury, M. Brown, I. N. Traver, P. Deghaye, B. Duesmann, B. Rosich, N. Miranda, C. Bruno, M. L'Abbate, R. Croci, A. Pietropaolo, M. Huchler, and F. Rostan (2012). "GMES Sentinel-1 mission". *Remote Sensing of Environment*. The Sentinel Missions - New Opportunities for Science 120, 9. DOI: 10.1016/j.rse.2011.05.028.

Tripathi, A. and R. K. Tiwari (2020). "Synergetic utilization of Sentinel-1 SAR and Sentinel-2 optical remote sensing data for surface soil moisture estimation for Rupnagar, Punjab, India". *Geocarto International* 0.0, 1. DOI: 10.1080/10106049.2020.1815865.

Tucker, C. J. (1979). "Red and photographic infrared linear combinations for monitoring vegetation". *Remote Sensing of Environment* 8.2, 127. DOI: 10.1016/0034-4257(79)90013-0.

Ulaby, F. T. and D. G. Long (2014). *Microwave radar and radiometric remote sensing*. Ann Arbor: The University of Michigan Press.

Ulaby, F. T., R. K. Moore, and A. K. Fung (1986). *Microwave Remote Sensing: Active and Passive, Volume II: Radar Remote Sensing and Surface Scattering and Emission Theory*. English. Norwood, MA: Artech House.

Vautard, R., P. Yiou, F. D'Andrea, N. d. Noblet, N. Viovy, C. Cassou, J. Polcher, P. Ciais, M. Kageyama, and Y. Fan (2007). "Summertime European heat and drought waves induced by wintertime Mediterranean rainfall deficit". *Geophysical Research Letters* 34.7. DOI: 10.1029/2006GL028001.

Vereecken, H., J. A. Huisman, H. Bogena, J. Vanderborght, J. A. Vrugt, and J. W. Hopmans (2008). "On the value of soil moisture measurements in vadose zone hydrology: A review". *Water Resources Research* 44.4. DOI: 10.1029/2008WR006829.

Vereecken, H., J. A. Huisman, Y. Pachepsky, C. Montzka, J. van der Kruk, H. Bogena, L. Weihermuller, M. Herbst, G. Martinez, and J. Vanderborght (2014). "On the spatio-temporal dynamics of soil moisture at the field scale". *Journal of Hydrology*. Determination of soil moisture: Measurements and theoretical approaches 516, 76. DOI: 10.1016/j.jhydrol.2013.11.061.

Vergopolan, N., J. Sheffield, N. W. Chaney, M. Pan, H. E. Beck, C. R. Ferguson, L. Torres-Rojas, F. Eigenbrod, W. Crow, and E. F. Wood (2022). "High-Resolution Soil Moisture Data Reveal Complex Multi-Scale Spatial Variability Across the United States". *Geophysical Research Letters* 49.15, e2022GL098586. DOI: 10.1029/2022GL098586.

Vergopolan, N., S. Xiong, L. Estes, N. Wanders, N. W. Chaney, E. F. Wood, M. Konar, K. Caylor, H. E. Beck, N. Gatti, T. Evans, and J. Sheffield (2021). "Field-scale soil moisture bridges the spatial-scale gap between drought monitoring and agricultural yields". *Hydrology and Earth System Sciences* 25.4, 1827. DOI: 10.5194/hess-25-1827-2021.

Vilasa, L., D. G. Miralles, R. A. M. d. Jeu, and A. J. Dolman (2017). "Global soil moisture bimodality in satellite observations and climate models". *Journal of Geophysical Research: Atmospheres* 122.8, 4299. DOI: 10.1002/2016JD026099.

Vliet, M. van der, R. van der Schalie, N. Rodriguez-Fernandez, A. Colliander, R. de Jeu, W. Preimesberger, T. Scanlon, and W. Dorigo (2020). "Reconciling Flagging Strategies for Multi-Sensor Satellite Soil Moisture Climate Data Records". *Remote Sensing* 12.20, 3439. DOI: 10.3390/rs12203439.

Vroege, W., J. Bucheli, T. Dalhaus, M. Hirschi, and R. Finger (2021). "Insuring crops from space: the potential of satellite-retrieved soil moisture to reduce farmers' drought risk exposure". *European Review of Agricultural Economics* 48.2, 266. DOI: 10.1093/erae/jbab010.

Wada, Y., L. P. H. v. Beek, N. Wanders, and M. F. P. Bierkens (2013). "Human water consumption intensifies hydrological drought worldwide". *Environmental Research Letters* 8.3, 034036. DOI: 10.1088/1748-9326/8/3/034036.

Wagner, W., G. Lemoine, and H. Rott (1999). "A Method for Estimating Soil Moisture from ERS Scatterometer and Soil Data". *Remote Sensing of Environment* 70.2, 191. DOI: 10.1016/S0034-4257(99)00036-X.

Wanders, N. and Y. Wada (2015). "Human and climate impacts on the 21st century hydrological drought". *Journal of Hydrology*. Drought processes, modeling, and mitigation 526, 208. DOI: 10.1016/j.jhydrol.2014.10.047.

Wanders, N., Y. Wada, and H. A. J. Van Lanen (2015). "Global hydrological droughts in the 21st century under a changing hydrological regime". *Earth System Dynamics* 6.1, 1. DOI: 10.5194/esd-6-1-2015.

Wang, H., R. Magagi, and K. Goita (2018). "Potential of a two-component polarimetric decomposition at C-band for soil moisture retrieval over agricultural fields". *Remote Sensing of Environment* 217, 38. DOI: 10.1016/j.rse.2018.08.003.

West, H., N. Quinn, and M. Horswell (2019). "Remote sensing for drought monitoring & impact assessment: Progress, past challenges and future opportunities". *Remote Sensing of Environment* 232, 111291. DOI: 10.1016/j.rse.2019.111291.

Western, A. W. and G. Bloschl (1999). "On the spatial scaling of soil moisture". *Journal of Hydrology* 217.3, 203. DOI: 10.1016/S0022-1694(98)00232-7.

Wiel, K. van der, T. J. Batelaan, and N. Wanders (2023). "Large increases of multi-year droughts in north-western Europe in a warmer climate". *Climate Dynamics* 60.5, 1781. DOI: 10.1007/s00382-022-06373-3.

Wilhite, D. A. and M. H. Glantz (1985). "Understanding the Drought Phenomenon: The Role of Definitions". *WATER INTERNATIONAL* 10.3, 111.

WMO (2017). *WMO Guidelines on the Calculation of Climate Normals*. Tech. rep. WMO-No. 1203. Geneva, Switzerland: World Meteorological Organization.

Wood, E. F., J. K. Roundy, T. J. Troy, L. P. H. van Beek, M. F. P. Bierkens, E. Blyth, A. de Roo, P. Doll, M. Ek, J. Famiglietti, D. Gochis, N. van de Giesen, P. Houser, P. R. Jaffé, S. Kollet, B. Lehner, D. P. Lettenmaier, C. Peters-Lidard, M. Sivapalan, J. Sheffield, A. Wade, and P. Whitehead (2011). "Hyperresolution global land surface modeling: Meeting a grand challenge for monitoring Earth's terrestrial water". *Water Resources Research* 47.5. DOI: 10.1029/2010WR010090.

Yadav, V. P., R. Prasad, R. Bala, and A. K. Vishwakarma (2020). "An improved inversion algorithm for spatio-temporal retrieval of soil moisture through modified water cloud model using C- band Sentinel-1A SAR data". *Computers and Electronics in Agriculture* 173, 105447. DOI: 10.1016/j.compag.2020.105447.

Yin, D., Z. G. Xue, D. Bao, A. RafieeiNasab, Y. Huang, M. Morales, and J. C. Warner (2022). "Understanding the role of initial soil moisture and precipitation magnitude in flood forecast using a hydrometeorological modelling system". *Hydrological Processes* 36.10, e14710. DOI: 10.1002/hyp.14710.

Yuan, X., L. Wang, P. Wu, P. Ji, J. Sheffield, and M. Zhang (2019). "Anthropogenic shift towards higher risk of flash drought over China". *Nature Communications* 10.1, 4661. DOI: 10.1038/s41467-019-12692-7.

Yurekli, K. and A. Kurunc (2006). "Simulating agricultural drought periods based on daily rainfall and crop water consumption". *Journal of Arid Environments* 67.4, 629. DOI: 10.1016/j.jaridenv.2006.03.026.

Zampieri, M., F. D'Andrea, R. Vautard, P. Ciais, N. d. Noblet-Ducoudré, and P. Yiou (2009). "Hot European Summers and the Role of Soil Moisture in the Propagation of Mediterranean Drought". *Journal of Climate* 22.18, 4747. DOI: 10.1175/2009JCLI2568.1.

Zappa, L., S. Schlaffer, B. Bauer-Marschallinger, C. Nendel, B. Zimmerman, and W. Dorigo (2021). "Detection and Quantification of Irrigation Water Amounts at 500 m Using Sentinel-1 Surface Soil Moisture". *Remote Sensing* 13.9, 1727. DOI: 10.3390/rs13091727.

Zargar, A., R. Sadiq, B. Naser, and F. I. Khan (2011). "A review of drought indices". *Environmental Reviews* 19, 333. DOI: 10.1139/A11-013.

Zhang, D. and G. Zhou (2016). "Estimation of Soil Moisture from Optical and Thermal Remote Sensing: A Review". *Sensors* 16.8, 1308. DOI: 10.3390/s16081308.

Zhang, M., F. Lang, and N. Zheng (2021). "Soil Moisture Retrieval during the Wheat Growth Cycle Using SAR and Optical Satellite Data". *Water* 13.2, 135. DOI: 10.3390/w13020135.

Zhao, J., R. Pelich, R. Hostache, P. Matgen, S. Cao, W. Wagner, and M. Chini (2021). "Deriving exclusion maps from C-band SAR time-series in support of floodwater mapping". *Remote Sensing of Environment* 265, 112668. DOI: 10.1016/j.rse.2021.112668.

Zheng, J., T. Zhao, H. Lu, J. Shi, M. H. Cosh, D. Ji, L. Jiang, Q. Cui, H. Lu, K. Yang, J.-P. Wigneron, X. Li, Y. Zhu, L. Hu, Z. Peng, Y. Zeng, X. Wang, and C. S. Kang (2022). "Assessment of 24 soil moisture datasets using a new in situ network in the Shandian River Basin of China". *Remote Sensing of Environment* 271, 112891. DOI: 10.1016/j.rse.2022.112891.

Zhu, L., J. P. Walker, and X. Shen (2020). "Stochastic ensemble methods for multi-SAR-mission soil moisture retrieval". *Remote Sensing of Environment* 251, 112099. DOI: 10.1016/j.rse.2020.112099.

Zhu, L., J. P. Walker, L. Tsang, H. Huang, N. Ye, and C. Rudiger (2019). "Soil moisture retrieval from time series multi-angular radar data using a dry down constraint". *Remote Sensing of Environment* 231, 111237. DOI: 10.1016/j.rse.2019.111237.

Zscheischler, J., O. Martius, S. Westra, E. Bevacqua, C. Raymond, R. M. Horton, B. van den Hurk, A. AghaKouchak, A. Jézéquel, M. D. Mahecha, D. Maraun, A. M. Ramos, N. N. Ridder, W. Thiery, and E. Vignotto (2020). "A typology of compound weather and climate events". *Nature Reviews Earth & Environment* 1.7, 333. DOI: 10.1038/s43017-020-0060-z.

Zscheischler, J., R. Orth, and S. I. Seneviratne (2015). "A submonthly database for detecting changes in vegetation-atmosphere coupling". *Geophysical Research Letters* 42.22, 9816. DOI: 10.1002/2015GL066563.

Zscheischler, J., S. Westra, B. J. J. M. van den Hurk, S. I. Seneviratne, P. J. Ward, A. Pitman, A. AghaKouchak, D. N. Bresch, M. Leonard, T. Wahl, and X. Zhang (2018). "Future climate risk from compound events". *Nature Climate Change* 8.6, 469. DOI: 10.1038/s41558-018-0156-3.

Acknowledgements

There are many people without whom I wouldn't have been able to finish this thesis. I'd like to take the opportunity of the last pages of this thesis to thank my colleagues, my friends and my family for supporting me and getting me to finish this piece of work.

First of all, my three supervisors, who've been with me for this PhD from start to finish. Marco, thank you for your daily support, your never-dwindling interest in my work and your ever helpful feedback. I really enjoyed getting to know you through this process and already miss the office chats! Ryan, thank you for the push to apply for this position: these four years have given me a lot of experiences that I might have missed otherwise. Our many discussions during the PhD have been very helpful in shaping this thesis towards its current state. I thank you for your support from afar and your determination in getting my work out there. Patrick, thank you for using your limited time to help me wherever possible. Your critical insights on my work have been invaluable for the contents of this thesis. Your efforts have also made navigating LIST and its endless documentation lots easier.

Jeff and Olivier, you have both been of great importance during the data collection phases of this work. Thank you for spending time with me in the office and in the field. Without your help, I couldn't have finished this thesis.

Anne and Saskia, thank you for agreeing to be my paranymphs. Saskia, you've been one of my best friends ever since the Afroeicie. My Wageningen time before and during my PhD would have been very different without you - thank you for being amazing! Anne, it was great having you as a colleague and friend both in Wageningen and in Luxembourg. Always having someone to share the highs and lows of a PhD and to go through part of that together was really valuable. Thank you for being you, for the coffees and for the chats!

At LIST I was lucky to have a great group of colleagues surrounding me. I thank you for sharing your knowledge and your time with me. Thanks, colleagues and friends in the office and hallways, for always being there for a short break or chat. You've all helped making me feel at ease at LIST. Laurent, thank you for your continued efforts to keep the DTU going. Adnan, Alessandro, Anne, Carol, Concetta, Dhruv, Enrico, Henry, Jasper, Jie, Judith,

Nicolaus and Perrine, thank you for the good times at the DTU meetings, the DTU retreats and the fun side-events outside of work. Guilhem, Nicolaus, Loic, Louis and Ginevra, thank you for spending your lunch breaks with me.

Thanks to my HWM colleagues for always making me feel at home in Wageningen. This especially goes for the people that were so kind to let me invade their offices. I had so many nice experiences thanks to HWM that I am forever grateful for: three writing weeks, two iceland excursions and one tour the PhD. Linda, Femke and Rahel, thank you for your friendship, the sleepovers, the runs and for a really fun weekend in Luxembourg! Thank you Janneke, Jelte, Joost, Lieke, Martine, Roel, Ryan, Sjoukje, Victor and Bram for making the two Iceland trips so memorable (although I probably have a volcano to thank for that, too..!). The tour the PhD was one of my personal highlights, thanks for the good times while organising Steven, Harro, Rose, Joris and Sjoukje, and Harro, thank you for spending many hours online with me in writing that opinion paper. Finally, thank you to the HWM PhDs who helped write this thesis through their feedback during the thesis rings.

Alexandre and Paris, thank you for being a-ma-zing housemates, friends and cycling buddies. Angela, thank you for the weekly bouldering outings, the good talks and your emotional support. Without the three of you, my time in Luxembourg would not have been the same. I loved our cycling trips, game nights, drinks, festivals and movies and look forward to our future adventures! When's the next bike trip, cookies?

Lotta & Nicole, Jolanda, R80 friends, bestuurtjes & Hageveld girls, I thank you for being part of my life. Your friendship means the world to me and I'm looking forward to seeing more of most of you now that I moved back to the Netherlands.

A big thanks goes out to my entire family. Thank you for your loving support throughout this process, for your calls and messages to keep me close while I was away, and for your visits to far-far-away Luxembourg. Mama, thank you for making the cover of this thesis, it turned out great! Thanks to both my parents for making me the person I am today. Dr. Hans & Lisa, thank you for having us so often, a visit to your place always made for a nice distraction. Noor & Nina, thank you for always being happy, it's a pleasure watching the two of you grow up. Emma en Kyra, thank you for always being there for a nice day out (like a random 90k bike trip), hope we can have more of those now that I live closer by! Yvonne, bedankt voor jouw steun, vooral tijdens de korte periode waar we ongepland even samen woonden. Oma Nel, dankjewel voor de lieve mails, die hebben mij erg gesteund op de soms wat eenzame ochtenden in Luxemburg.

Last but certainly not least, Ruben, thank you for sticking with me throughout this chaotic period, thank you for always having my back, thank you for making your house my home away from home and then our home, and thank you for being the kindest, most good-humoured and best partner in life I could imagine.

List of publications

Peer-reviewed Journal Publications

Buitink, J., **T. C. van Hateren**, and A. J. Teuling (2021). "Hydrological System Complexity Induces a Drought Frequency Paradox". *Frontiers in Water* 3. DOI: 10.3389/frwa.2021.640976.

Hateren, **T. C. van**, M. Chini, P. Matgen, L. Pulvirenti, N. Pierdicca, and A. J. Teuling (2023a). "On the potential of Sentinel-1 for sub-field scale soil moisture monitoring". *International Journal of Applied Earth Observation and Geoinformation* 120, 103342. DOI: 10.1016/j.jag.2023.103342.

Hateren, **T. C. van**, M. Chini, P. Matgen, and A. J. Teuling (2021a). "Ambiguous Agricultural Drought: Characterising Soil Moisture and Vegetation Droughts in Europe from Earth Observation". *Remote Sensing* 13.10, 1990. DOI: 10.3390/rs13101990.

Hateren, **T. C. van**, M. Chini, P. Matgen, L. Pulvirenti, N. Pierdicca, and A. J. Teuling (2023b). "On the Use of Native Resolution Backscatter Intensity Data for Optimal Soil Moisture Retrieval". *IEEE Geoscience and Remote Sensing Letters* 20, 1. DOI: 10.1109/LGRS.2023.3264732.

Hateren, **T. C. van**, H. J. Jongen, H. Al-Zawaidah, J. G. Beemster, J. Boekee, L. Bogerd, S. Gao, C. Kannen, I. van Meerveld, S. I. de Lange, F. Linke, R. B. Pinto, J. O. Remmers, J. Ruijsch, S. R. Rusli, R. C. van de Vijsel, J. P. Aerts, S. M. Agoungbome, M. Anys, S. Blanco Ramírez, T. van Emmerik, L. Gallitelli, G. Chiquito Gesualdo, W. Gonzalez Otero, S. Hanus, Z. He, S. Hoffmeister, R. O. Imhoff, T. Kerlin, S. M. Meshram, J. Meyer, A. Meyer Oliveira, A. C. Muller, R. Nijzink, M. Scheller, L. Schreyers, D. Sehgal, P. F. Tasseron, A. J. Teuling, M. Trevisson, K. Waldschlager, B. Walraven, C. Wannasin, J. Wienhofer, M. J. Zander, S. Zhang, J. Zhou, J. Y. Zomer, and B. W. Zwartendijk (2023d). "Where should hydrology go? An early-career perspective on the next IAHS Scientific Decade: 2023–2032". *Hydrological Sciences Journal* 68.4, 529. DOI: 10.1080/02626667.2023.2170754.

Hateren, **T. C. van**, S. J. Sutanto, and H. A. J. Van Lanen (2019). "Evaluating skill and robustness of seasonal meteorological and hydrological drought forecasts at the catchment scale – Case Catalonia (Spain)". *Environment International* 133, 105206. DOI: 10.1016/j.envint.2019.105206.

Hoek van Dijke, A. J., R. Orth, A. J. Teuling, M. Herold, M. Schlerf, M. Migliavacca, M. Machwitz, **T. C. van Hateren**, X. Yu, and K. Mallick (2023). "Comparing forest and grassland drought responses inferred from eddy covariance and Earth observation". *Agricultural and Forest Meteorology* 341, 109635. DOI: 10.1016/j.agrformet.2023.109635.

Authorship contribution statement

This PhD project was part of the Hydro-CSI Doctoral Training Unit, led by Laurent Pfister at LIST. The general research direction of this thesis was based on the topic outlined in that project proposal. I then formulated the research plan and research questions that resulted in the chapters presented in this thesis. I wrote the introduction (Chapter 1) and the synthesis (Chapter 6) with minor suggestions from my promotors. Some introductory parts of Chapter 1 are based on an opinion paper that I co-wrote with Harro Jongen and 47 other authors. Chapters 2 to 5 result from a collaboration with the authors listed here. Each of their contributions are summarised per chapter below.

JZ:	Jie Zhao
LP:	Luca Pulirenti
MC:	Marco Chini
NP:	Nazzareno Pierdicca
PM:	Patrick Matgen
RT:	Ryan Teuling
TH:	Tessa van Hateren

Chapter 2

Conceptualisation:	TH, MC, PM, RT
Data collection:	TH
Data analysis and interpretation:	TH in consultation with MC, PM, RT
Writing:	TH
Revision and approval:	TH, MC, PM, RT

Chapter 3

Conceptualisation:	TH, MC, PM, LP, NP, RT
Data collection:	TH
Data analysis and interpretation:	TH in consultation with MC, PM, LP, NP, RT
Writing:	TH
Revision and approval:	TH, MC, PM, LP, NP, RT

Chapter 4

Conceptualisation:	TH, MC, PM, LP, NP, RT
Data collection:	TH
Data analysis and interpretation:	TH in consultation with MC, PM, LP, NP, RT
Writing:	TH
Revision and approval:	TH, MC, PM, LP, NP, RT

Chapter 5

Conceptualisation:	TH, MC, PM, RT
Data collection:	TH, JZ
Data analysis and interpretation:	TH in consultation with MC, PM, RT
Writing:	TH
Revision and approval:	TH, MC, PM, JZ, RT

Graduate school certificate

Netherlands Research School for the
Socio-Economic and Natural Sciences of the Environment

D I P L O M A

for specialised PhD training

The Netherlands research school for the
Socio-Economic and Natural Sciences of the Environment
(SENSE) declares that

Theresa Catharina van Hateren

born on the 22nd of December 1994 in Hillegom, The Netherlands

has successfully fulfilled all requirements of the
educational PhD programme of SENSE.

Wageningen, the 22nd of November 2023

Chair of the SENSE board

Prof. dr. Martin Wassen

The SENSE Director

Prof. Philipp Pattberg

The SENSE Research School has been accredited by the Royal Netherlands Academy of Arts and Sciences (KNAW)

KONINKLIJKE NEDERLANDSE
AKADEMIE VAN WETENSCHAPPEN

The SENSE Research School declares that **Theresa Catharina van Hateren** has successfully fulfilled all requirements of the educational PhD programme of SENSE with a work load of 42.6 EC, including the following activities:

SENSE PhD Courses

- Environmental research in context (2019)
- Research in context activity: Writing of community opinion paper: "an early-career perspective on the theme of the next IAHS scientific decade" (2022)

Other PhD and Advanced MSc Courses

- Summer School on InSAR: Split Band Interferometry and displacement time series, European Centre for Geodynamics and Seismology (2019)
- Hillslope hydrology: past, present and future, LIST (2019)
- Geostatistics, Wageningen University (2019)
- R and big data, Wageningen University (2019)
- Brain training, Wageningen Graduate Schools (2020)
- Project and time management, Wageningen Graduate Schools (2020)
- Scientific writing, Wageningen Graduate Schools (2021)

Management and Didactic Skills Training

- Supervising MSc student with thesis entitled 'Hydrological drought across different size basins in the Rhine and Meuse catchments' (2021)
- Assisting with the drought practical in the ITEE course (2021)
- Giving tutorials in the BSc course "Water I" (2019-2022)
- Organizing and teaching in the Iceland practical of the MSc course "Catchment & Climate hydrology" (2019, 2022)
- Giving practicals in the MSc course "Catchment & Climate hydrology"(2020-2022)
- Organized the "Tour the PhD" for 18 people of the HWM group (2022)

Oral Presentations

- *Evaluating skill and robustness of seasonal meteorological and hydrological drought forecasts at the catchment scale – Case Catalonia (Spain).* EGU General assembly, 4-8 May, 2020, Online
- *Optimal Spatial Resolution of Sentinel-1 Surface Soil Moisture Evaluated Using Intensive in Situ Observations.* IGARSS, 12-17 July, 2021, Online
- *Optimal soil moisture resolution and retrieval method for S1 data.* IGARSS, 17-22 July 2022, Kuala Lumpur, Malaysia

SENSE coordinator PhD education

Dr. ir. Peter Vermeulen

The research presented in this thesis was financially supported by the Luxembourg National Research Fund (FNR) under the grant agreement No. PRIDE15/10623093/HYDRO-CSI. The research was carried out at the Remote Sensing and Natural Resources Modelling group, Department of Environmental Research and Innovation, Luxembourg Institute of Science and Technology (Esch-sur-Alzette, Luxembourg) and at the Hydrology and Environmental Hydraulics Group, Department of Environmental Sciences, Wageningen University & Research (Wageningen, The Netherlands).

Financial support from Wageningen University for printing this thesis is gratefully acknowledged.

Cover design by	C. J. Osselton & T. C. van Hateren
Layout design by	T. C. van Hateren
Printed by	ProefschriftMaken on FSC-certified paper